ENHANCING TRAFFIC SAFETY WITH THE IMPLEMENTATION OF

CROWDSENSING SOLUTIONS IN THE MOBILE ERA

A Dissertation

by

XIAO LI

Submitted to the Office of Graduate and Professional Studies of
Texas A&M University
in partial fulfillment of the requirements for the degree of

DOCTOR OF PHILOSOPHY

Chair of Committee,	Daniel W. Goldberg
Committee Members,	Anthony Filippi
	Tracy Hammond
	Yunlong Zhang
Head of Department,	David Cairns

December 2019

Major Subject: Geography

ABSTRACT

Traffic injuries are one of the most severe public health problems. Fueled by the growing availability of traffic-related data sources, data-driven safety studies have been extensively utilized to model traffic risks and enhance driving safety. Among these data sources, mobile crowd sourced (MCS) data shows significant potential to advance current safety studies substantially; however, the implementation of MCS-based solutions is still underexplored. This dissertation explores the potential of MCS-based solutions for enhancing traffic safety. It contains four distinctive research works to re-evaluate and capture traffic risks using MCS data.

In the first study, I utilized crowdsourced Waze data to re-assess freeway traffic risks. Traditionally, police crash reports (PCR) have been used as the primary source of crash data in safety studies, which cannot capture the unreported risks (near-crashes and traffic incidents). This study provides a new procedure to capture unreported traffic risks by combining PCRs and Waze data. The results demonstrated that Waze could capture a broad range of unreported traffic risks and be potentially used as a surrogate safety measure in the absence of crash data.

The second and third studies introduce MCS-based solutions for monitoring road surface conditions. Road surface roughness assessment is essential in road maintenance, which is also closely related to traffic safety. However, continuously monitoring road surface roughness with a high-efficient solution remains a challenging research question. In these two studies, we proposed new solutions to achieve large-scale monitoring of

road surface conditions and the detection of road anomalies using MCS data. The results demonstrated, by mining the MCS data, road surface conditions can be effectively assessed.

The last study introduces an innovative approach to characterize hazardous driving scenes, in which drivers are prone to making driving mistakes. This study marks the first attempt to explore the correlation between driving error occurrence and geospatial features. In this study, mobile sensed driving errors were integrated with driving-related geospatial features to form "scenic tuples" to characterize the occurrence of each error. Through mining a long-term collection of scenic tuples, we can extract the individualized hazardous scenes, which has the potential to aid in reducing driving risks.

DEDICATION

To my grandparents, my mother, my father, and everyone who is beside me along the

way.

ACKNOWLEDGEMENTS

CONTRIBUTORS AND FUNDING SOURCES

Contributors

This work was supervised by a dissertation committee consisting of Professor Daniel Goldberg [advisor] and Professor Anthony Filippi of the Department of Geography, Professor Tracy Hammond of the Department of Computer Science & Engineering, and Professor Yunlong Zhang of the Department of Civil and Environmental Engineering.

Assistance with the analyses in Section 2 was provided by Bahar Dadashova of Texas A&M Transportation Institute and is under review by Transportation Research Record Journal. Assistance with analyses in Section 4 was provided by Professor Daniel Goldberg of the Department of Geography and Dr. Tianxing Chu of Texas A&M University-Corpus Christ and was published in 2018. Assistance with analyses in Section 5 was provided by Da Huo of the Department of Geography and was published in 2019.

All other work conducted for the dissertation was completed by the student independently.

Funding Sources

NOMENCLATURE

AADT	Annual Average Daily Traffic
API	Android Application Program Interface
BD	Baseline Dataset
CAN	Controller Area Network
CCP	Connected Citizens Program
CD	Comparison Dataset
CFS	Correlation-Based Feature Selection
CMF	Crash Modification Factor
CRIS	Crash Records Information System
CR-3	Texas Peace Officer's Crash Report
CWT	Continuous Wavelet Transform
DB3	Daubechies 3 Wavelet
DBSCAN	Density-Based Spatial Clustering of Applications with Noise
DFO	Distance from Origin
DTW	Dynamic Time Wrapping
DWT	Discrete Wavelet Transform
ECEF	Earth-Centered, Earth-Faxed
ETA	Estimated Time of Arrival
FHWA	The U.S. Federal Highway Administration

GIS	Geographic Information Science
GPS	Global Positioning System
HC	Hierarchical Clustering
HCPC	Hierarchical Clustering on Principal Components
HDBSCAN	Hierarchical Density-Based Spatial Clustering of Applications with Noise
HWT	Haar Wavelet Transform
IRI	International Roughness Index
LiDAR	Light Detection and Ranging
LSTM	Long-Short-Term-Memory
MCA	Multiple Correspondence Analysis
MCS	Mobile Crowd Sensing/Sensed
MEMS	Microelectromechanical System
MLA	Machine Learning Algorithm
OLS	Ordinary Least Square Regression
PCR	Police Crash Report
PSI	Present Serviceability Index
RMS	Root Mean Square
SPF	Safety Performance Function
SVM	Support Vector Machine
TxDOT	Texas Department of Transportation
WHO	World Health Organization

WIR   Waze Incident Report

WT   Wavelet Transform

TABLE OF CONTENTS

LIST OF FIGURES

xv

LIST OF TABLES

1. INTRODUCTION

1.1. Background

Traffic injuries are one of the most severe public health problems in the world (World Health Organization 2015). Driving behavior (*what*), as a crucial contributing factor, closely relates to road safety. Driving mistakes (such as speeding, drunken driving, and irregular overtaking) not only threaten driving safety but also put pedestrians at significant risk. Meanwhile, driving safety also relates to two other factors, *when* and *where* (J. D. Lee 2008; Jinfeng Zhao 2011; World Health Organization 2015; Yao, Loo, and Yang 2016).

Since 1976, numerous studies have been conducted to analyze traffic risks. Among these studies, GIS plays an important role, not only in managing and manipulating crash data but also in providing abundant spatiotemporal, data sources, methods, and theories for better understanding and facilitating traffic safety (Goodchild 2015; Bham et al. 2017). Especially in the past decade, massive volumes of traffic-related data sources were becoming available (e.g., traffic volume, road geometry, weather condition, etc.) These spatiotemporal data sources offer a great opportunity for road safety researchers to discover new insights into the crash distribution and model the traffic risk scenarios. Among all the emerging data sources, mobile crowdsourced data shows significant potential to advance current road safety analysis substantially. For example, as one of the most successful crowdsourcing mobile applications, Waze takes advantage of the crowdsourced traffic information to provide driving information

1

services in near real-time. With more than 110 million monthly active users reporting on traffic, Waze delivers an accurate representation of what's happening on the road every day.

Mobile sensing technology has advanced rapidly over the past few years (Li et al. 2019; W. Xu et al. 2015; R. Chen, Chu, Liu, Chen, et al. 2014). Equipped with miniaturized sensors (e.g., accelerometer, gyroscope, GPS, camera), smartphones have become promising data acquisition and computing platforms, which could achieve a high-sampling rate with little or zero economic cost. Smartphones are ubiquitous today, which empower the citizens to sense their surroundings, generate data, and contribute their observations to achieve a continuous monitoring system in an unprecedented manner (Guo et al. 2016, 2014; Panichpapiboon and Leakkaw 2017). By leveraging the power of citizens and the rich sensing resources, mobile crowd sensing (MCS) has become a popular researching paradigm for large-scale sensing and monitoring in recent years. Mobile crowd sensed data sources are transforming our life, which has been proven extremely efficient and successfully deployed to solve real-world issues, such as noise monitoring, traffic density estimation, route planning, among others (Guo et al. 2015; Zappatore, Longo, and Bochicchio 2016). Meanwhile, mobile sensing technology also shows great potential to sense the driving environment, synthesize real-time traffic information, even identify and alert aggressive driving behaviors (N. Silva et al. 2018; Li et al. 2019; Zappatore, Longo, and Bochicchio 2016). However, to date, the implementation of mobile crowdsourced data in road safety analysis is still at a preliminary stage.

2

1.2. Research Objectives

This dissertation innovatively explores the utilization of mobile crowdsourced data in road safety analysis, which aims to re-think the traffic safety and characterize the hazardous driving context from three perspectives: traffic incident, road, and driver. In this dissertation, I focus on the implementation of mobile sensing solutions for achieving the following three research objectives:

1) Re-evaluate traffic safety by comprehensively considering both official police-reportable crashes and crowdsourced traffic incidents using Waze data.

2) Estimate road surface conditions and identify road surface anomalies using mobile crowdsensing solutions.

3) Depict individual-based hazardous driving scenes using GIS and mobile sensing.

1.3. Overview of Substantive Sections

This dissertation consists of four substantive sections. Each section represents a unique MSC-based research work written in the journal article format, which describes the implementation of mobile sensed data for solving traffic-safety-related problems.

1.3.1. Section 2 Overview

Section 2 explores the utilization of crowdsourced Waze data for recognizing unreported traffic risks and re-evaluate highway traffic safety (Research Objective 1).

Identification of traffic crash hot spots is of great importance for improving roadway safety. Traditionally, police crash reports (PCR) have been used as the primary source of crash data in safety studies. However, using PCR as the sole source of information has several drawbacks. For example, some crashes, which do not cause

3

extensive property damage, are mostly underreported. Underreporting of crashes can significantly influence the effectiveness of data-driven safety analysis and prevent safety analysts from reaching statistically meaningful results. Crowdsourced traffic incident data such as Waze can add a new dimension to the traditional safety analysis by providing real-time crash and traffic incident data.

In this section, we explore the potential of using crowdsourced Waze incident reports (WIRs) to identify high-risk road segments. The researchers use WIRs and PCRs from an I-35 corridor in North Texas to conduct the safety analysis. Results demonstrated that WIRs and PCRs are spatially correlated; however, their temporal distributions are significantly different. WIRs have a broader coverage with 60.24 percent of road segments in our study site receiving more WIRs than PCRs. Moreover, by combining WIRs with PCRs, more high-risk road segments can be identified compared to the results generated from PCRs.

1.3.2. Section 3 & 4 Overview

Section 3 and Section 4 are together to investigate the implementation of mobile crowdsensing solutions for monitoring road surface conditions and detecting road surface anomalies (e.g., bumps and potholes) (Research Objective 2).

Road surface assessment (Section 3) and road anomaly detection (Section 4) are essential in road maintenance and management. Bumpy road surface and road anomalies can not only discomfort driving experience, but they also damage vehicle components, cause economic loss, even lead to car crashes. However, to date, continuously

monitoring road surface condition with a low-cost and high-efficient solution remains to be a challenging research question.

To address this question, I have proposed some crowdsensing solutions to detect road anomalies and assess road surface roughness using mobile sensed data. The results demonstrated that mobile sensors (e.g., accelerometer) could effectively capture the vehicle vibrations caused by the unevenness of the road surface. Through analyzing these mobile sensors' signals, we can successfully identify road anomalies and assess road surface roughness. However, a single user's detection result can be influenced by various factors, such as vehicle models, phone models, driving skills, etc. Therefore, I implemented crowdsensing solutions to optimize the detection results by mining public contributed data. Results demonstrate that the proposed solution can accurately distinguish road surface qualities and successfully detect road anomalies with a high positioning accuracy (within 3.29 meters in average) and an acceptable size estimation error (with a mean error of 14 cm).

1.3.3. Section 5 Overview

Section 5 details an innovative research work, in which we integrate mobile sensed data with traditional data sources to depict individualized hazardous driving senses.

Aggressive driving behaviors are significant contributors to driving risks; however, few studies have detected and integrated them into road safety analysis, especially into individual-based driving safety analysis. In this section, I proposed a novel approach to discovering the significant spatiotemporal similarities among

individual's driving errors to answer a fundamental but underexplored road safety research question: *when* and *where* drivers are prone to making driving errors?

In this research work, we integrated different types of driving-related data to depict individualized hazardous driving scenes. We first utilized mobile sensed data collected by smartphone built-in accelerometer and gyroscope to capture the "jerk energy" when performing aggressive driving behaviors. Our experiment demonstrated that different driving errors generate unique sensors' data patterns, which can be, in turn, utilized to classify the detected driving errors. Meanwhile, by integrating the mobile sensed driving errors with road networks and driving trajectories, we depicted and characterized each driving error with some carefully selected spatiotemporal factors. Through an in-depth analysis of long-term collected driving errors, we not only can help drivers to identify their hazardous driving patterns (e.g., hazardous driving time periods, most visited roads, and driving error hotspots), but more, assist drivers with recognizing their dangerous driving habits and hazardous driving scenes.

2. RETHINKING HIGHWAY SAFETY ANALYSIS BY LEVERAGING CROWDSOURCED WAZE DATA[*]

2.1. Introduction

How dangerous can traffic crash be in our life? As one of the biggest public health concerns, traffic crashes cause nearly 1.3 million fatalities worldwide every year (World Health Organization 2018). In 2016, there was more than 7 million police-reported traffic crashes in the U.S., leading to 34,439 deaths and 2.17 million traffic injuries (U.S. National Highway Traffic Safety Administration 2016). Meanwhile, roadway crashes are estimated to cost the economy as much as 277 billion dollars every year(U.S. National Highway Traffic Safety Administration 2016). Prior studies have demonstrated that traffic crashes are not randomly distributed along with roadway network. Crash frequency and severity may increase on some specific road segments (i.e., hotspots) due to various roadway, roadside, and operational characteristics of these locations. Therefore, effectively identifying crash hotspots has become essential for improving road safety, which requires immediate attention.

Police crash report (PCR) is the most commonly used data source in the existing roadway safety studies. The police-reportable crashes are characterized as the crash which occurs on a public roadway and results in a fatality, injury, or property damage exceeding certain thresholds dollar value. For example, in Texas, this threshold is USD

---

[*] Under Review by Transportation Research Record: Journal of the Transportation Research Board.

1,000. Therefore, most of the near-crashes or traffic incidents are left unreported, which may significantly limit the effectiveness of using PCRs for identifying hotspots. Moreover, these officially recorded crashes can have a several-month time lag before they become public. Although using traffic cameras and sensors can help to obtain near real-time traffic incident data, it is not suitable for monitoring traffic conditions of the whole roadway network because of the high cost of monitoring traffic cameras. To date, the assessment of road safety using traffic incident data remains to be a challenging research question.

In recent years, safety researchers and transportation agencies alike, have considered leveraging crowdsourced data in the roadway safety analysis. With the help of smartphones, a massive volume of traffic-related information can be contributed by the public, which offers us an excellent opportunity to understand the occurrence of crashes(Li and Goldberg 2018; Fire et al. 2012; T. H. Silva et al. 2013). Waze, as a leading crowdsourcing platform, collects enormous volumes of timely traffic information, which has proven tremendously helpful to the traffic engineers concerned with safety, operations, and planning (Waze 2019). By integrating PCRs with the crowdsourced Waze incident reports (WIRs), safety analysts are more likely to identify the high-risk hot spots more effectively. However, the relevant study is missing. Meanwhile, using crowdsourced data has some challenges. Different users may report on the same traffic event, which causes severe data redundancy. Therefore, effectively reducing data redundancy is crucial for utilizing Waze data, which needs to be further explored.

8

This study aims to investigate the potential of using the crowdsourced WIRs to better access traffic risks on freeways. The study attempts to address the following research questions:

1) What are the spatiotemporal distribution characteristics of WIRs and PCRs?

2) Can WIRs be used as a surrogate data source when PCRs are unavailable?

3) Can the crash hotspots be better captured by integrating WIRs and PCRs?

To address these questions, the researchers analyzed four weeks WIRs and PCRs obtained from the I-35 corridor in North Texas. The researchers collected a whole week data from four different months respectively: August, October, November, and December of 2016. First, the authors developed a new method to reduce data redundancy and obtain unique Waze incidents (unique WIRs). The researchers then matched the unique WIRs with the observed crashes and compared their spatial and temporal distributions. Besides, the researchers estimated predicted crashes through safety performance functions (SPFs) and crash modification factors (CMFs), to assess whether the WIR data can be used as a reliable surrogate of these safety measures (i.e., observed crash frequency and predicted crashes) for identifying high-risk locations.

The remainder of this section is organized as follows: in Section 2.2, the researchers conduct the Literature Review. Section 2.3 discusses Data and Methodological Approaches, including redundancy elimination and data integration methods. In Section 2.4, the researchers present the Results of data analysis. The section ends with Discussion and Conclusion.

2.2. Literature Review

Table 2.1 Summary List of Relevant Literature.

Topics	Publication	Research Purpose	Data
Comparison Between Waze Data and Other Data Sources	Goodall and Lee (2019)	Evaluate the accuracy of crash & disabled vehicle Waze reports	Traffic camera and Waze
	Amin-Naseri et al. (2018)	Compare Waze with other official and unofficial data sources to evaluate its reliability and coverage	Official and unofficial incident data sources
	Dos Santos, Davis, and Smarzaro (2016)	Compare Waze report with the official incident report and their spatial distribution.	Official incidents data
	Fire et al. (2012)	Find the correlation between the number of Waze reports and the number of police reports	Police reports and Waze
Using Waze Data in Prediction Model	Flynn, Gilmore, and Sudderth (2018)	Investigate the relationship between Waze reports and official crash report	Historical fatal crash count and traffic-related variables.
	Parnami et al. (2018)	Estimate the time of travel from point A to point B using prior Waze data.	Waze only
Waze Data Characterization and Visualization	T. H. Silva et al. (2013)	Characterize Waze data (e.g., most common report, user participation pattern, etc.)	Waze only
	Monge-Fallas et al. (2016)	Visualize the most congested routes, traffic density, and users' travel speed using Waze data.	Waze only
	Perez Espinosa et al. (2016)	Identify heavy traffic zones based on Waze using clustering method.	Waze only
	Perez et al. (2018)	Identify Waze-intense areas and road segments using a clustering method.	Waze only

To the best of the authors' knowledge, the first study using Waze data in road safety analysis was conducted by Fire et al. (2012), in which the researchers used WIR to identify high-risk road intersections. Up to now, however, the Waze-related studies are still at a preliminary stage. Only a few studies have been published, which are mainly centered around three topics (Table 2.1): a) Waze data characterization and visualization; b) Waze data quality assessment; and c) Waze data implementation in prediction models.

2.2.1. Related Work

Exploring the spatial, temporal distribution of WIRs is an essential step in Waze studies. T. H. Silva et al. (2013) analyzed 162,212 geotagged WIRs collected from Twitter, using different statistical tools such as word clouds, heatmaps, cumulative distribution functions, etc. This study demonstrated the highly unequal frequency of Waze users' participation, both spatially and temporally. More WIRs are submitted during rush hours in the urban area. Monge-Fallas et al. (2016) compared four different visualization tools for mapping traffic density using Waze. This study shows that Heatmap is the best among the four tools for visualizing WIRs in terms of usability, efficiency, and the ease of understanding. Some researchers treat the high mount of Waze reports as a reliable indicator of traffic risks. Perez et al. (2018)utilized K-means clustering to map the Waze-active areas. They performed Expectation Maximization to determine the number of clusters. These reports were further grouped based on their geolocations, timestamps, and subtypes using K-means. Finally, they identified high-risk road segments by overlapping these clusters with road networks. A similar study was

11

conducted by Perez Espinosa et al. (2016). In this study, the researchers identified heavy

traffic zones using Waze traffic reports.

Studies have been conducted to compare Waze data with other official traffic

datasets to evaluate its accuracy, response efficiency, and reliability. Goodall and Lee

(2019) assessed the accuracy of WIRs and disabled vehicle records using video ground

truth. This study utilized traffic camera videos to validate 40 Waze reported crashes.

This study has approved that Waze data is a valuable supplementary data source for

monitoring traffic incidents with a low false alarm rate of 5 percent. Thirty-three percent

of the road incidents were first reported by Waze users, which can help the police

department to make a faster response and potentially save lives. Amin-Naseri et al.

(2018) evaluated the accuracy and efficiency of Waze data by comparing it with other

three different traffic data sources. This comparison suggested that Waze is an

invaluable data source for monitoring traffic incidents with broader coverage and faster

reporting time. Meanwhile, it also states that Waze may not be reliable from midnight to

6 a.m.

Some studies have investigated the relationship between Waze reports and other

traffic events (such as official crash statistics, travel time, etc.). Flynn, Gilmore, and

Sudderth (2018) investigated the relationship between Waze reports and the PCRs. In

this study, the researchers first converted Waze data points to the aggregated Waze grids.

Then, they generated twenty spatial, temporal, and contextual features to estimate if

there is an observed PCR in a specific space-time unit using Random Forest classifier.

Parnami et al. (2018) created a low-cost traffic flow prediction model using Waze

estimated time of arrival (ETA). This study assumed that the ETA obtained from Waze

could accurately represent the actual traffic. Based on this assumption, the researchers

used Long-Short-Term-Memory (LSTM) networks to predict the traffic flow at a 5-

minute interval based on the previous 60 days of training data.

2.2.2. Knowledge Gaps and Solutions

Existing studies have proven that Waze is a reliable traffic data source for

understanding traffic risk better. However, how to eliminate the redundant WIRs is still

an unanswered question. The relationship between PCRs, WIRs, and estimated crashes

through predictive models remains underexplored. This study proposes a new procedure

to identify and eliminate duplicate WIRs. It also explores the correlations between

WIRs, police-reportable crashes, and the predicted crashes. Meanwhile, the researchers

innovatively conducted monthly hot spot analysis using different data sources to explore

further if WIRs could aid in better capturing traffic risks.

2.3. Data and Methodological Approaches

Figure 2.1 illustrates the flow chart of the research methodology used in this
study.

The researchers utilized three data sources, including PCRs, WIRs, and roadway

inventory shapefiles. The researchers first selected freeway crashes from PCRs and

WIRs, by removing frontage road, and ramp exit and entrance crashes. Then, the

duplicate WIRs were eliminated to identify unique Waze incident events (unique WIRs).

A similar process was performed to match the unique WIRs with PCRs to create a

merged dataset (PCRs + WIRs). Meanwhile, the researchers calculated the predicted

crash frequency using freeway SPFs and CMFs. Finally, the researchers created four

safety datasets: WIRs, PCRs, merged dataset, and predicted crashes.
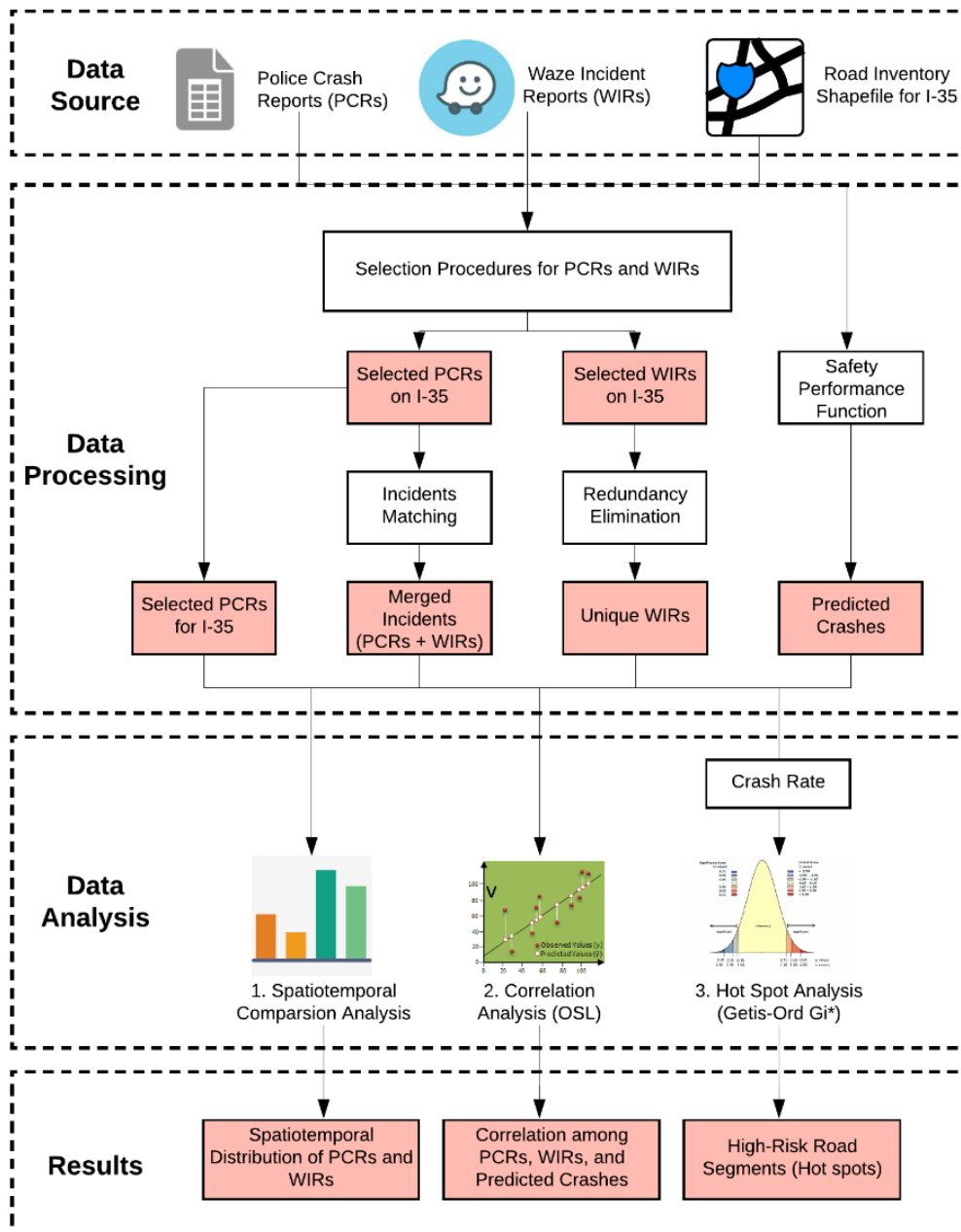
Figure 2.1 Flow chart of research methodology.

To better explore the potential of WIRs in road safety analysis, three analyses were conducted, including:

1) *Spatiotemporal comparison analysis*: characterize the spatiotemporal distributions of PCRs and WIRs.

2) *Correlation analysis*: investigate the relationship between PCRs, WIRs, and predicted crashes to test further if WIRs could be used as a surrogate safety measure when PCRs are unavailable.

3) *Hot spot analysis*:

    a. Calculate crash rates for each road segment using PCRs, unique WIRs, merged dataset, and predicted crashes respectively.

    b. Perform hot spot analysis (Getis-Ord Gi*) using different crash rates to identify high-risk road segments. This analysis aims to evaluate if WIRs could capture more traffic risks which are ignored by the conventional crash datasets (e.g., PCRs).

2.3.1. Data Overview

This section explores the data sources and elements used in this study.

2.3.1.1. Waze Incidents Reports (WIRs) Acquisition and Selection

In 2014, Waze launched a two-way data exchange program—Connected Citizens Program (CCP). Program partners can receive real-time user-reported traffic data from a customized polygon (Figure 2.2) through CCP data portal. Waze formats the crowdsourced data as an XML/JSON file. Each data file has a "traffic alerts" section, which contains user-reported traffic events. Four main types of traffic events are

specified, including accident, jam, weather hazard, and road closure. In this study, WIRs

refer to the Waze *traffic accident alerts*.
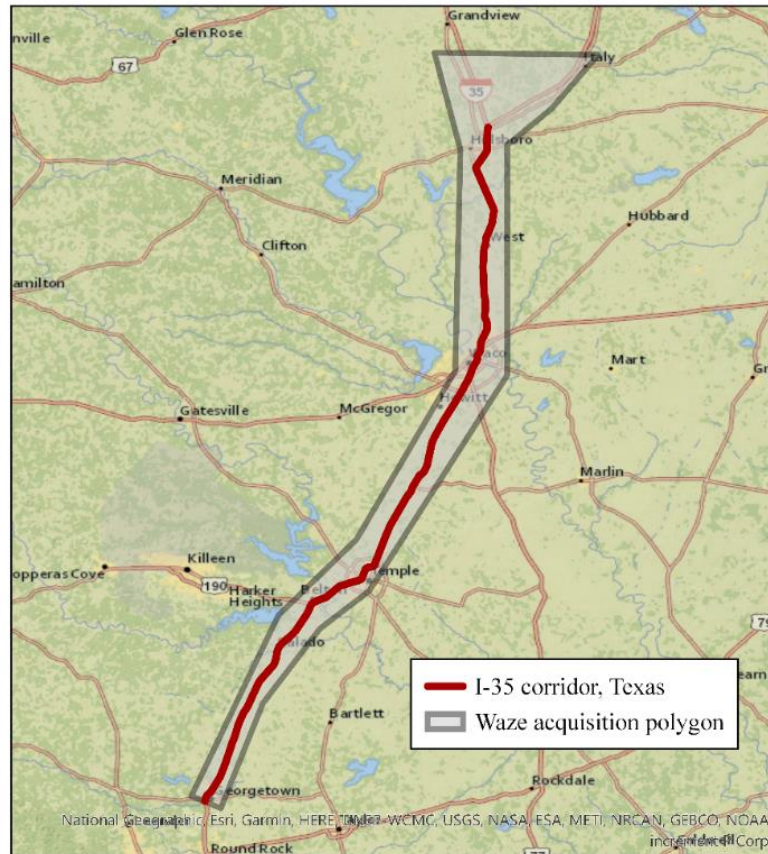
Figure 2.2 Study site and Waze reports acquisition polygon.

Waze generates a reliability score (0-10) for each reported traffic alert to indicate

how reliable the report is. Because the current CCP does not support historical Waze

data retrieval, the researchers carefully selected four weeks Waze data files from a 109

miles-long corridor on Interstate 35 (I-35) in North Texas (Figure 2.2). 2,767 WIRs were

collected from four weeks during August, October, November, December of 2016 – one

full week for each month; no holidays within the selected weeks. To extract the highly reliable WIRs, a selection procedure was implemented to filter out the unrelated and unreliable WIRs based on two criteria:

- Criteria 1: reliability score > 5 **AND** street name = I-35

- Criteria 2: reliability score > 5 **AND** road type = Freeways **AND** distance to I-35< 60 meters (~200 feet).

If a WIR could satisfy any one of the criteria, it would be counted as a reliable WIR. Through this procedure, 1,807 highly reliable WIRs were selected and then mapped to the nearest road segments identified from the roadway inventory shapefiles.

2.3.1.2. Police Crash Reports (PCRs) Acquisition and Selection

PCRs were collected from Texas Department of Transportation (TxDOT) Crash Records Information System (CRIS) (Texas DOT 2019a). Data for crashes deemed "TxDOT reportable" are characterized as the crash which occurs on a public roadway and results in a fatality, injury or a minimum of $1,000 in damage. It contains information collected in Texas Peace Officer's Crash Report (CR-3), interpreted data based on CR-3 information, system-generated data based on CR-3 information, and roadway attribute data from Texas Inventory.

First, the researchers selected the crashes, which were reported during the same period of WIRs and within 60 meters (~200 ft) of I-35. This buffer was selected based on the roadbed width of the freeway. Then, a selection procedure was applied based on the attributes of PCRs to eliminate unrelated crash reports (e.g., frontage road or ramp

crashes). After filtering, 177 freeway crashes were identified, which occurred in the

study site during the four-week study period:

- Criteria: roadway part (on which crash occurred) = main/proper lane **AND**

  roadway system = Interstate **AND** whether a crash occurred at an interaction and

  ramp = No.

2.3.1.3. Roadway Characteristics

The researchers obtained roadway design elements and traffic volumes (annual

average daily traffic-AADT) from TxDOT's Roadway Inventory shapefiles (Texas DOT

2019b). The corridor stretches for 109.956 miles and consists of 294 segments.

Descriptive statistics of roadway characteristics are detailed in Table 2.2.

Table 2.2 Descriptive Statistics of Road Inventory Data in Study Site.

Roadway Design Elements	Maximum	Minimum	Mean	Std. Dev.
Length (in miles)	4.136	0.001	0.374	0.530
AADT	132,225	56,176	73,685.068	14,747.346
Lane Width (in feet)	20	11	12.238	1.135
Inside Shoulder Width (in feet)	32	0	13.745	5.699
Outside Shoulder Width (in feet)	44	0	20.065	4.460
% of Trucks in AADT	30.3	1.2	25.260	4.089
Median Width (in feet)	50	3	28.432	9.076
Typical Segment Types (Number of Segments)	*Urban 6-lane*	*82*	*Urban 4-lane*	*58*
	Rural 6-lane	*108*	*Rural 4-lane*	*46*

2.3.2. Data Processing and Integration

This section explores the data processing and integration methods used in this

study.

2.3.2.1. WIRs Redundancy Elimination and Matching with PCRs

Since Waze users voluntarily contribute WIRs, different users may report the same incident, which generates a massive volume of redundant WIRs. Meanwhile, studies have proven that Waze can report on crashes from 20 minutes earlier to several hours later than PCRs with up to several miles positioning difference (Amin-Naseri et al. 2018). Following the recommended matching thresholds in (Amin-Naseri et al. 2018)— 2.5-mile radius (spatial unit) and two hours of time lag (temporal unit), the researchers tested different combinations of spatial and temporal thresholds for merging duplicate WIRs and matching them with PCRs:

- Spatial threshold range: from 0 – 3,500 meters (~2.5 miles) with 250 meters (~0.15 miles) increments

- Temporal threshold range: from -20 (minutes earlier than PCRs) – 120 (minutes later than PCRs) with a 10-minute increments

The researchers hypothesize that the number of matched WIRs should experience a significant increase when the increasing thresholds reach their optimal values. Hence, *t*-test was adopted to identify the significant increase to aid in determining the optimal thresholds. Please note that all the WIRs and PCRs were pre-processed through the selection procedure as mentioned above to make sure they report on the traffic information that had occurred on I-35 during the selected study period.

Unique WIRs: The duplicate WIRs can be further identified and grouped using the selected spatial and temporal thresholds, which refers to different traffic incidents. To merge the duplicate WIRs, the researchers proposed a weighting method to

recalculate the location of each unique traffic incident based on the geolocations and reliability scores of the duplicate WIRs using Equations (2.1) - (2.2), as shown below:

$$x = \frac{\sum_{i=1}^{n} x_i w_i}{\sum_{i=1}^{n} w_i} \qquad (2.1.a)$$

$$y = \frac{\sum_{i=1}^{n} y_i w_i}{\sum_{i=1}^{n} w_i} \qquad (2.1.b)$$

where, x, y are the recalculated latitude and longitude of the unique incident, i is the i-th duplicate WIRs, n is the number of duplicate WIRs reporting on the same incident, w_i is the weight signed to the i-th WIR using Equation 2.2, which depends on the generated reliability score for the i-th WIR:

$$w_i = \frac{r_i}{\sum_{i=1}^{n} r_i} \qquad (2.2)$$

Merged Dataset: After generating the unique WIRs, the same thresholds were utilized to match WIRs with PCRs. The matched WIRs were treated as redundant reports and removed. The rest of WIRs were combined with PCRs to form a new merged dataset, which covers both officially reported crashes and crowdsourced traffic incidents.

2.3.2.2. Predictive Models for Crash Frequency Estimation

To better evaluate the ability of WIRs for representing traffic risks, this study also compared WIRs with the predicted crashes calculated through the Highway Safety Manual's (HSM) predictive methods (American Association of State Highway and

Transportation Officials 2010). According to this method, the predicted crashes are

calculated as Equation 2.3:

$$N_{predicted} = N_{SPF_x} \times (CMF_{1x} \times CMF_{2x} \times \cdots CMF_{nx}) \times C_x \qquad (2.3)$$

where $N_{predicted}$ is the predicted crash frequency for a study site x, N_{SPF_x} is the

predicted crash frequency based on a given base condition using SPF for study site x,

CMF_{nx} is the n-th CMF, and C_x is the calibration factor for the jurisdiction of study site

x.

In this study, the researchers used four SPFs developed by Bonneson and Pratt

(2009) to estimate the base condition highway crashes on four facility types in Texas:

urban four-lane freeways, rural four-lane freeways, urban six-lane freeways, and rural

six-lane freeways. The researchers then used five CMFs to estimate the predicted

crashes: lane width, outside shoulder width, inside shoulder width, median width (no

barrier), and truck presence. Refer to (Bonneson and Pratt 2009) for a detailed

explanation of how to calculate SPFs and CMFs. As mentioned above, this study focuses

on freeway crashes. Therefore, all the frontage and ramp entrance and exit SPFs and

CMFs were excluded.

2.3.3. Data Analysis Methods

This study conducted three types of data analyses to evaluate the performance of

using WIRs in highway safety analysis. The researchers first performed spatiotemporal

comparison analysis between PCRs and unique WIRs to assess the coverage of WIRs.

Then, the researchers investigated the relationship between PCRs, unique WIRs, and

predicted crashes to further explore if WIRs could be used as a surrogate data source

when PCRs are unavailable. Last, high-risk road segments were identified by performing hot spot analysis (Getis-Ord Gi*) on the crash rates of road segments. In this study, four crash rates were calculated for each road segment based on different data sources, including PCRs, unique WIRs, merged dataset, and predicted crashes.

2.3.3.1. Crash Rate Calculation

Crash risk is commonly defined as "the number of crashes compared to the level of exposure," which can better represent the likelihood of crash occurrence for a road segment (The U.S. National Highway Safety Administration 2019). In this study, crash rate was calculated to indicate the "Risk-Level" of road segments. Equation 2.4 was adapted from (The U.S. National Highway Safety Administration 2019) with:

$$R = \frac{C \times 100,000,000}{T \times V \times L} \tag{2.4}$$

where R represents the crash rate of a road segment defined as "crashes per 100 million vehicle-miles of driving"; C is the number of crashes occurred along a road segment; T depicts time span (number of days); V is Average Annual Daily Traffic (AADT) volumes; and L is road segment length in miles.

In this study, four data sources including PCRs, unique WIRs, WIR-PCR, and predicted crashes were used to calculate different crash rates for each road segment.

2.3.3.2. Hot Spot Analysis (Getis-Ord Gi*)

The Getis-Ord Gi* statistic has been widely adopted to identify the significant spatial clusters of high values (hot spots) and low values (cold spots) (Songchitruksa and Zeng 2010; Esri 2016). It examines each sample within the context of its neighboring samples. The Gi* statistic is calculated using Equations (2.5) – (2.7) (Esri 2016):

$$G_i^* = \frac{\sum_{j=1}^{n} w_{i,j} x_j - \bar{X} \sum_{j=1}^{n} w_{i,j}}{S \sqrt{\frac{\left[n \sum_{j=1}^{n} w_{i,j}^2 - \left(\sum_{j=1}^{n} w_{i,j} \right)^2 \right]}{n-1}}}$$ (2.5)

where,

$$\bar{X} = \frac{\sum_{j=1}^{n} x_j}{n}$$ (2.6)

$$S = \sqrt{\frac{\sum_{j=1}^{n} x_j^2}{n} - (\bar{X})^2}$$ (2.7)

n represents the number of samples, x_j is the value of j-th sample, and $w_{i,j}$ indicates the spatial weight between two samples (i, j).

Gi * statistic generates a *z*-score and *p*-value for each feature. The statistically significant positive *z*-scores indicate hot spots—clusters of high values, the negative *z*-scores refers to cold spots—clusters of low values. In this study, Gi* statistic was performed to identify hot spots of high-risk road segments—statistically significant clusters of high crash rates. By comparing the hot spots generated from different data sources, the researchers could further examine whether the WIRs could aid in better representing traffic risks.

2.4. Results

This section covers the redundancy elimination result of WIRs, the merged dataset by matching WIRs with PCRs. It details the results of three analyses, including spatiotemporal comparison analysis, correlation analysis, and hot spot analysis.

2.4.1. Result for WIRs Redundancy Elimination and Matching with PCRs

The researcher used the "true" incident, i.e., the PCR as the starting point and tested different combinations of spatial and temporal thresholds to a) remove the redundant WIRs that correspond to the same PCR; and b) match unique WIRs with the PCRs. The researchers hypothesize that when spatial and temporal "distances" from the true incident (i.e., PCR) to the surrogate incident (i.e., WIR) reach their optimal value, the number of matched WIRs should experience a significant increase since more redundant WIRs can be captured. After the optimal threshold is attained, the number of matched WIRs should not be significantly different than the optimal number of matched WIRs.
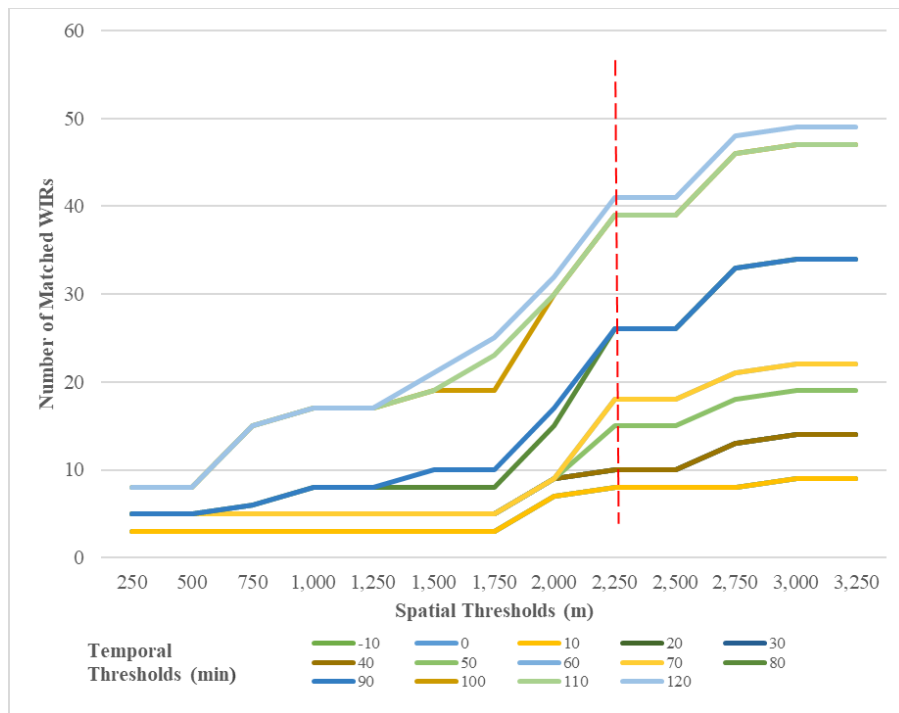
Figure 2.3 Number of matched WIRs when using different spatial and temporal thresholds.

Figure 2.3 illustrates the number of WIRs that are matched with PCRs when using each combination of spatial and temporal thresholds. As can be observed, regardless of the time interval, the number of unique WIRs are increasing consistently until the distance from the true incident (i.e., PCR) reaches 2,250 meters (~1.4 miles). After this distance, the number of WIRs matched with the PCR become steady. A new jump is observed at 2,500 meters, although it does not seem to be very significant. It is possible that this "second" jump in number of unique WIRs matching with the PCR refer to a secondary event that was related to the primary event. However, this hypothesis cannot be verified because, as indicated earlier, non-PDO traffic incidents are not reported by police. Hence, the researchers selected the 2,250 (or 1.4 miles) as the spatial threshold for identifying the redundant WIRs.

To determine the best temporal threshold, the researchers used t-test to check the significant difference in the number of matched WIRs for different time intervals. Studies have found that Waze can report a crash from 20 minutes earlier to several hours later than the police-reported crash time (Amin-Naseri et al. 2018). Therefore, the researchers tested different temporal intervals to match WIRs with PCRs. These temporal intervals have the same start-timestamp (-20 minutes earlier than PCRs) and a different end-timestamp. The temporal thresholds t in Figure 2.3 represents the end-timestamps for each temporal matching interval. For example, $t = 10$ represents a 30-minute temporal matching interval—from 20 minutes earlier to 10 minutes later than PCR occurred. The researchers tested different temporal thresholds ranging from -10

minutes (i.e., 10 minutes earlier than PCRs) to 120 minutes (i.e., two hours after the

PCR) in 10-minute increments.

Figure 2.3 shows that the number of WIRs matched with a PCR remains the

same when temporal threshold increases from -10 to 10, hence they are used as a

baseline dataset (BD) to compare to the number of matched WIRs reported at higher

time intervals. This dataset is denoted as BD = $[N_{WIR,-10}, N_{WIR,0}, N_{WIR,10}]$, where

$N_{WIR,t}$ refers to the number of WIRs matched with the PCR with a temporal matching

interval, $t = -10$ (from 20 minutes earlier to ten minutes earlier), $t = 0$ (from the 20

minute earlier to the same time as the PCR) and $t = 10$ (from the 20 minute earlier to 10

minutes later than the PCR). The comparison datasets (CD$_r$) were then generated by

adding 10-minute intervals to the baseline dataset and compared with BD using *t-test* to

identify the significant difference between the number of baseline and comparison

WIRs. For example, CD$_{30}$ refers to: $[N_{WIR,-10}, N_{WIR,0}, N_{WIR,10}, N_{WIR,20}, N_{WIR,30}]$).

Table 2.3 T-Test Results Between Base Dataset and Comparison Datasets.

Goodness of Fit Statistics	CD$_{20}$	CD$_{30}$	CD$_{40}$	CD$_{50}$	CD$_{60}$	CD$_{70}$
t Stat	-1	-1.63299	-2.23607	-1.98248	-2.2088	-2.6295
P(T<=t) one-tail	0.195501	0.088904	0.037793	0.047349	0.031454	0.015101
t Critical one-tail	2.353363	2.131847	2.015048	1.94318	1.894579	1.859548
P(T<=t) two-tail	0.391002	0.177808	0.075587	0.094698	0.062909	0.030201
t Critical two-tail	3.182446	2.776445	2.570582	2.446912	2.364624	2.306004

The results of t-test (Table 2.3) show that after 70 minutes, the number of matched WIRs was observed to be significantly different than the previous results.

As the results of these analyses, the researchers determined the optimal spatial and temporal thresholds for identifying the redundant WIRs as:

- Spatial threshold: in a 2,250-meter radius.

- Temporal thresholds: 90 minutes, (-20 to 70 minutes).

By applying these thresholds, 1,807 WIRs were finally consolidated into 381 unique WIRs. The location for each unique WIRs was recalculated using the proposed weighting method (Equations 2.1- 2.2).

A similar process was conducted to match unique WIRs with PCRs. In this study, only 13 out of 177 PCRs (7.34%) were matched with the unique WIRs (13 out of 381). These results align with prior studies that found 7 to 13.4 percent of reported crashes can be matched with the Waze reports (Amin-Naseri et al. 2018; Dos Santos, Davis, and Smarzaro 2016).

Finally, the researchers created a merged database by combining PCRs with un-matched unique WIRs. This dataset contains 545 traffic incidents and crashes.

2.4.2. Spatiotemporal Comparison Analysis

The spatiotemporal distribution of PCRs and unique WIRs are plotted in Figure 2.4. Figure 2.4 (a) and Figure 2.4 (b) represent the counts of PCRs and unique WIRs for each road segment. These two figures show a similar spatial data pattern, which implies that crash-intense road segments can potentially be captured using WIRs. Figure 2.4 (c) shows the differences between PCRs and WIRs. Among 109.96 miles of roadway

segments in this study, 66.24 miles road segments experienced more WIRs than PCRs, which means that WIRs have broader spatial coverage than PCRs.

The temporal distribution of WIRs and PCRs are depicted in Figure 2.4 (d) and Figure 2.4 (e). These figures show that PCRs tend to occur during the daytime, while WIRs were more intensively reported at nighttime. However, the previous studies state that Waze is less reported during the midnight period, which conflicts with the researchers' finding (Amin-Naseri et al. 2018). This finding implies that the temporal pattern of WIRs may vary in different study areas.

Figure 2.4 (f) shows the hourly comparison result, which indicates that more PCRs are recorded than WIRs from 8:00 to 14:00. From 18:00 to 5:00, more Waze reports incidents observed than officially reported crashes.

2.4.3. Correlation Analysis

This study investigated the relationship between PCRs, unique WIRs, and the estimated crashes through predictive models to statistically test if WIRs could be used as a surrogate data source or safety measures in absence of crash data. The correlation among these three datasets are detailed in Figure 2.5. This figure illustrates that PCRs are highly correlated with WIRs (0.63) than with predicted crashes (0.57). It also suggests that WIRs can better represent the predicted safety risk than PCRs (0.70 vs. 0.57).
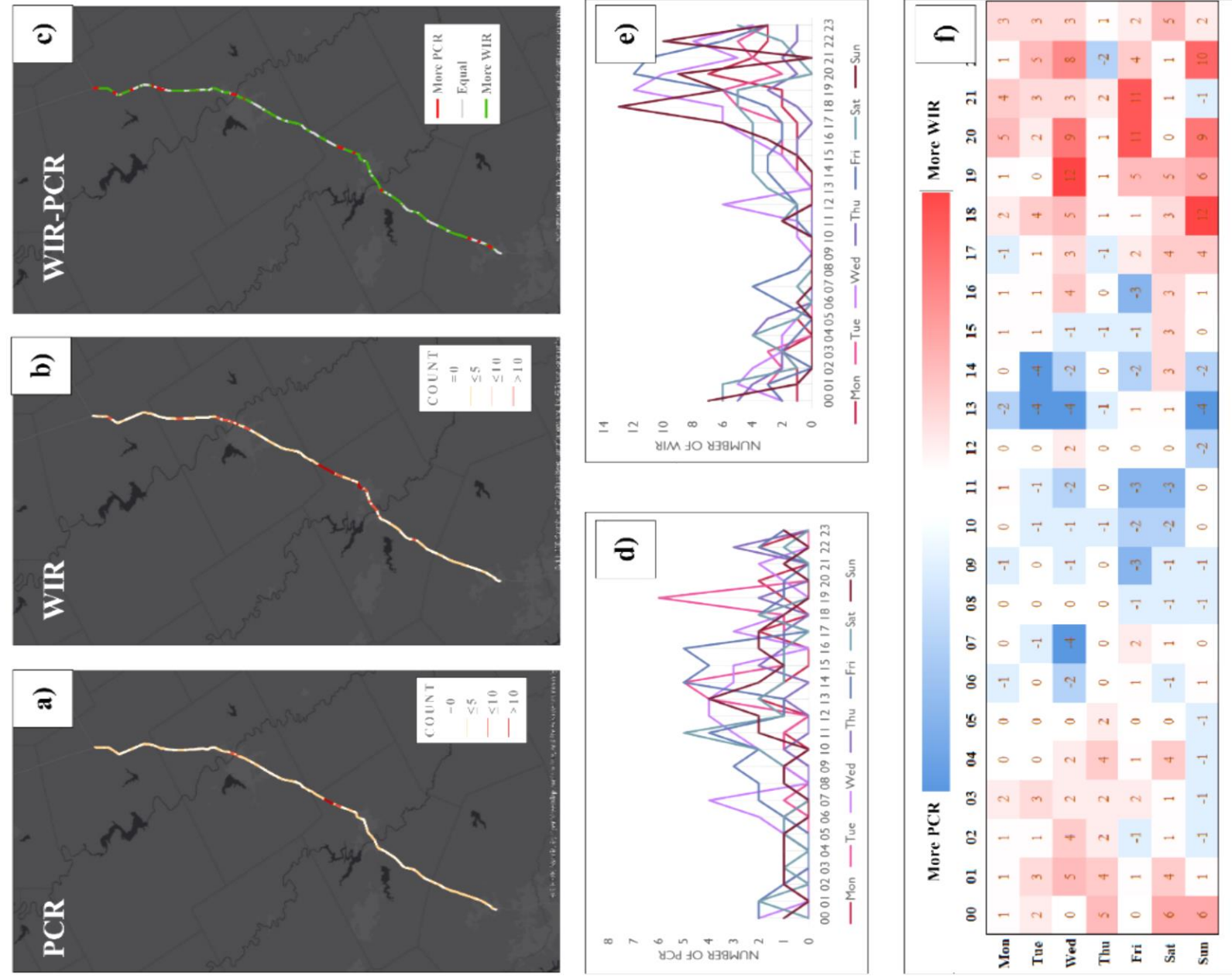
Figure 2.4 Spatiotemporal comparison between PCRs and unique WIRs. a) spatial distribution of PCRs. b) spatial distribution of unique WIRs. c) spatial comparison between PCRs and unique WIRs. d) hourly distribution of PCRs. e) hourly distribution of unique WIRs. f) hourly comparison between PCRs and unique WIRs.
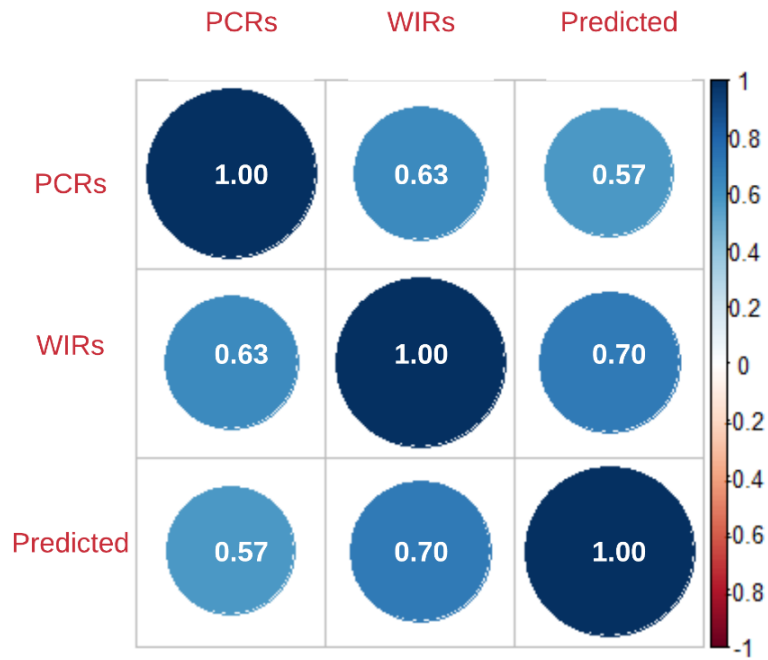
Figure 2.5 Correlations among PCRs, unique WIRs, and predicted crashes.

The researchers also developed Ordinary Least Square (OLS) regression model to further investigate the relationship between the three safety measures: PCR, WIR and predicted crashes. Two regression models were constructed. One uses unique WIRs alone as independent variable (Equation 2.8), another uses both WIRs and predicted crashes as independent variables (Equation 2.9). The estimation results are shown in Table 3.4 and have the following functional forms:

$$N_{PCR} = 0.144 + 0.354 \times N_{WIR} \qquad (2.8)$$

$$N_{PCR} = 0.30 + 0.255 \times N_{WIR} + 0.123 \times N_{Predicted} \qquad (2.9)$$

where N_{PCR} is the calculated number of PCRs for a road segment, N_{WIR} is the number of

unique WIRs, and $N_{Predicted}$ is the predicted number of crashes using SPFs and CMFs.

Table 2.4 Liner Regression Results for PCRs.

Model Parameters	Model 1	Model 2
	Estimate (St. D.)	Estimate (St. D.)
Intercept	0.144 (0.069)	0.030 (0.072)
Unique WIRs	0.354*** (0.025)	0.255*** (0.035)
Predicted Crashes		0.123*** (0.031)
R-squared	0.402	0.434
Adjusted R-squared	0.400	0.430
No. observations	294	
Standard errors are included in parenthesis.		
*, **, *** represents significance at 90%, 95%, and 99% level based on p-value.		

The regression results indicate that the number of unique WIRs is a significant

predictor for estimating crashes reported on each road segments. When taking both

unique WIRs and predicted crashes as predictors, the performance of the model can be

slightly improved with R-squared increased from 0.4 to 0.43.

2.4.4. Hot Spot Analysis

This study also assessed the performance of WIRs for identifying high-risk road

segments. The researchers first calculated crash rates for each road segment using four

different data sources, including PCRs, unique WIRs, merged dataset, and predicted

crashes. Then, Getis-Ord Gi* statistics were conducted based on different crash rates respectively to identify hot spots—high-valued road segments surrounded by high-valued neighboring segments. Figure 2.6 illustrates the sample result of detected hot spots, which were generated using one-week unique WIRs collected from December 2016.
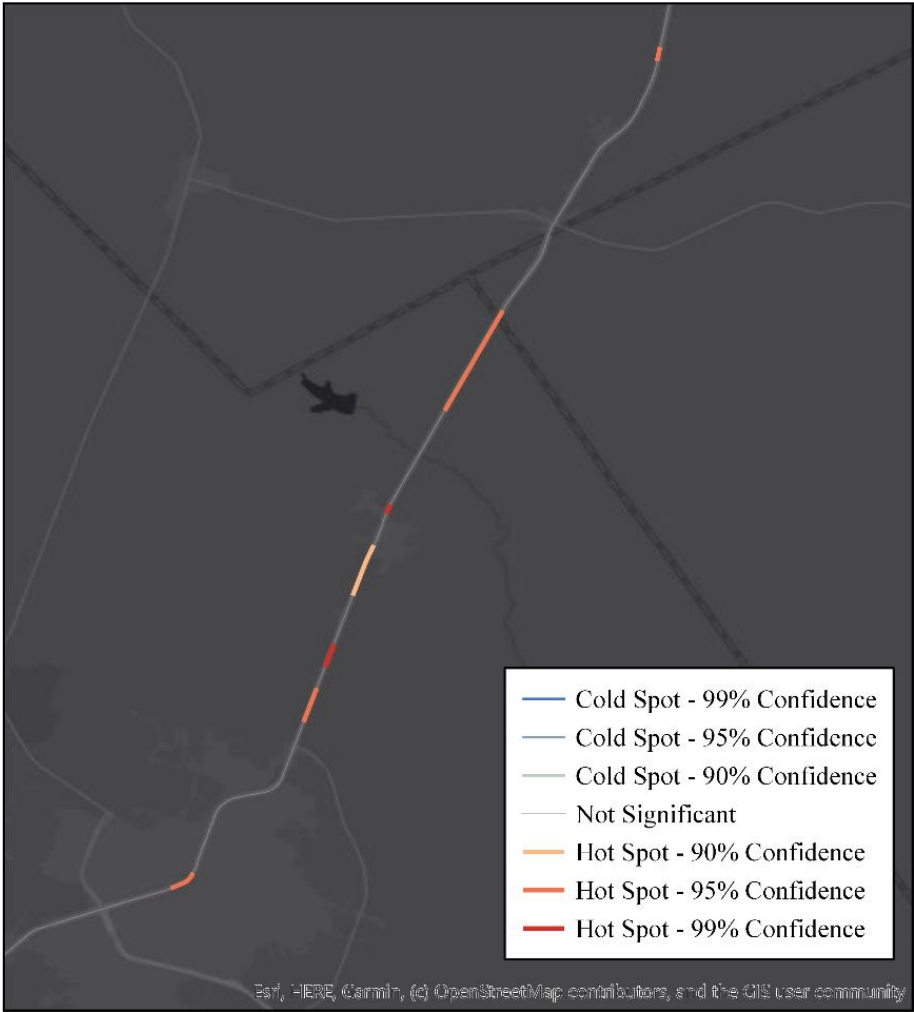
Figure 2.6 Sample results of detected hot spots.

This study compared hot spots detected from different data sources in different months to investigate if the distribution of hot spots varies from month to month. The researchers also examined the monthly results with the hot spots detected from four-month datasets to identify constant hot spots. This study defines *constant hot spots* as a segment, or its neighboring segments (within ± 1mile) that 1) are determined as hot spots in more than two different months and 2) also need to be identified as hot spots in the four-month dataset.

Table 2.5 Hot-Spot Detection and Comparison Results.

Datasets	August	October	November	December	Four-month
PCRs	266, 278, 318, 323, 334, 337, 341, 350, 352, 354, 355, 357, 363	266, 276, 298, 299, 303, 306, 308, 310, 317, 327, 351, 356, 358, 368	291, 292, 303, 306, 308, 318, 333, 334, 343, 351, 353, 358, 363, 367	266, 288, 303, 306, 317, 332, 334, 342	266, **298**, **303**, **317**, **334**, 342, **358**, **363**
WIRs	294, 318, 319, 356, 363, 364	298, 299, 303, 305, 307, 308, 310, 315, 319, 344, 350, 356, 357, 366, 368	291, 303, 315, 318, 336, 344, 357, 363, 368	291, 299, 303, 305, 306, 308, 310, 318, 327, 332, 350, 359	**284**, **294**, **303**, 307, **315**, **317**, 319, 344, **356**, **357**, **363**, **364**, **368**
Merged dataset (WIR-PCR)	264, 266, *294*, 318, 319, 337, 352, 354, 355, 356, 363, 364, 366, 367	248, 298, 299, 303, 307, 308, 310, 315, 317, 319, 336, 351, 356, 357, 358, 366, 368	291, 292, 303, 315, 317, 318, 334, 344, 358, 363, 368	266, 291, 305, 308, 327, 332, 342, 334, 350, 359,	**284**, **294**, **298**, **303**, **315**, **317**, **334**, **336**, **356**, **357**, **358**, **363**, **364**, **368**
Predicted Crashes (2016)	**317, 363, 293, 317, 385**				
- Numbers represent DFOs for road segments. - Underscore represents constant hot spots. **Bold text** indicates hot spots matched with merged dataset hot spots.					

Table 2.5 details the results of hot-spot detection using PCR, WIR, merged dataset and predicted crashes. The numbers listed in this table represent the integer part of distance from origin (DFO) for the detected high-risk road segments, which are easier for locating the identified hot spots. In this study, if any portion of a one-mile-segment was recognized as a hot spot, the researchers would count the entire one-mile-segment as high-risk road segment. Constant hot spots are highlighted with underscores. The matched segments are marked with bold text.

This table shows that the hot spots may vary in different months; however, there are still some constant hot spots which may be considered as true high-risk segments. By combing PCRs with WIRs, more high-risk road segments can be detected, which could cover the results generated from PCRs, unique WIRs, and predicted crashes.

2.5. Discussion and Conclusion

As an emerging data source, Waze shows excellent potential to capture a broad range of unreported traffic risks. However, current Waze-related studies are still at a preliminary stage. How to better leverage Waze into road safety analysis is still an unanswered research question. This study is among the first to systemically evaluate the performance of Waze incident reports (WIRs) for capturing unreported near-crashes and traffic incidents. The researchers first proposed a new procedure to eliminate duplicate WIRs to extract unique WIRs. Meanwhile, these unique WIRs were further matched with police crash reports (PCRs) to form a new merged dataset, which covers both officially reported crashes, and crowdsourced incidents. This study also calculated the crash frequency of road segments based on the road inventory shapefile using the HSM

predictive methods. Three analyses were conducted to comprehensively assess the effectiveness of WIRs in road safety analysis. Through this study, the researchers finally answered the following three essential but underexplored research questions.

Question 1: What are the spatiotemporal distribution characteristics of WIRs and PCRs?

Through the spatiotemporal comparison of PCRs and WIRs, the researchers found these two data sources shows a very similar spatial distribution. However, the temporal comparison shows a significant difference between them. In this study, PCRs were reported during daytime, while. WIRs were more intensively reported during nighttime. It is also worth noting that 60.24 percent of the road segments in the study site received more WIRs than PCRs. 27.1 percent received the same amount of WIRs and PCRs. It implies that unreported traffic incidents more intensively occurred on most of the road segments. These traffic incidents should be considered into road safety studies.

Question 2: Can WIRs be used as a surrogate data source when PCRs are unavailable?

By matching WIRs with PCRs, the researchers found that only 7.34 percent of the PCRs can be paired with WIRs, which aligns with prior studies—13.4 percent (Amin-Naseri et al. 2018) and 7 percent (Dos Santos, Davis, and Smarzaro 2016). Therefore, it can be concluded that WIRs and PCRs report on different traffic risks. Correlation analysis shows that PCRs are highly correlated with WIRs (0.63) than with predicted crashes (0.57). It also indicates that WIRs can better represent the predicted traffic risk than PCRs (0.70 vs. 0.57). The regression models suggest that both WIRs and

predicted crashes are significant predictors for estimating PCRs. However, using WIRs

alone may not be capable enough, since the model performance is relatively unsatisfying

with an R-squared of 0.4. Meanwhile, the similar spatial distributions of WIRs and PRCs

suggest that Waze data might be able to identify crash-intense road segments when

PCRs are unavailable. This finding has very significant implications for highway safety

researchers and practitioners. It indicates that WIRs could be potentially used as a

surrogate safety measure in absence of crash data (e.g., when evaluating the safety

effectiveness of new safety treatments). However, further research is required in order

to confirm this very important finding.

**Question 3: Can the crash hotspots be better captured by integrating WIRs
and PCRs?**

By comparing the hot spots generated from different months, the researchers

found the detected high-risk road segments may vary in different months. However, it is

worth noting that some hot spots can be persistent in different months, which are

constant high-risk segments and should be given more attention. This study has found

that, by combining WIRs with PCRs, more high-risk road segments can be identified (14

miles) comparing to the results generated from PCRs (8 miles), unique WIRs (13 miles),

and predicted crashes (5 miles). Most of the hot spots detected from PCRs (75%), unique

WIRs (77%), and predicted crashes (100%) could be identified from the merged data.

Therefore, it can be concluded that integrating WIRs and PCRs can better capture traffic

risks and discover more unidentified high-risk road segments.

This study shows that overall Waze is an invaluable source of data for safety researchers, which is tremendously useful for capturing unreported traffic incidents. However, there are still some gaps that were not adequately addressed by this study. Although the findings are promising, the researchers used Waze data only from an interstate corridor, which is generally assumed to experience more Waze reports. This gap may also affect some of the findings; for example, temporal and spatial threshold for consolidating the WIRs and matching them with PCRs may not be applicable to other facility types. The future research will focus on these areas.

3. TOWARD A MOBILE CROWDSENSING SYSTEM FOR ROAD SURFACE ASSESSMENT[*]

3.1. Introduction

Road surface roughness has been assessed as a significant factor in road maintenance, management, and construction. Road surface transient events, such as potholes and bumps, not only impact road quality but also affect driver safety, fuel consumption and road maintenance (Beuving et al. 2004; Vittorio et al. 2014). The World Bank has identified road roughness as a primary factor in the analysis of road quality vs. user cost. Many studies have demonstrated that the improvement of road surface conditions could directly promote fuel efficiency as well as driving safety (Beuving et al. 2004; Vittorio et al. 2014).

Studies have been carried out on the road surface roughness assessment since the 1950s. Several approaches, which require the use of costly and sophisticated vehicular instruments have been proposed and widely accepted, such as using laser profilometers to calculate the international roughness index (Paterson and Attoh-Okine 1992; Watanatada et al. 1987), computing deflection basin parameters by deflectometers (Kim 2001; B. Xu, Ranjithan, and Kim 2002) or using ground penetrating radar to determine the conditions of the roads(Cao, Labuz, and Guzina 2011). However, these traditional

assessment methods are labor-intensive and time-consuming requiring professional knowledge and high-end instrumentation. Most local governments and small municipalities cannot afford the high cost of these methods with a limited budget.

New detection methods have been proposed over the past few years, which can achieve a higher road revisiting rate and lower equipment cost (Allouch et al. 2017; Astarita et al. 2012; Bhoraskar et al. 2012; Eriksson et al. 2008; Macias, Suarez, and Lloret 2013). These methods are used to monitor the ever-changing road surfaces by extracting the road surface anomalies and their corresponding locations. With various sensor technologies and the powerful computing capabilities, the use of smartphone sensing in research is proliferating. Smartphones equipped with a number of built-in sensors can be used to support various customized applications, which have been identified as promising platforms and can be used for mobile geospatial computing (R. Chen and Guinness 2014). Built-in smartphone accelerometers have been utilized to detect ground vehicle jitters caused by the non-flatness of the road surface (Bhoraskar et al. 2012; R. Chen and Guinness 2014). More importantly, by combining the accelerometer and GPS data obtained from a smartphone, the road roughness can be automatically geo-referenced (Aleadelat et al. 2017; Astarita et al. 2012; Das et al. 2010; Eriksson et al. 2008; Perttunen et al. 2011).

3.1.1. Related Work

Threshold techniques have been broadly used to extract road surface transient events. A real-time pothole detection system was designed by Mednis et al. (2011). Four different transient events detection techniques were compared in this study. The system

is designed mainly based on threshold technique. The overall accuracy can reach 90%. Harikrishnan and Gopi (2017) applied Gaussian Model on the Z-axis readings of built-in smartphone accelerometer for detecting and classifying bumps and potholes. The research hypothesis is that the Z-axis acceleration should fit on a Gaussian distribution. In this study, the vehicle vibration data was collected from a horizontally fixed smartphone and segmented into groups. A newly designed Max-Abs filter was applied on the segmented data for minimizing the small acceleration spikes and highlighting the abnormal events. Threshold technique was applied to classify the abnormal events as potholes and bumps. The accuracy of detection and classification of this method can up to be 100%.

Several studies investigated the relationship between road surface roughness and accelerometer readings. Amador-Jiménez and Matout (2014) have proposed a low-cost solution for road surface evaluation using tablets' built-in accelerometer. In this study, the Root Mean Square (RMS) of the Z-axis acceleration normalized by vehicle speed was confirmed as a proxy for the International Roughness Index (IRI), which can be used to examine the road quality. Aleadelat and Ksaibati (2017) tested the relationship between the Z-axis acceleration and the present serviceability index (PSI). PSI is a widely used index for assessing pavement condition. In this study, two smartphones were horizontally fixed on the vehicle's dashboard. An Android app "AndroSensor" was used for data collection at two driving speeds: 40 mph and 50 mph. The result demonstrates that the Z-axis acceleration has a strong linear relationship with PSI.

Many different machine learning methods have also been employed for assessing road surface condition. Eriksson et al. (2008) proposed a signal processing and machine learning based approach to extract potholes from the readings of external GPS and accelerometer. 7 taxis were used in the test for data collection. Sensors were fixed at different positions inside the vehicle. The result demonstrated the pothole and other transient events can be effectively identified by the proposed method. Perttunen et al. (2011) proposed a solution to extract road surface anomalies (e.g. pothole, bumps) from acceleration data and GPS readings. Kalman filter was implemented to reduce the noise of GPS signal. A spectral analysis was performed on the acceleration signal to extract road features. Support Vector Machine (SVM) was used to predict three categories of transient events (i.e., speed bump, bump, and large pothole). Bhoraskar et al. (2012) designed a traffic monitoring system, which uses the detected braking events and vertical acceleration peaks to estimate the traffic congestion and examine potholes. To translate the acceleration from the frame of the portable device to the frame of the vehicle, a 3-axis accelerometers re-orientation was carried out in the system. SVM and K-means Clustering were implemented to predict road surface condition (identified as "bumpy road" or "smooth road") and optimize the assessment result of each road segment. Singh, Bansal, and Sofat (2017) proposed a new method to detect bumps and potholes using smartphone sensors. An Android app "Smart-Patrolling" was created and employed for data collection. Five filters (Speed, Virtual Re-Orientation, Filtering Z-axis, SMA and Band-Pass filter) and Dynamic Time Warping (DTM) techniques are applied. In this study, smartphones were fixed inside the vehicle at different places including front

dashboard pilot, font dashboard co-pilot, and back seat. The ground truth (unique patterns of accelerometer readings corresponding to these bumps and potholes) was collected during training phase and used as the template references. The accuracy of this method for detecting potholes and bumps is 88.66% and 88.89%. Allouch et al. (2017) implemented a machine learning method to estimate road surface condition. An Android app "Road Data Collector" is created for data. In the training phase, the real road quality was manually labeled as "Smooth" or "Potholed" using designed smartphone app. Different road segments' features were extracted from the readings of accelerometer and gyroscope. Correlation-based Feature Selection (CFS) approach was applied to the training dataset to optimize the feature selection. Three different machine learning methods (C4.5 Decision Tree, Support Vector Machines, and Naïve Bayes) were tested in this study. The result demonstrated that C4.5 classifier has the best performance with an overall accuracy of 98.6%.

Utilizing a crowdsensing method to obtain road surface roughness data would be exceptionally beneficial, as it would allow the data to be frequently updated, resulting in more accurate result, and would involve a minimal cost for local governments. Some researchers have tried to design a crowdsensing system, which can continuously monitor the changes of road surface condition. K. Chen et al. (2014) designed a system called CRSM, which has the potential to detect the potholes and assess the road surface quality effectively. This approach takes advantages of the crowd sensed data by utilizing specialized hardware modules (low-cost GPS receiver and accelerometer) mounted on the vehicles. A lightweight data mining approach was employed in this system with 100

taxis recruited for data collection. The accuracy of this system is about 90%. Lima et al. (2017) proposed a simple lightweight smartphone-based approach, which can recognize road quality as "Good", "Normal", "Bad", and "Terrible". This study makes use of threshold technique with a bunch of thresholds are set through the empirical tests to recognize road quality. This study performed a crowdsourcing solution. Crowd sensed results were simply averaged and then mapped using GoogleMaps API.

A comparison of existing methods is detailed in Table 3.1, which reflects the following problems that need to be addressed:

1) The repeatability of threshold-based methods is limited. Thresholds need to be adjusted and retested when applied under different conditions;

2) Machine learning methods require an extensive training phase, which is time-consuming and not suitable for the crowdsensing system;

3) Most studies just focus on the transient events detection. A comprehensive road surface assessment is lacking;

4) Very few studies utilize crowdsensing approaches, which just simply averages the crowd sensed data. An improved crowdsensing solution for assessing road surface condition need to be further explored.

Table 3.1 Comparison of Existing Methods.

	Method	Smartphone Sensors	Roughness Assessment	Pothole &Bump Detection	Crowd-sensing	Accuracy
(Mednis et al., 2011)	Threshold (Z-Thresh, Z-Diff, STDEV, G-Zero)	Accelerometer, GPS	No	Yes	No	TP = 90% (Pothole)
(Harikrishnan & Gopi, 2017)	Threshold, Gaussian Model, & A newly designed Max-Abs filter	Accelerometer, GPS	No	Yes	NO	TP = 100% (Pothole)
(Amador-Jiménez & Matout, 2014)	Threshold	Tablet Accelerometer **(Not phone sensors)**	Predict IRI using Z-axis Acceleration	No	No	Produce a repeatable indicator of road condition
(Aleadelat & Ksaibati, 2017)	Exponential Transformation & Simple Linear Model	Accelerometer	Predict PSI using Z-axis Acceleration	No	No	Z-acceleration has a strong liner relationship with and can be used to predict PSI
(Eriksson et al., 2008)	Signal processing and machining learning-based approach	External GPS, Accelerometer **(Not phone sensors)**	No	Yes	No	FP < 0.2% (Pothole)
(Perttunen et al., 2011)	Spectral Analysis & SVM	Accelerometer, GPS	No	Yes	No	FPR = 3% FNR = 18% (Potholes)
(Bhoraskar et al., 2012)	K-means Clustering & SVM	Accelerometer, GPS, Magnetometer	"Smooth" Or "Bumpy"	Yes	No	FPR = 0% FNR = 10% (Potholes)
(Singh et al., 2017)	DTM	Accelerometer, GPS	No	Yes	No	TP (Pothole, Bump) = 88.66%, 88.89%.
(Allouch et al., 2017)	Machine Learning (C4.5 Decision Tree, SVM, and Naïve Bayes)	Accelerometer, Gyroscope	"Smooth" or "Potholed"	Yes	No	Accuracy = 98.6% (Pothole)
(Chen et al. 2013)	Improved Gaussian Mixture Model; Threshold	Hardware modules **(Not phone sensors)**	"Good", "Fair", "Poor", "Bad"	Yes	Average Crowd Sensed Results	Accuracy = 90% (Pothole); Can evaluate road roughness levels correctly
(Lima et al., 2016)	Threshold	Accelerometer, GPS	"Good", "Normal", "Bad", "Terrible"	Yes	Average Crowd Sensed Results	Not reported

3.1.2. Key Contributions

This study presents a preliminary mobile crowdsensing system for road surface roughness detection, which includes a mobile data-collecting component and a web-based data server component. It takes advantages of previous studies but differs in following three aspects: 1) **a detailed crowdsensing solution**: An iOS app *Crowdsense* and an Android app *AndroSensor* are utilized in this study for data collection. This study provides a detailed result optimization by integrating crowd sensed data; 2) **with comprehensive road condition assessment**: Instead of just focusing on the pothole or bump detection, a more comprehensive assessment of road conditions is introduced including an overall road condition estimation, IRI-proxy calculation, and transient events (bumps/potholes) detection; 3) **a cloud-based data server**: A low-cost, lightweight, cloud-based system framework, which takes advantages of free Google services, is developed in the study. Google Fusion Table is tested and innovatively applied in the model for data visualization.

To verify the proposed solution, a preliminary model for crowdsensing road surface roughness is created, and a detailed experiment is designed and conducted in the city of College Station, Texas.

3.2. Methodology

This section discusses the research methodologies. First, the system architecture is introduced. The strategy of the proposed road surface assessment is elaborated upon. A detailed explanation of the mathematical algorithm, which is used for evaluating road

surface conditions and computing two assessment indexes, is also given in this section. The rest of this section covers the result optimization, visualization, and publication.

3.2.1. System Architecture

In this study, a crowdsensing approach was employed to assess road surface conditions. The whole system mainly includes two components: a mobile data-collecting component and a web-based data server component as shown in Figure 3.1. The mobile data-collecting component requires a user to run the mobile application *AndroSensor* in an Android smartphone or the mobile application *Crowdsense* in an iOS smartphone. Smartphones are used to collect the raw data in real-time including the GPS positions and the raw measurements of the accelerometer and upload the road surface conditions to a cloud-based data server. The server periodically processes the road roughness information contributed from different crowdsourcers and integrates the detection results accordingly.
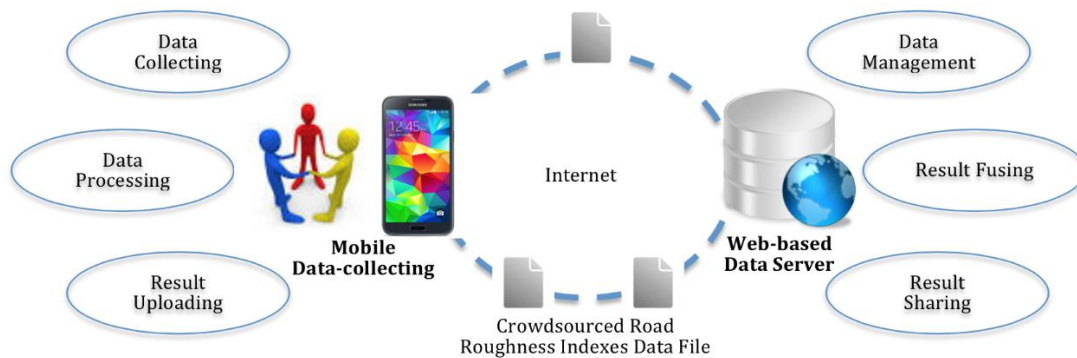
Figure 3.1 System architecture.
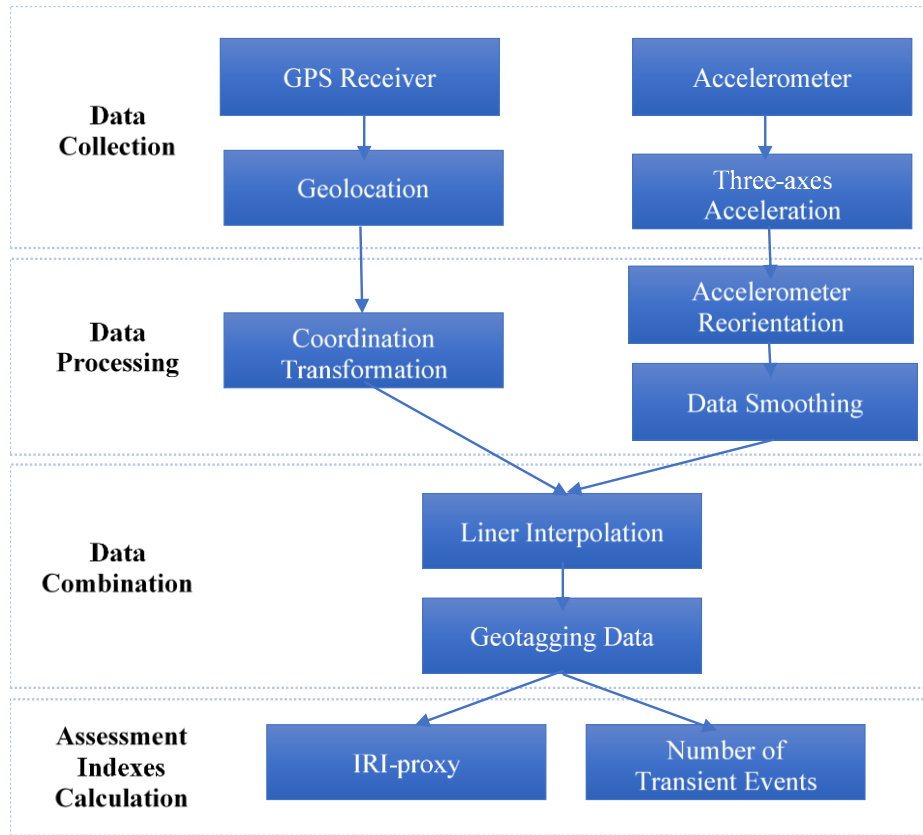
Figure 3.2 The flow chart of real-time road surface assessment using smartphone.

3.2.2. Real-Time Road Surface Condition Assessment

The process of road surface assessment is described in Figure 3.2. It consists of four steps: data collection, data process, data integration and assessment indexes calculation.

3.2.2.1. Accelerometer Reorientation

Microelectromechanical systems (MEMS) accelerometers in smartphones have a high sampling rate and are sensitive to detect the jerks of a ground vehicle when transient events occur (i.e., hitting potholes or bumps) (Bhoraskar et al. 2012; R. Chen

and Guinness 2014). To distinguish between the acceleration anomaly caused by a
transient event and vehicle regular acceleration/deceleration, it would be ideal to reorient
smartphone accelerometer to make the smartphone axes align with the vehicle axes,
which means the X- and Y-axes of the smartphone directly sense the vehicle's horizontal
acceleration/deceleration. On the other hand, Z-axis acceleration, which is perpendicular
to the vehicle, can be used to identify the acceleration anomaly caused by vehicle
vibration. If the condition is satisfied, the accelerometer is called well-oriented,
otherwise disoriented. Equations (3.1) - (3.4) are adapted from (Astarita et al. 2012),
which can be used to perform accelerometer orientation achieved through the Euler
Angles.

$$\alpha = \tan^{-1}(a_y'/a_z') \quad \beta = \tan^{-1}(-a_x'/(\sqrt{(a_y')^2 + (a_z')^2})) \tag{3.1}$$

$$a_{xreor} = \cos(\beta)\, a_x' + \sin(\beta)\sin(\alpha)\, a_y' + \cos(\alpha)\sin(\beta)\, a_z' \tag{3.2}$$

$$a_{yreor} = \cos(\alpha)\, a_y' - \sin(\alpha)\, a_z' \tag{3.3}$$

$$a_{zreor} = -\sin(\beta)\, a_x' + \cos(\beta)\sin(\alpha)\, a_y' + \cos(\beta)\cos(\alpha)\, a_z' \tag{3.4}$$

a_x', a_y', a_z' are the three directions' accelerations gathered from a disoriented
accelerometer, $a_{xreor}, a_{yreor}, a_{zreor}$ are the reoriented three-axes accelerations. α is the
roll angle which shows a rotation around X-axis, β is the pitch angle which shows the
rotation around Y-axis.

Figure 3.3 illustrates the differences in orientation between a disoriented
accelerometer which doesn't match the measurements of the data and the well-oriented

accelerometer. After reorientation, the X-axis acceleration is roughly below zero, Y-axis

is now at zero, and the Z-axis is now at negative one.
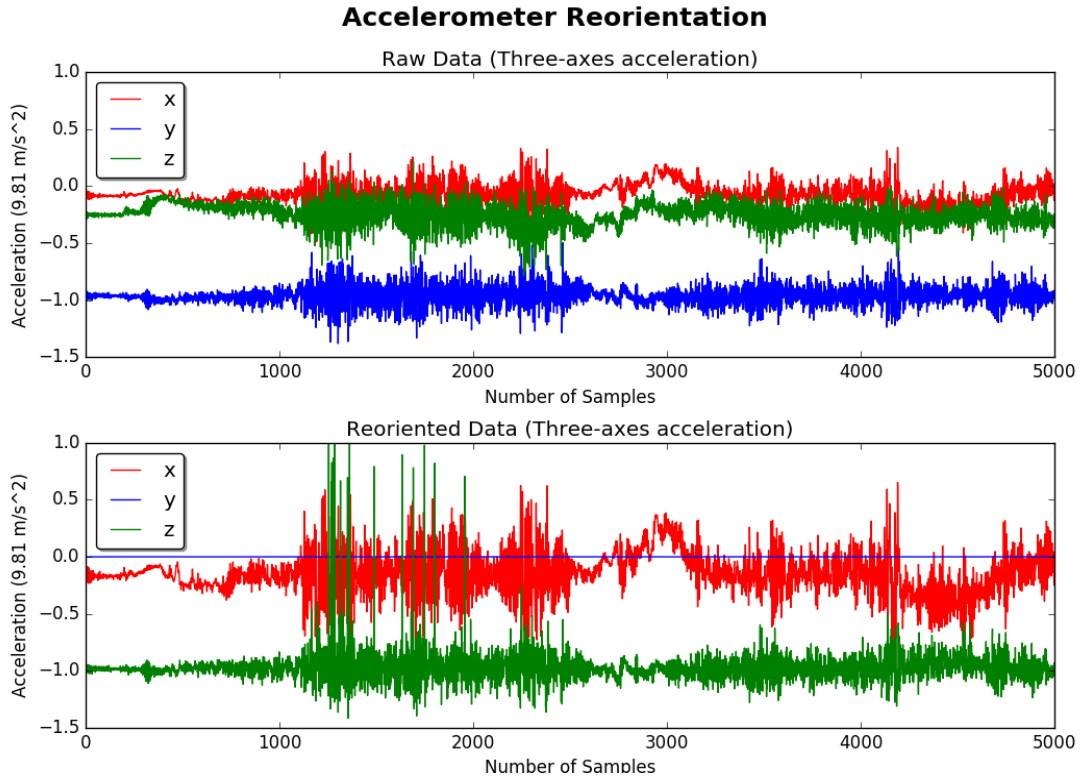
Figure 3.3 A comparison between raw data and reoriented data following the reorientation using Euler Angles.

3.2.2.2. Geotagging Data

Accelerometers measure specific force, which is the acceleration relative to free-

fall. To extract acceleration signals generated by the road roughness, a high-pass filter as

well as a low-pass filter applied to the Z-axis acceleration measurements. The low-pass

filter is used to extract the force of Earth gravity from the measured acceleration. Then

the high-pass filter is applied to eliminate the contribution of the Earth gravity to obtain

a corrected acceleration. Equations (3.5) - (3.7) are adapted from ("Motion Sensors"

n.d.), the low-pass filter is applied as:

$$Y_n = \alpha \cdot Y_{n-1} + (1 - \alpha) \cdot X_n \tag{3.5}$$

where,

$$\alpha = \frac{t}{t+dT}, \tag{3.6}$$

t is the current time tag, dT is the event delivery rate, Y_{n-1} is the filtered output of the last

epoch, Y_n is the current filtered output, and X_n is the current observation.

Having applied the low-pass filter, the following high-pass filter is used to

eliminate the Earth gravity:

$$Z_n = X_n - Y_n = \alpha \cdot X_n - \alpha \cdot Y_{n-1} \tag{3.7}$$

where Z_n is the corrected acceleration.

The output rate of the built-in GPS receiver (typically 1 Hz) is far lower than the

built-in accelerometer (typically 100 Hz). To geo-reference each accelerometer

measurement, a linear interpolation scheme is applied, given the hypothesis that the

ground vehicle moves with a constant speed between two adjacent GPS positions.

To calculate the distance between two adjacent GPS positions, the original

geodetic coordinates are transformed into ECEF (Earth-Centered, Earth-Fixed)

coordinates, which are coordinates in a Cartesian coordinate system. Equations (3.8) -

(3.11) are adapted from (Clynch 2006). Given the geodetic latitude φ, longitude λ, and

ellipsoidal height h, where the radius of curvature in the prime vertical, N, is given by:

$$N = \frac{a}{\sqrt{1-e^2 \sin^2 \varphi}} \tag{3.8}$$

where the semi-major axis $a = 6378137$, the first eccentricity $e = 8.1819190842622 - e^2$,

then the ECEF coordinates xyz can be obtained with:

$$x = (N + h) \cos \varphi \cos \lambda \tag{3.9}$$
$$y = (N + h) \cos \varphi \sin \lambda \tag{3.10}$$
$$z = ([1 - e^2]N + h) \sin \varphi \tag{3.11}$$

Due to the short time interval of one second between two GPS sample points, it

is reasonable to assume that the velocities of the ECEF coordinate components are

constant, therefore, we can apply the following equations to estimate the coordinates of

accelerometer measurement sampled at time t:

$$x = x_0 + \frac{(t - t_0)(x_1 - x_0)}{t_1 - t_0}$$

$$y = y_0 + \frac{(t - t_0)(y_1 - y_0)}{t_1 - t_0}$$

$$z = z_0 + \frac{(t - t_0)(z_1 - z_0)}{t_1 - t_0}$$

$$\tag{3.12}$$

where (x_0, y_0, z_0) and (x_1, y_1, z_1) are the coordinates of two consecutive GPS locations

sampled at time t_0 and t_1 , respectively. With the coordinate (x, y, z), we can then geo-

referencing each accelerometer measurement sampled on the roads. The distance S between accelerometer sampled point and the first GPS location (x_0, y_0, z_0) can then be estimated with:

$$S = \sqrt{(x - x_0)^2 + (y - y_0)^2 + (z - z_0)^2} \qquad (3.13)$$

3.2.2.3. Two Road Surface Condition Assessment Indexes

Several studies have verified that Z-axis acceleration gathered from smartphones can be used as an effective and reliable signal to estimate road surface condition (Amador-Jiménez and Matout 2014; Bhoraskar et al. 2012; Harikrishnan and Gopi 2017). In this study, two assessment indexes are calculated from the geotagged Z-axis acceleration measurements including 1) IRI-proxy for each road segment, and 2) the number of transient events. The IRI-proxy is employed to depict the overall road quality. A transient event occurs when root mean square (RMS) of the Z-axis acceleration exceeds the preset threshold and meets specific criterion that is discussed later. RMS is a statistical measure of the magnitude of a varying quantity. It is especially useful when the function alternates between positive and negative values, e.g., sinusoids. Calculating RMS of Z-axis acceleration can effectively wipe off data noise from signals, smooth the raw data, and highlight the pattern of the vehicle vibration.

IRI-proxy: The International Roughness Index (IRI), which is generally measured by special instruments, is the roughness index commonly used to examine the road surface condition (Sayers and Karamihas 1998). Since 1986, IRI has been worldwide used as the most common index for examining and evaluating road systems.

52

Some studies indicate that there is a close correlation between IRI and the speed-normalized Z-axis acceleration. Equation 3.14 is generated based on (Amador-Jiménez and Matout 2014). A proxy for IRI (IRI-proxy) can be calculated by multiplying the speed-normalized RMS by 100.

For each road segment, its IRI-proxy can be calculated with:

$$IRI_{proxy} = \frac{n \cdot R}{\sum_{i=1}^{n} V_i} \cdot 100 \qquad (3.14)$$

where n is the numbers of measurements gathered from a 50-meter road segment, R is the RMS of this road segment, V_i is the real-time speed of the vehicle at the location of the i-th acceleration measurement. Based on the IRI-proxy, the road roughness condition is classified into 4 levels. These four road condition indexes are summarized in Table 3.2 (Douangphachanh and Oneyama 2013).

Table 3.2 Four Levels of Road Surface Condition Based on IRI-proxy.

Road Surface Condition	IRI-proxy
Excellent/Good	$0 \leq IRI < 4$
Fair	$4 \leq IRI < 7$
Poor	$7 \leq IRI < 10$
Bad/Failed	$IRI \geq 10$

These indexes are generated from the road roughness condition bands used in Lao Road Management System, which contains 6 road condition indexes: 1) Excellent ($0 \leq IRI < 2$), 2) Good ($2 \leq IRI < 4$), 3) Fair ($4 \leq IRI < 7$), Poor ($7 \leq IRI < 10$), 5) Bad ($10 \leq IRI < 18$), and Failed ($IRI \geq 18$) (Douangphachanh and Oneyama 2013).

Transient Event: Transient events detection is to identify and locate potential

potholes/bumps on the road surface (Tan et al. 2014). The vehicle vibration on rough

road segments is greater than that on the smooth segments, so transient events are

typically represented as events with large amplitude and short wavelength in a RMS

curve. Many transient events detection methods have been proposed such as Z-PEAK,

Z-DIFF, Z-STDEV et al. (Mednis et al. 2011). Based on the existing methods, an

improved method was proposed in this study. Figure 3.4 shows the workflow of the

proposed transient event detection. It mainly consists of four steps as follows:
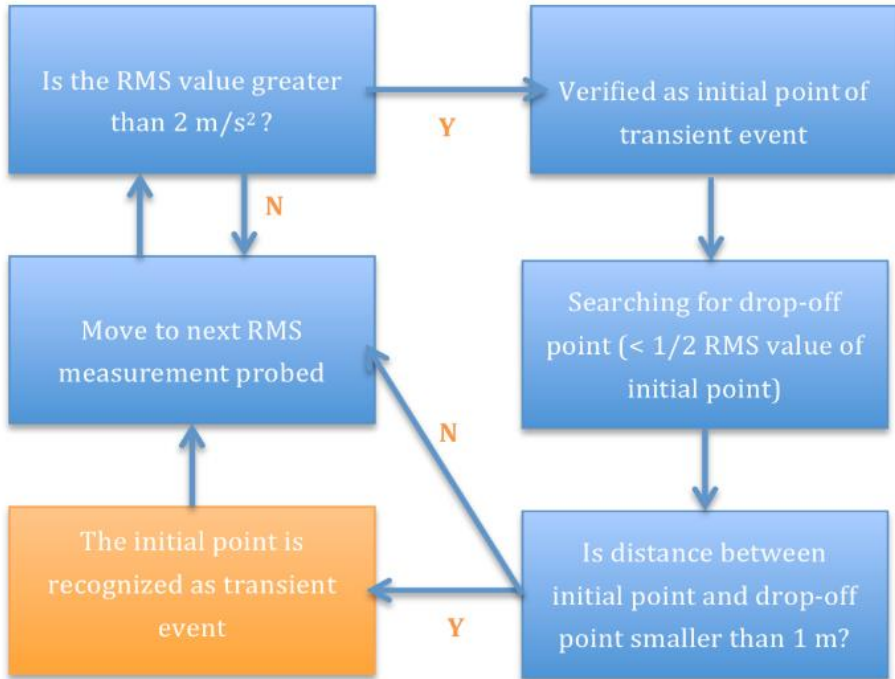
Figure 3.4 Workflow of transient event identification.
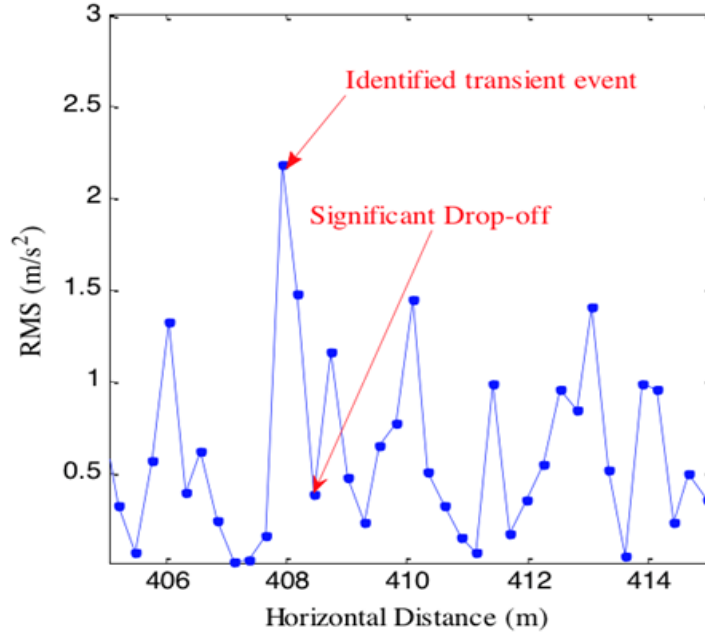
Figure 3.5 Illustration of transient event identification along a RMS curve.

1) Detect the initial point of the transient event: The search is performed along the RMS curve as shown in Figure 3.5. When an RMS value of greater than a preset threshold (through the empirical test, 2 m/s^2 is set as the threshold value) is detected, an initial point is identified;

2) Detect the drop-off point: The searching is continued from the initial point until a point with an RMS value of less than half of RMS value of the initial point. If such a point in the RMS curve occurs, a drop-off point is then identified;

3) Transient event validation: If the distance between the initial point and the drop-off point is less than 1 meter, a transient event is detected. The threshold value 1 meter is selected based on the assumption that the pothole size should be smaller than 1 meter.

4) Repeat steps 1-3 from the current point in the RMS curve.

To remove the anomalous transient events, two pothole filters are adapted from (Eriksson et al. 2008) and applied as follows:

1) The speed filter: reject the transient event with zero or very low speed. A threshold of 5 km/h is set to verify each new event.

2) Z-axis acceleration filter: the events, whose Z-axis acceleration is lower than the threshold of 2 m/s^2, will be removed.

3.2.3. Result Optimization by Integrating Crowd Sensed Data

As each road condition assessment is performed based on the wheel trajectory, which cannot cover the entire pavement, a slight difference exists in the results from different users. This is mainly caused by different driving attempts although the driving routes and vehicles were the same. The detection of the transient events purely relies on where the tire meets the road. For example, a driver may tend to avoid a pothole while another driver may just hit it. Besides, the road surface is a slow, dynamic changing surface. After a long-term use, road surface quality will become worse with more new potholes. Therefore, it is beneficial to take advantages of a crowdsensing solution, which integrates contributions from the public and provides a better assessment of the entire pavement. In this study, a cloud storage service is employed to synergy the contributions from multiple crowdsourcers and publish the integrated results.

Result Optimization: Two data files, one for storing the RMS and IRI-proxy, while the other for transient events, are automatically outputted. The newly submitted

data files are processed on the server to optimize and update the crowd sensed road surface conditions.
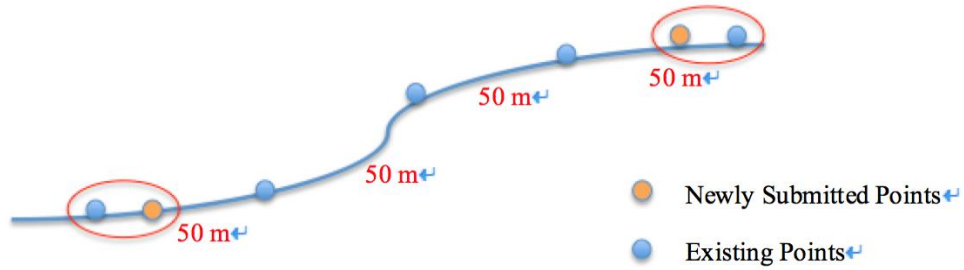
Figure 3.6 The process of data synergy from multiple crowdsourcers.

In this study, the dataset RIRI−proxy = {R1, R2, · · ·, Rn} represents a set of IRI-proxy values for each 50-meter road segment. For the same road segment, each newly submitted dataset would be merged to the existing dataset as shown in Figure 3.6.

A weighting scheme based on the distance between newly submitted points and their nearest existing points is proposed. For each existing point, its IRI-proxy is recalculated based on newly submitted data with:

$$u_i(x) = \frac{w_i(x) \cdot u_i + u_0(x)}{w_i(x) + 1} \tag{3.15}$$

where,

$$w_i(x) = 1 - \frac{d(x, x_i)}{d} \tag{3.16}$$

$u_0(x)$ is the original IRI-proxy value at an existing point, $u_i(x)$ is the recalculated IRI-proxy value at an existing point, d is the distance tolerance (50 meters, in this study), $d\ (x,\ x_i)$ is the distance between a newly reported point x_i and its nearest existing point x, u_i is the IRI-proxy value of the newly submitted point, and $w_i(x)$ is the weight signed to the IRI-proxy value at the newly submitted point.

Numerous studies indicate that the positioning accuracies of the smartphone GPS receivers ranged from 5 to 10 meters (Zandbergen and Barbeau 2011; Zandbergen 2009). Therefore, the positioning error of detected potholes can be as large as 10 meters. For this reason, all potholes within a circle with a radius of 10 meters are considered as one pothole. Thus,

1) If the distance between the newly detected pothole to its nearest existing pothole is less than 10 meters, the position of the existing pothole will be recalculated as the average of these two positions;

2) If the distance between these two potholes is longer than 10 meters, the newly detected pothole will be considered as a new pothole and added to the database.

Furthermore, the server also counts the number of reports for each potential pothole. If a potential pothole has been detected and reported by three different crowdsourcers, then it will be published. In this way, the accuracy of the crowd sensed results can be improved.

3.2.4. A Cloud-based Framework for Data Visualization and Sharing

In this study, a lightweight, cloud-based framework, which takes advantages of free Google services, is developed in the study. Cloud storage services have been widely

used by consumers, business and governments to host, manage and collaborate on a huge amount of information. As one of the most popular customer clouds, Google Drive offers users a cost-effective ability to access, host, collaborate on, and disseminate files. Each user is given 15GB of free storage. Google Drive supports users to share their files or folders with individuals and with groups so that they can view, manage and comment on it. In this study, the administrator builds connections with all crowdsourcers using Google Drive and authorizes them to submit data to our server.

A Cloud Mapping Method - Google Fusion Table is used to map the potholes and road surface conditions in this study. Google Fusion Table is an experimental data visualization web application that allows users to gather, manage, collaborate on, visualize, and publish data tables online. Google Fusion Table provides a simple and effective approach, which is accessible to inexperienced users and empowers these users to develop their database-driven web-based application (Shen 2012). It allows users to map various kinds of features in minutes including points, lines, polygons, customer addresses, and countries. The newly generated map will appear with several small red placemarks based on the location data.

3.3. Experiments and Results

This section covers a brief introduction about the field tests, data analysis, and result integration and visualization.

3.3.1. Field Tests

To verify the proposed solution, some driving tests were carried out on a road segment of about 50km containing different levels of surface roughness in College

Station, Texas. Test data was collected from five different drivers who drove routes for

15 days. The iOS app *Crowdsense,* was installed on 3 iOS phones (i.e., two iPhone 6,

one iPhone 7), and the Android app *AndroSensor* was installed on 2 Android phones

(i.e., Moto X Pure). All these phones are equipped with a high-sensitivity built-in 3-axis

accelerometer and a GPS receiver. Each smartphone was fixed in the car using

smartphone holder. The GPS and Z-axis accelerometer data from the smartphones were

collected. The smartphones measured acceleration data with an output rate of 100 Hz

while generating GPS position information at 1 Hz. In this test, the cars were driven

normally, with a maximum speed of approximately 70 km/h. Even at maximum speed,

the smartphones could log 5 or 6 acceleration measurements per meter, which enabled

analysis of the road surface roughness with a high spatial resolution. To protect user

privacy seriously, all sensed data were completely anonymized. Users' explicit

permission is required prior to enabling the sensors.

3.3.2. Result Evaluation

Figure 3.7 shows the result of a 5-kilometer road segment. In this figure, the

upper subplot shows the raw data, the middle subplot shows RMS of Z-axis acceleration,

the lower subplot shows IRI-proxy for every 50-m traveled along the horizontal plane is

calculated to indicate the road surface roughness.
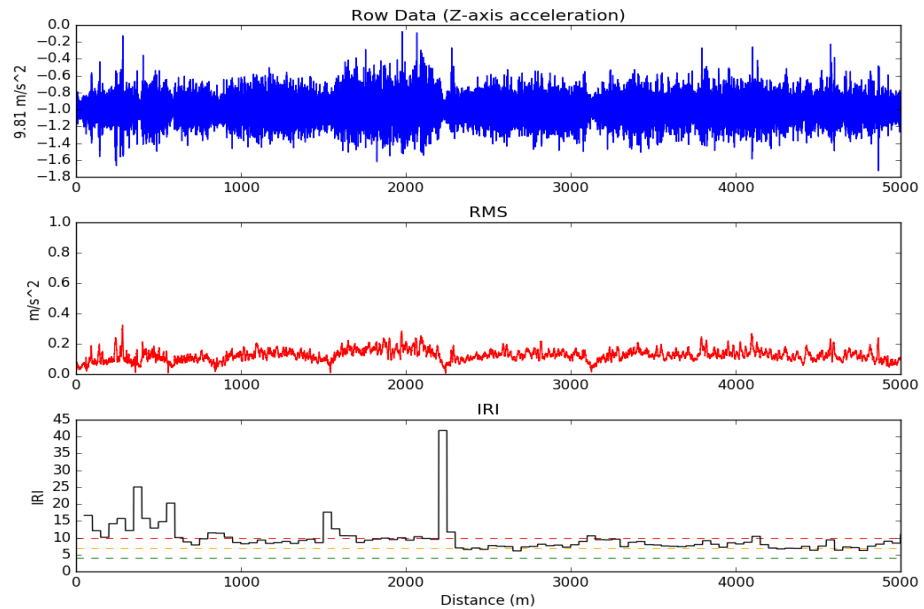
Figure 3.7 The raw data, RMS of raw data, and IRI-proxy of a 5-kilometer road segment.
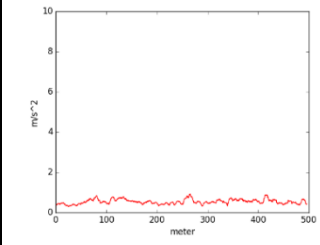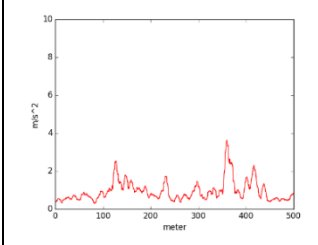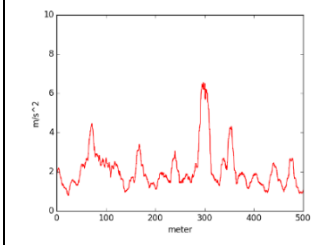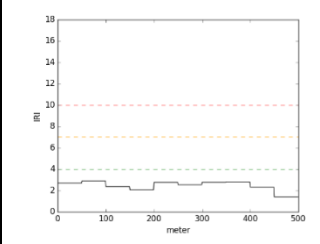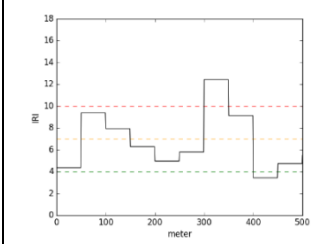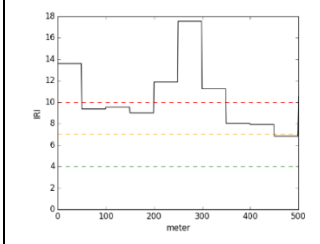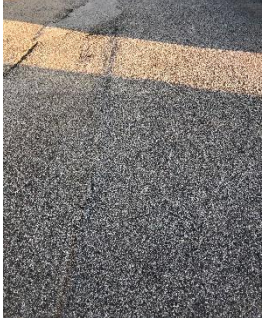
Table 3.3 Description of Three Typical Road Segments.

	Road Name	Length (meter)	Road Surface Description	Overall Condition	Data Acquisition Time
Segment A	Luther Street West, College Station, TX	1071	Smooth concrete road surface	Good	08/26/2017 4:20 pm
Segment B	Marion Pugh Drive, College Station, TX	1093	Fair good gravel road with some tars on the surface	Moderate	08/26/2017 4:45 pm
Segment C	Welsh Avenue, College Station, TX	1630	Bumpy gravel road surface with several **potholes**	Bad	08/26/2017 5:10 pm
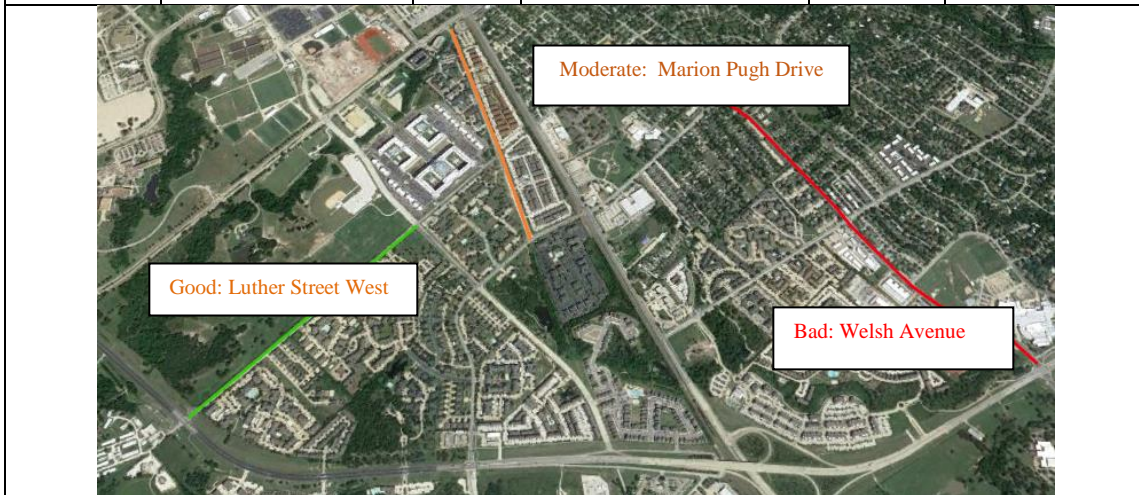
Three typical road segments (A, B, C) are selected from the testing routes to verify the proposed assessment strategy. A detailed description of these road segments is listed in Table 3.3. An iPhone 6 smartphone was used to run *Crowdsense* for data collection. This smartphone was fixed in the cabin of a 2009 Toyota Corolla.

Table 3.4 The Comparison of Three Typical Road Segments.

	Segment A	Segment B	Segment C
RMS of Z-acceleration	0.4347 m/s^2	0.9258 m/s^2	2.8826 m/s^2
IRI-proxy	2.5734	7.2624	11.6374
Quality Assessment	Good	Poor	Bad
RMS			
IRI			
Road Image			

Statistical results of mean RMS values, IRI-proxy, and road surface images of

three road segments (i.e., A, B and C) are presented in Table 3.4. Segment A, which has

the highest road quality, was labeled "Good". The mean IRI-proxy of Segment A is

2.5734, the mean value of RMS is $0.4347\ m/s^2$. Segment B, which has a medium-level

of road quality, was labeled "Poor" based on the calculated IRI-proxy 7.2624, and with

the mean value of RMS is $0.9258 m/s^2$. Segment C, which has the worst road quality,

was labeled "Bad". The mean IRI-proxy of Segment C is 11.6374, with the mean value

of RMS is $2.8826 m/s^2$.

Table 3.5 The Comparison of Three Different Smartphone Models.
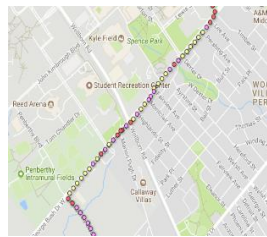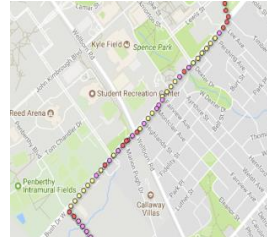
	Moto X Pure	iPhone 6	iPhone 7	Standard Deviation
RMS mean m/s²	0.3435	0.3384	0.3291	0.0075
IRI-proxy mean	10.8241	10.8187	10.4341	0.2236
Estimated Road Surface Condition				Data Acquisition Time: 10/13/2017 8:20 AM Location: George Bush Drive, College Station, Tx.

Table 3.5 shows the statistical results of three smartphone models (i.e., Moto X

Pure, iPhone 6, iPhone7) under test to illustrate the repeatability by using different

smartphones. These three smartphones were fixed on the same car (i.e., 2009 Toyota

Corolla) for testing the same road segment (i.e., George Bush Drive, College Station,

TX). The differences of the mean RMS and mean IRI-proxy of the above smartphone

models are small. The IRI-proxy maps generated based on different phones are all very similar, which indicates that the proposed approach is suitable for different phone models.

Speed VS Z-axis acceleration
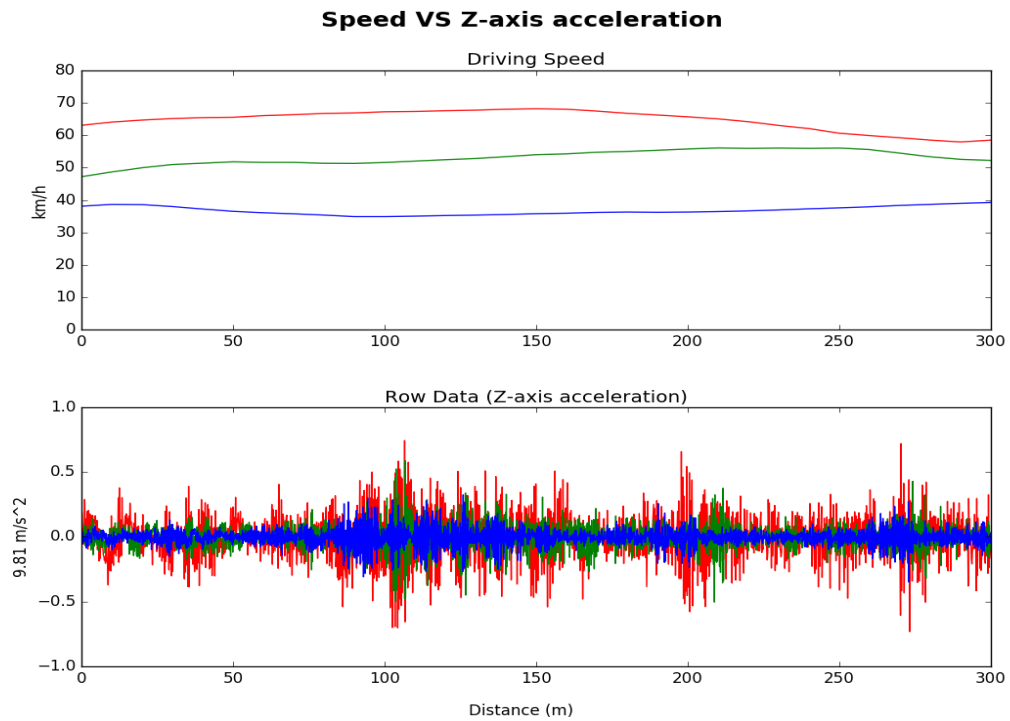
Figure 3.8 Three driving speed (low, medium, high) with their corresponding Z-axis acceleration gathered from the same road segment.

Studies have demonstrated Z-axis acceleration is influenced by the driving speed (Lima et al., 2017). To test the relationship between the driving speed with Z-axis acceleration, Road segment A was tested three times at different driving speeds: low (30-40 km/h), medium (40-50 km/h), high (50-60 km/h). Figure 3.8 shows three different driving speeds and their corresponding Z-axis acceleration. This figure

indicates that the high driving speed will increase the vibration of Z-axis acceleration. The IRI-proxy was calculated three times based on the datasets gathered with different driving speed detailed in Table 3.6. The table indicates that these three tests' results are similar, just one 50-meter "Good" road segment was mislabeled as "Fair". It indicates that the proposed speed-normalized method could handle the data difference which is caused by the different driving speed.

Table 3.6 The Comparison of IRI-proxy Calculated with Different Driving Speeds.

IRI-Proxy (Low)	IRI-Proxy (Medium)	IRI-Proxy(High)
1.809354497	1.949075566	1.901084422
2.713605347	1.862560789	2.596207585
2.946428568	1.701830928	2.624650091
2.302405857	2.547429886	2.142437912
2.032438854	1.7268601	2.829025458
2.786624122	2.115270482	**4.136784105**
2.576768388	2.136877558	3.278992175
2.763603782	1.897341655	3.417223982
1.809354497	1.949075566	1.901084422

To verify the accuracy of proposed crowdsensing solution for the pothole detection, a road test was carried out in Texas A&M University Parking Lot 50, where contains a lot of distinguishable potholes. The test was repeated 10 times by a tester with different smartphones for data collection. Four pothole detection methods: Z-PEAK, Z-DIFF, Z-STEDV and the method we proposed are respectively utilized to extract and

label potholes. The true pothole number is 28, which were manually counted prior to the

test. Half-meter-accuracy positions of these 28 potholes were geotagged by using a

hand-held GPS.

Figure 3.9 True pothole distribution and four pothole detection methods' results from 5 laps (red dot: true pothole; blue dot: detected pothole; light blue buffer: positioning error tolerance).

The performance of Z-PEAK, Z-DIFF, Z-STEDV and the proposed

crowdsensing solution was evaluated by comparing the truth reference with their results

from five laps and the results from ten laps from two respects: 1) coverage rate

(#correctly detected potholes / #true pothole); 2) false positive rate (#mislabel potholes /

66

#detected potholes). Figure 3.9 shows the true potholes distribution (red dots) and 4

different methods' pothole detection results from five laps (blue dots). The positioning

error tolerance is set as 5 meters (light blue buffer) in this figure, which means the

detected pothole with a distance less than 5 meters from the nearest true pothole, is

judged as a correct detection.

Table 3.7 The Performance of Four Pothole Detection Methods.

False Positive Rate				
Positioning Error Tolerance	5 Meters		10 Meters	
Number of Laps	5	10	5	10
Z-PEAK	22.22%	17.38%	11.76%	5.88%
Z-DIFF	57.14%	50%	16.66%	10.58%
Z-STEDV	35.29%	23.59%	16.66%	11.11%
IMPROVED	27.27%	16.67%	6.73%	6.14%
Coverage Rate				
Positioning Error Tolerance	5 Meters		10 Meters	
Number of Laps	5	10	5	10
Z-PEAK	25.92%	37.03%	40.74%	62.06%
Z-DIFF	37.04%	51.85%	66.67%	81.84%
Z-STEDV	59.25%	74.07%	77.78%	85.18%
IMPROVED	62.96%	88.89%	88.89%	92.59%

Table 3.7 details the false positive rates and the coverage rates of these four

methods gathered from five laps and ten laps. Two positioning error tolerances (5 meters

and 10 meters) are respectively adapted for the detection performance evaluation. The test indicates that Z-Peak has a high accuracy for pothole detection. However, the coverage rate of Z-Peak method is the lowest. Another two pothole detection algorithms (Z-DIFF and Z-STEDV) which are low in detection accuracy and coverage rate compared to the improved algorithm. The improved algorithm does a better job of properly detecting potholes by integrating crowd sensed data, increasing the coverage rate and lowering the false positive rate of the pothole detection.

Battery consumption is an important issue for crowdsensing. In this study, battery consumption of different phones (i.e., Moto X Pure, iPhone 6, and iPhone 7) was also tested as shown in Figure 3.10. The sampling rate of accelerometers was set to 100 Hz and GPS receivers were enabled for all three phones. The result shows that the battery of Android-based Moto X Pure can offer 8 - 9 hours of data collection. iPhone 6 and iPhone 7 can support more than 12 hours' data collection. To date, several studies (Abdesslem, Phillips, and Henderson 2009; Constandache et al. 2009; Peng et al. 2017; J. Wang et al. 2017; Zhuang, Kim, and Singh 2010) have been carried out, which can effectively minimize the energy consumption of built-in smartphone sensors. In the future study, a more energy-efficient crowdsensing system will be built by taking advantages of the former studies, choosing more appropriate sampling rate of sensors, and optimizing algorithms.
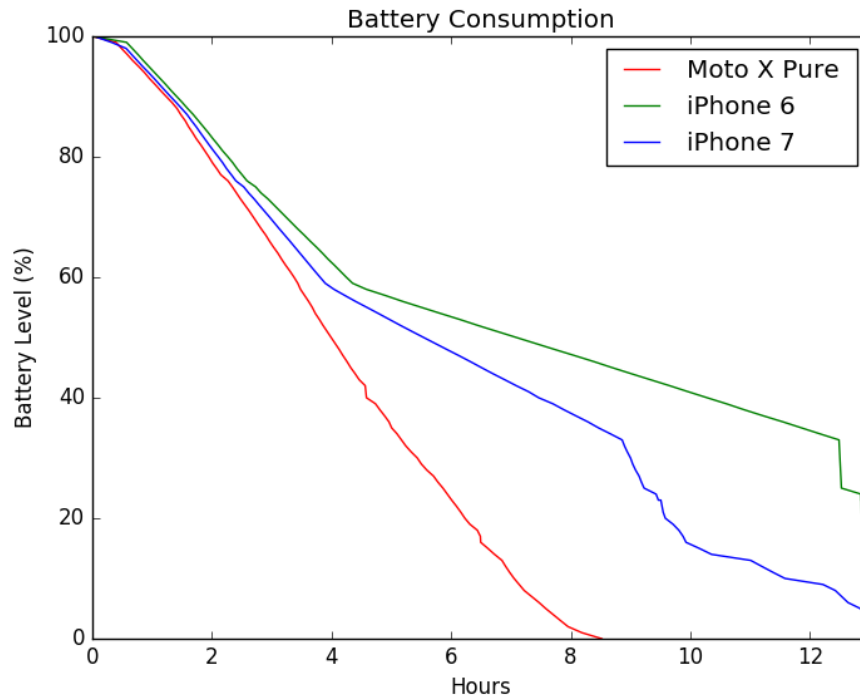
Figure 3.10 Battery consumption test.

As mentioned above, the contribution from crowdsourcers were mapped using Google Fusion Table. Three maps, as shown in Figure 3.11, were generated from the 15-day detection data to depict road surface condition. Figure 3.11-A presents pothole distribution. The pothole density map was obtained by enabling the heat map layer as shown in Figure 3.11-B. Meanwhile, Figure 3.11-C shows the overall road roughness map based on IRI-proxy, in which each point was colored based on its IRI-proxy. In this map, "Good" in yellow, "Fair" in Green, "Poor" in purple, and "Bad" in red. These three maps give the public a clear view of the most up-to-date road surface condition for some road segments in College Station, Texas.
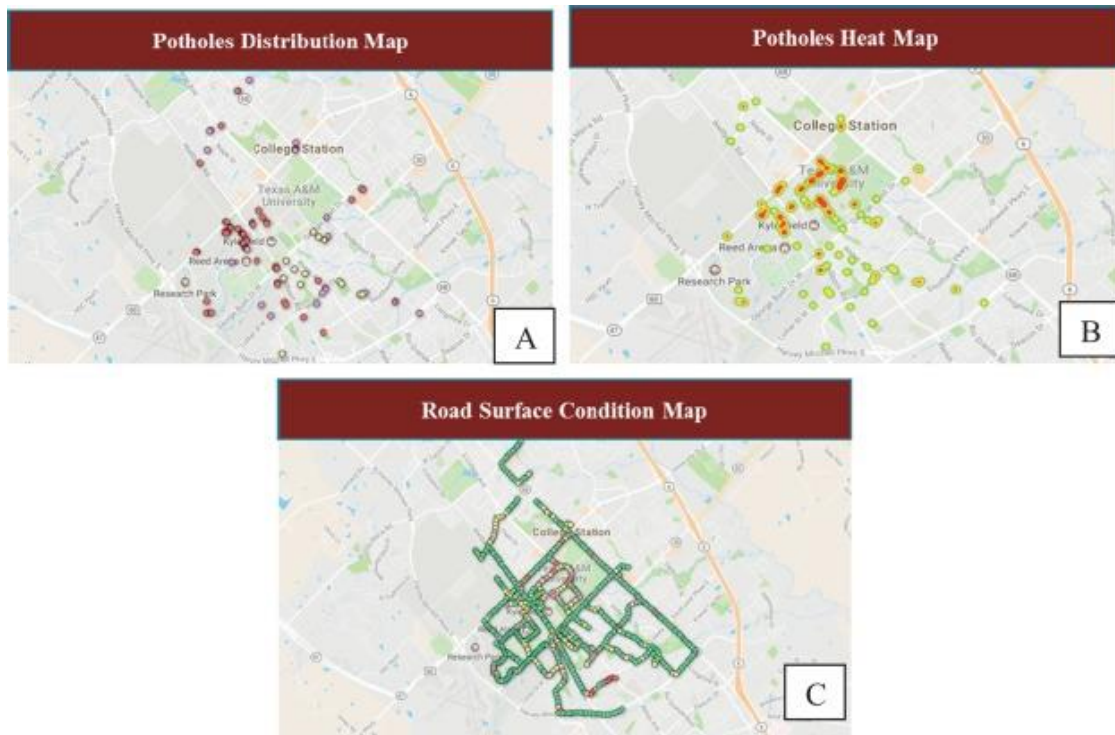
Figure 3.11 Road surface roughness maps (A: potholes distribution map, B: potholes density map, C: IRI-proxy map).

3.4. Discussion and Conclusion

In the study, a labor-saving and low-cost crowdsensing system for road surface condition assessment was introduced, and it has verified the feasibility of using built-in smartphone sensors for road surface condition assessment in terms of two detection indexes: IRI-proxy and the number of the transient events. In order to examine the proposed solution, test data were collected from five users driving routes around College Station, Texas. The drivers drove 50 km road segments with different surface roughness levels. The field tests demonstrated that the built-in smartphone sensors can effectively assess road quality and detect the transient events. The overall road surface condition

can be accurately judged and labeled by the IRI-proxy and the transient events can be efficiently identified. By implementing a crowdsensing solution, the road surface condition can be constantly monitored. Meanwhile, the most up-to-date and more accurate assessment results were achieved by mining crowd sensed data. What's more, the Google Fusion Table can offer powerful access for data management and visualization.

However, it has shown that using different devices in different driving attempts can generate different assessment results, even though they were carried out on the same routes. It is mainly because ground vehicles always move in a line-scan rather than area-scan pattern. Due to the limited accuracy of the built-in smartphone GPS receiver, a high-accuracy positioning result cannot be guaranteed. "How accurate are smartphone GPS receivers?" is the most often asked question related to crowdsensing. The positioning accuracy of smartphones has been significantly enhanced over the past decade. Zandbergen (2009) examined the positioning accuracy of the 3G iPhone - the first mobile device which integrates three different positioning technologies. The result indicates an average positioning accuracy is 8 meters. In Zandbergen and Barbeau (2011), the result shows the positioning accuracy of smartphones has been improved to 5-8 meters, which is sufficient for most location-based services. R. Chen et al. (2014) proposed a novel "DGNSS-C" algorithm which can enhance the positioning accuracy of smartphones by 30% - 40% (2-3 meters). (Pesyna, Heath, and Humphreys 2014) created a "centimeter-accurate" mobile system by combining the GPS recordings with a smartphone-quality Global Navigation Satellite System antenna. The latest news

71

published on IEEE SPECTRUM (Moore 2018) said Broadcom Limited (a global semiconductor leader) designed a more accurate GPS chip (BCM47755), which enables 30-centimeter positioning accuracy and 50% less battery drains for the next generation of smartphones releasing in 2018.

With the rapid development of the modern smartphone technologies and the increasing number of public crowdsensing smartphone participants, the proposed solution is promising for providing accurate real-time road surface roughness information and offering comprehensive and timely road service information to road maintenance works as well as drivers.

4. EMBRACING CROWDSENSING: AN ENHANCED MOBILE SENSING SOLUTION FOR ROAD ANOMALY DETECTION[*]

4.1. Introduction

"No one knows how many potholes are out there, but we all agree there are a ton of them." The U.S. Federal Highway Administration (FHWA) estimates that about 52% of the U.S. highways are in a miserable condition (Bruce 2001). A newly released report—*Repair Priorities 2019* shows that the percentage of "poor condition" roads in the U.S. has rapidly increased from 14% to 20% between 2009 and 2017 (Bellis, Osborne, and Davis 2019). The category of "poor condition" road is defined by FHWA, which contains excessive road anomalies, such as potholes, bumps, and ruts. Road anomalies can not only discomfort driving experience, but they also damage vehicle components, cause economic loss, even lead to car crashes. The American Automobile Association estimates that pothole damage costs three billion U.S. dollars in vehicle repairs nationwide annually (AAA 2016). Meanwhile, approximately one-third of traffic fatalities occur on poor-condition roads each year ("The Pothole Facts" 2019). Therefore, effectively detecting road anomalies has become a fundamental social need, which requires immediate attention.

Traditional road anomaly detections were conducted through three main types of approaches, including 3D laser scanning, vision-based image processing, and vehicular vibration-based analysis (Sattar, Li, and Chapman 2018). However, implementing these approaches requires costly and sophisticated instruments (e.g., profilometer, 3D laser scanner), which also consumes extensive time, workforce, and expertise. It is worth noting that road surface conditions can vary day by day. Existing potholes can grow larger, driven by heavy traffics. How to continuously monitor road anomalies with a low-cost and high-efficient solution remains to be a challenging question.

Mobile sensing technology has developed rapidly over the past few years (Li et al. 2019; W. Xu et al. 2015; R. Chen, Chu, Liu, Chen, et al. 2014). Equipped with various sensors, smartphones have become promising data acquisition and computing platforms, which could achieve a high-sampling rate with little or zero economic cost. Recent studies attempt to investigate the ability of mobile sensors in road anomaly detection. Studies have proven that smartphone accelerometers can effectively capture the vehicle vibrations caused by the unevenness of the road surface (Astarita et al. 2012; Li and Goldberg 2018; Li, Chen, and Chu 2014). Through analyzing these mobile sensors' signals, we can potentially identify road anomalies.

4.1.1. Related Studies

Different studies have been conducted to identify road anomalies (e.g., potholes and bumps) using smartphone sensors. Among the available mobile sensors, accelerometers are most sensitive for capturing vehicle jerks when hitting bumps and potholes. Various methods have been implemented to analyze acceleration signals,

which can be broadly classified into two categories: 1) threshold-based methods and 2) machine learning methods. In recent studies, some researchers start to adopt signal processing techniques, such as wavelet transforms, to analyze mobile sensed signals. Meanwhile, implementing crowdsensing solutions has become a promising research direction, which shows a significant potential to obtain more reliable detect results by synthesizing public contributed data.

Threshold-based methods detect road anomalies through extracting extreme values from acceleration signals. Astarita et al. (2012) explored the effectiveness of built-in smartphone accelerometers for detecting speed bumps and potholes using threshold-based method. In this study, the extreme peak values along the curve of z-axis acceleration were treated as direct indicators for identifying bumps and potholes. Three filters were utilized to eliminate data noise and enhance the peak signals. The result demonstrated that speed bumps could be successfully identified by the extreme peak values of filtered z-axis acceleration with an accuracy of 90%. However, this method was less useful for locating potholes with a detection rate of around 65%. Mednis et al. (2011) compared different threshold-based methods for identifying road anomalies from acceleration signals. A dedicated accelerometer was installed on a vehicle to sense its vibration. The authors found a specific data pattern while hitting potholes—acceleration readings near to be 0 m/s2 for all three axes. Therefore, they created a G-ZERO algorithm and compared with the other three methods, including Z-THRESH, Z-DIFF, and STDEW(Z). The results demonstrated this new method achieve 90% accuracy for detecting road anomalies. Rishiwal and Khan (2016) proposed a simple threshold-based

solution to measure the severity of bumps and potholes. Continuous series of z-axis acceleration were collected to represent vehicle vibrations when driving along a road. A set of thresholds were generated through empirical tests to examine z-axis acceleration, which could extract road anomalies and label their severity levels (1 to 3) with an accuracy of 93.75%. Zang et al. (2018) attempted to use bicycle-mounted smartphones to measure the conditions of pedestrian and bicycle lanes. This study also implemented a threshold-based method to extract significant spikes from the curve of vertical acceleration. These spikes were recognized as road anomalies. The authors validated their result with ten ground truth sample and achieved 100% detection accuracy.

Machine learning methods have also been intensively utilized in road anomaly detections. Kalim, Jeong, and Ilyas (2016) created a new mobile app called CRATER to identify potholes and speed bumps through machine learning methods. In this study, the authors also used the built-in accelerometer to capture the vehicle shocks and vibrations while driving. A set of features (e.g., mean, maximum, minimum speed, etc.) were generated from the collected signals. Five classifiers were compared, including naïve Bayes, support vector machine (SVM), decision tables, decision tree, and supervised clustering. The results demonstrated that SVM did the best among the five methods, which could successfully identify potholes and speed bumps with accuracy rates of 90% and 95%. Meanwhile, this paper also attempted to obtain more reliable results by leveraging crowdsourced data. The potholes had to be reported by more than five different users before publishing on the web map. Celaya-Padilla et al. (2018) utilized a different machine learning approach to check the existence of speed bumps. The authors

first installed some hardware sensors (e.g., three-axis accelerometer and gyroscope) on a vehicle to measure vehicle vibration. The collected data series were split into two-second subsets. Each subset was manually labeled as with or without a speed bump. Then, seven statistical features (e.g., mean, variation, skewness, etc.) were generated from each axis of the two sensors' measurements for each subset. These features were selected through a multivariate feature section strategy supported by genetic algorithms. Finally, the selected features were fed to logistic regression models to identify whether a speed bump exists in each subset. This study achieved a detection accuracy of 97.14%. A similar study was conducted by Silva et al. (2018). The authors used random forest classifier to detect road anomalies from mobile sensed data. Fifty statistical features were generated from each subset of the collected data series. Each subset contained 125 continuous three-axis accelerometer measurements. Through applying feature selection procedure, twenty-five features were selected and used in the classification model. This method achieved a 77.23% - 93.91% accuracy for distinguishing road with and without anomalies in different experimental settings.

Wavelet analysis has a superior ability for analyzing continuous changing signals, which shows a great potential to aid in interpreting mobile sensed data. Wei, Fwa, and Zhe (2005) calculated wavelet statistics using an official roughness dataset to characterize road surface roughness. Results demonstrated that the obtained wavelet statistics showed a high correlation with officially measured roughness indexes. Recent studies attempted to use wavelet transforms to recognize bumps and potholes from mobile sensed data series. For example, Bello-Salau et al. (2018) were the first to

77

integrate wavelet transform (WT) into road anomaly detection. In this study, the authors combined a discrete WT model with the scale-space filtering algorithm to denoise the vehicle vibration signals collected from a dedicated accelerometer—NI myRIO-1950. Then, a fixed threshold was used to extract abnormal values from the denoised signals to identify the road anomalies (e.g., bumps and potholes). This study achieved relatively high accuracy for detecting bumps (96%) and potholes (94%). Silveira Rodrigues et al. (2019) conducted a similar study to evaluate the effectiveness of a different discrete WT—Haar wavelet transform (HWT) for detecting potholes. In this study, the authors first created an Android-based mobile app to collect data from the built-in smartphone accelerometer. Then, HWT was applied to the z-axis accelerations in different decomposition levels to generate wavelet coefficients, which could highlight the abnormal variations when hitting potholes. Thresholds were generated based on the mean value and the standard deviation of the calculated wavelet coefficients. These thresholds were used to label the collected signals as potholes, intermediate irregularities, and acceptable perturbations. However, the authors only used two manually collected potholes to validate their result, which was not statistically sufficient.

Implementing crowdsensing solutions would be exceptionally beneficial in road anomaly detection, as it allows continuous monitoring of road surface conditions by leveraging public contributed data with little or even zero economic cost. Xiao Li and Goldberg (2018) proposed a crowdsensing solution to assess road surface conditions. The authors first used an improved threshold-based method to detect potholes. Then, the crowd sensed potholes within a 10-meter radius were aggregated into one pothole

through a simple averaging procedure. Sabir, Memon, and Shaikh (2019) conducted a

similar study to enhance the accuracy of the detected road anomalies. In this study, the

public reported potholes within a 5-meter radius were clustered to eliminate duplicated

reports. Meanwhile, road anomalies had to be reported by different users before final

confirmed. This study could successfully detect 90% of speed breakers and 85% of

potholes.

4.1.2. Knowledge Gaps

Although existing studies have proven efficient to identify road anomalies using

mobile sensed data, they also expose some knowledge gaps which need to be addressed,

including:

1) **Existing detection methods have apparent limitations.** Threshold-based

   methods need extensive empirical studies to obtain high-reliable thresholds.

   However, these thresholds mostly need to be adjusted even re-tested when

   applied in different locations, which, in turn, significantly limits the repeatability

   of threshold-based methods. Machine learning methods usually require an

   extensive model training process based on a vast amount of labeled data, which

   is laborious and time-consuming. Utilizing wavelet transform (WT) can be more

   efficient to analyze mobile sensed data; however, integrating WT into road

   anomaly detection is still at a preliminary stage. To date, only a few studies

   reported on the utilization of discrete WT. The implementation of continuous

   wavelet transform (CWT) is still underexplored.

2) **Pothole size estimation is lacking.** Most existing studies focus only on identifying and locating potholes; however, few studies investigate how to estimate potholes' size using mobile sensed data. The damages caused by potholes vary by their sizes. Patching a pothole can cost about $35 to $50 U.S. dollars. Therefore, accurate and timely pothole size estimation is of great importance, which can help local governments allocate budget to fix hazardous potholes wisely.

3) **Prior crowdsourcing solutions are too simple to synthesize crowd sensed results efficiently.** How to leverage crowd sensed data to achieve a better road anomaly detection is still an underexplored question. Currently, only a few studies attempted to address this question with some simple crowdsensing strategies (e.g., average the crowd sensed data). However, these studies cannot effectively integrate public contributions to optimize detection result.

4.1.3. Solution and New Contributions

To fill above-referenced knowledge gaps, we propose an enhanced crowdsensing approach to detect road anomalies. In this study, we first create an Android-based mobile app—*PotholeAnalyzor* to acquire mobile sensors' data, including three-axis accelerometer and GPS. We then use wavelet analysis to identify road surface anomalies (such as bumps and potholes) and measure their sizes based on the mobile sensed data. Finally, we innovatively synthesize crowd sensed results through a spatial clustering method—Hierarchical Density-Based Spatial Clustering of Applications with Noise (HDBSCAN) to optimize the detection results.

Compared with prior studies, this study makes three new contributions for road anomaly detection, including:

1) **Implement a new method.** To the best of our knowledge, this study marks the first attempt to test the performance of CWT in road anomaly detection.

2) **Provide a solution for pothole size estimation.** Pothole size estimation plays an important role in road surface management; however, it is not considered in prior studies. This study uses an innovative wavelet-based approach to extract size information for road surface anomalies, which is a new solution to an existing problem.

3) **Put forward an enhanced crowdsensing approach.** There are some drawbacks associated with the crowd sensed data, such as data inaccuracy and redundancy. This study is among the first to investigate how to optimize road anomaly detection results by spatially clustering crowd sensed data.

4.2. Methods

In this study, we propose an enhanced crowdsensing approach to detect road anomalies by taking advantage of CWT and spatial clustering methods. The detection process goes through three main stages as shown in Figure 4.1, including 1) mobile sensors' data acquisition and preprocessing, 2) road anomaly detection and size estimation, and 3) result optimization by clustering crowd sensed data.

This section details the data and methods used in each processing stage, respectively. We first create an Android-based mobile app—*PotholeAnalyzor* to acquire research data from two smartphone sensors (e.g., GPS and accelerometer). Next, the

81

mobile collected raw data is preprocessed to clean, transform, and organize datasets before conducting analysis. Then, we make the first attempt to use CWT to analyze mobile sensed signals for identifying road anomalies and estimating their sizes. Finally, the detected bumps and potholes are confirmed and optimized by clustering crowd sensed results.
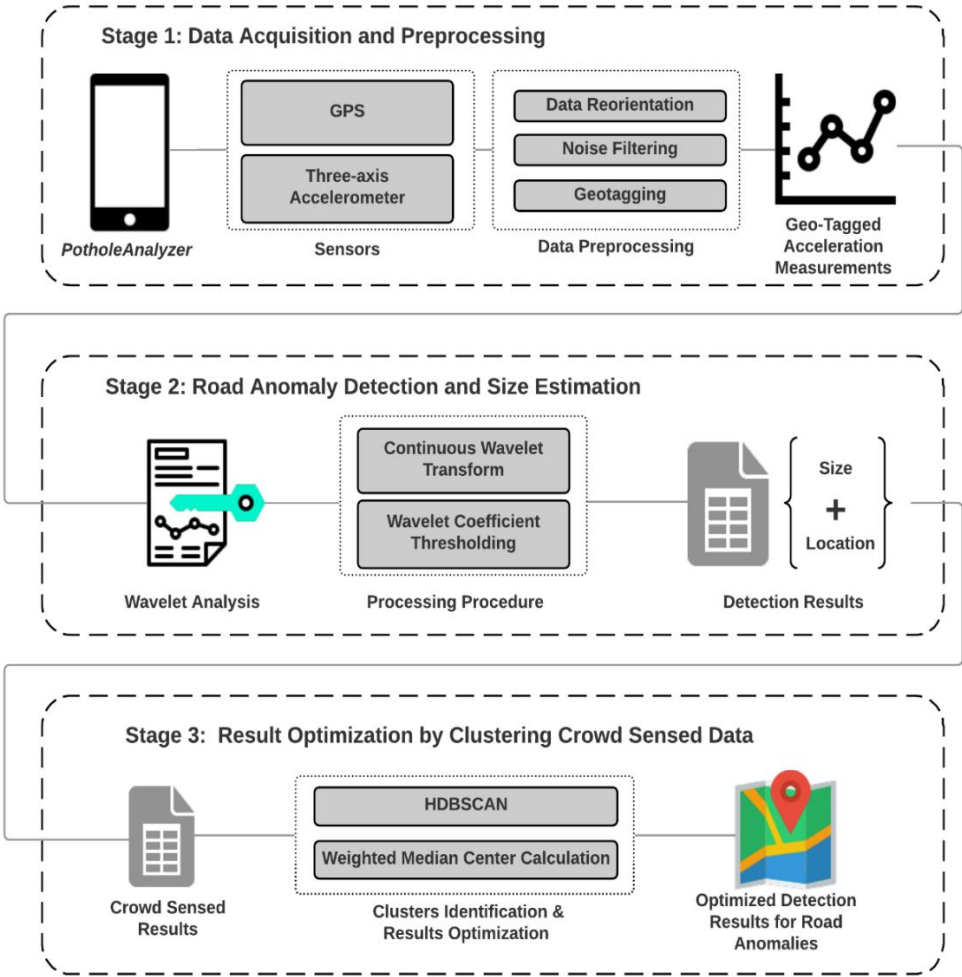
Figure 4.1 Research workflow.

4.2.1. Data Acquisition and Preprocessing

Studies have proven that smartphone accelerometer works well for capturing irregular vehicle vibrations when hitting potholes or bumps. By integrating with GPS data, we can geotag these abnormal acceleration signals, which can aid in identifying and locating road anomalies. In this study, we first create an Android-based mobile app—*PotholeAnalyzor* to collect data from smartphone accelerometer and GPS. The collected raw accelerometer's data is preprocessed through three steps: 1) data reorientation, 2) data smoothing, and 3) geotagging accelerometer's measurements using GPS data.

4.2.1.1. Mobile Sensor Data Collection

To obtain the mobile sensors' data, we create an Android-based mobile app—*PotholeAnalyzor* using Android application program interfaces (APIs). *PotholeAnalyzor* can record real-time sensed accelerometer measurements, timestamps, and GPS coordinates. Please note that smartphones must be fixed on the vehicle using smartphone holders during data collection, which can avoid some noises caused by devices sliding.

Accelerometer measures both the real acceleration force and earth gravity. To eliminate the influence of earth gravity, Android provides a linear acceleration sensor, which isolates and removes the force of gravity from accelerometer measurements using a low-pass filter and a high-pass filter. Refer to ("Motion Sensors" n.d.; Li and Goldberg 2018) for a detailed explanation.

This study analyzes linear accelerometer measurements to detect road anomalies. The sampling rate of the accelerometer is set to 100 Hz while GPS is set to 1 Hz. Figure

4.2 shows the app's user interface, which contains a dynamic chart showing the z-axis

acceleration and a Google Maps visualizer tracking the driving path using GPS. There

are some similar iOS-based apps such as CrowdSensor that can be installed on iPhones.

Figure 4.2 The user interface of *PotholeAnalyzor*.

4.2.1.2. Data Reorientation

Smartphone accelerometer can measure movement in three axes. To ensure the

effectiveness of mobile sensed acceleration for capturing vehicle jerks while hitting

potholes, data reorientation needs to be implemented to align the accelerometer's axes

with the vehicle's axes—x-axis and y-axis of the accelerometer should be used to measure the horizontal movement of the vehicle; z-axis should be perpendicular to the vehicle and senses its vertical vibration, which are directly caused by road anomalies (Sattar, Li, and Chapman 2018). Euler Angles have been widely proven effective for reorienting accelerometers. In this study, we reorient the accelerometer measurements through Euler Angles as follows (Astarita et al. 2012; Johnson and Trivedi 2011):

$$\alpha = \tan^{-1}\left(\frac{a_y}{a_z}\right), \beta = \tan^{-1}\left(\frac{-a_x}{\sqrt{a_y{}^2 + a_z{}^2}}\right), \tag{4.1}$$

$$a_x' = \cos\beta \times a_x + \sin\beta \times \sin\alpha \times a_y + \cos\alpha \times \sin\beta \times a_z, \tag{4.2}$$

$$a_y' = \cos\alpha \times a_y - \sin\alpha \times a_z, \tag{4.3}$$

$$a_z' = -\sin\beta\, a_x + \cos\beta \times \sin\alpha \times a_y + \cos\beta \times \cos\alpha \times a_z, \tag{4.4}$$

where α and β are two Euler Angles, roll and pitch, $a_x,\ a_y,\ a_z$ are the raw accelerometer measurements along three axis, and a_x', a_y', a_z' are the reoriented three-axis accelerations.

4.2.1.3. Data Smoothing

Removing data noise is an essential step in signal analysis. Mobile sensed measurements inevitably contain noises. In this study, we implement a high-pass filter to wipe off noises and enhance signal patterns, which is conducted as:

$$y_i = \theta \times y_{i-1} + \theta \times (x_i - x_{i-1}), i \in [1, n-1], \tag{4.5}$$

$$\theta = \frac{t}{t + dT}, \tag{4.6}$$

where x_i is the ith raw sample data, y_i is the ith smoothed data, t is the current time tag, dT is the event delivery rate, n is the number of samples, which refers to the number of z-axis accelerometer measurements in this study.

Figure 4.3 shows the comparison between raw data and processed data, which indicates noises can be efficiently eliminated with an enhanced data pattern after filtering.
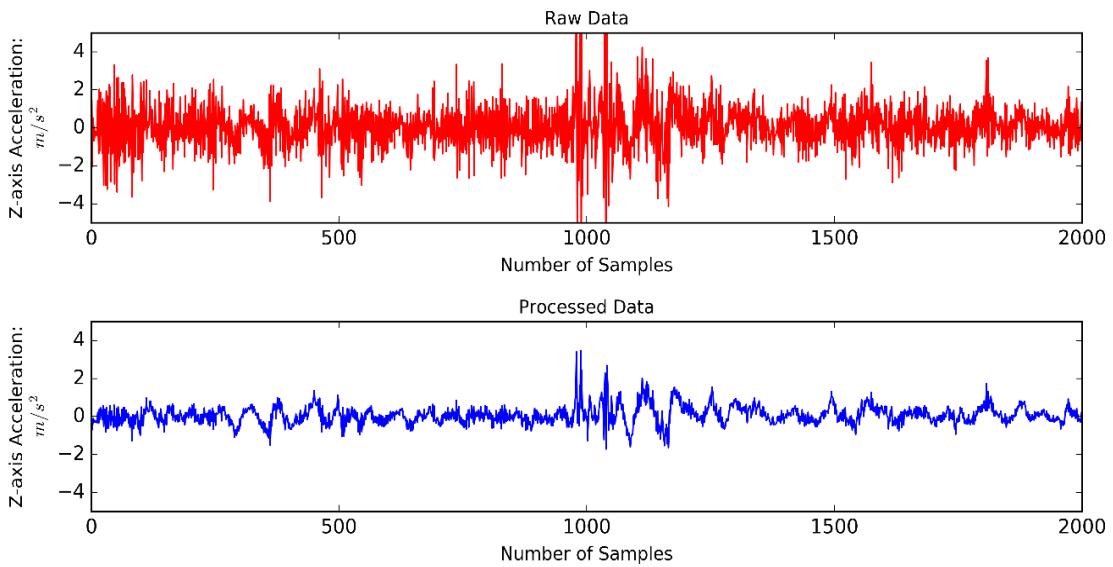
Figure 4.3 Comparison between raw data and processed data.

4.2.1.4. Geotagging

The sampling rates of GPS (1 Hz) and accelerometer (100 Hz) are quite different. To identify the locations of road anomalies, we need to geotag each accelerometer measurement by leveraging GPS readings. In this study, we adopt a scheme proposed in

(Li et al. 2019) to integrate these two sensors' data. First, the original GPS readings (latitude, longitude, height) are transformed into earth-centered earth-fixed (ECEF) coordinates (x, y, z). Then, we find two temporal-nearest GPS readings for each accelerometer measurement by matching their timestamps. Last, the accelerometer measurement can be geotagged through a linear interpolation scheme based on its temporal distance to its two nearest GPS points.

$$x = x_0 + \frac{(t - t_0)(x_1 - x_0)}{(t_1 - t_0)},$$

$$y = y_0 + \frac{(t - t_0)(y_1 - y_0)}{(t_1 - t_0)}, \tag{4.7}$$

$$z = z_0 + \frac{(t - t_0)(z_1 - z_0)}{(t_1 - t_0)}$$

where (x, y, z) is the calculated ECEF coordinates for the accelerometer measurement with a timestamp t, (x_0, y_0, z_0) and (x_1, y_1, z_1) are two consecutive GPS readings with timestamps t_0 and t_1, which are temporally nearest GPS points to the acceleration measurement.

4.2.2. Road Anomaly Detection and Size Estimation

From a digital signal perspective, each piece of accelerometer recording is a sum of multiple signals with varying frequencies and amplitudes. Therefore, spectral analysis can be very useful in decomposing this type of data and identifying unique frequency components that are indicative of surface roughness or irregular locations. Fourier analysis and wavelet analysis are the two most popular frequency-based approaches. The use of Fourier analysis in road surface roughness characterization (Sayers, Gillespie, and

Queiroz 1986; Hayhoe 2009), however, suffers from a major limitation which is the lack of association between the spatial domain and the frequency domain, such that locating a certain spectral anomaly on the distance profile is difficult with Fourier analysis. Wavelet analysis, on the other hand, is a superior option because it does not only reveal the frequency components of the road profile but also identify where a certain spectral anomaly exists in the spatial domain. Previous applications of wavelet analysis in this field have yielded satisfactory results in road roughness assessment and the detection of surface irregularities, e.g., (Wei, Fwa, and Zhe 2005). In this study, we extend this application and discuss the use of wavelet analysis in pothole detection and pothole size estimation.

4.2.2.1. Continuous Wavelet Transform

We detect potholes and estimate their sizes by performing the continuous wavelet transform on the preprocessed data. We chose CWT over the discrete wavelet transform (DWT) because CWT results are easier to interpret given that CWT operates at every scale (frequency) and the shifting of the wavelet function is continuous. The one-dimensional CWT is defined as (Daubechies 1992):

$$C(a, \tau) = \int_{-\infty}^{\infty} f(x) \frac{1}{a} \psi^* \left(\frac{x - \tau}{a} \right) dx, \tag{4.8}$$

where C is the output wavelet coefficient, $f(x)$ is the preprocessed input signal as a function of location x, a is the scale parameter (inversely related to spatial frequency), τ is position parameter and ψ^* is the complex conjugate of the mother-wavelet function that is chosen based on the feature of interest.

In this study, we use order 3 Daubechies wavelet (DB3) as the mother-wavelet (Figure 4.4) which is recommended by (Wei, Fwa, and Zhe 2005). There is a correspondence between wavelet scales and frequency, such that a smaller scale corresponds to a compressed wavelet, which is high in frequency, while larger scales correspond to a stretched wavelet, representing lower frequency. As defined in Equation 4.8, a wavelet coefficient is a function of both wavelet scale and position. Scale controls the compression or stretching of the wavelet and position controls the shifting of the wavelet function. For each scale (corresponds to a certain degree of wavelet compression or stretching), the wavelet examines every location on the input signal by continuously moving along the distance axis. Therefore, the final output is a two-dimensional matrix in scale (frequency)-location space, which is then converted to a matrix of percentage of energy (the sum of all elements in the matrix equals to 1).
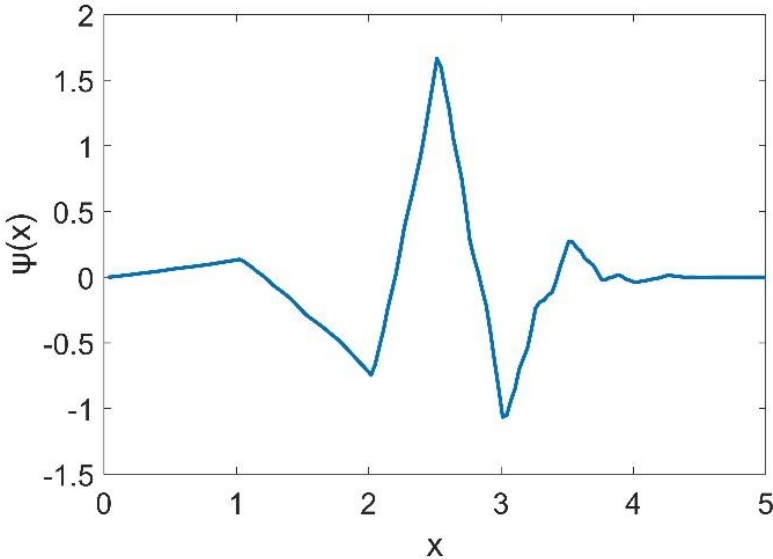
Figure 4.4 The order 3 Daubechies wavelet (DB3).

CWT produces high wavelet coefficient values at scales where the oscillation in the wavelet correlates best with the signal feature. With a proper choice of mother-wavelet that approximates the target signal (in this case, our target signal is the accelerometer recording when hitting a pothole), the wavelet coefficient image will highlight the target location at the right scale (Figure 4.5).
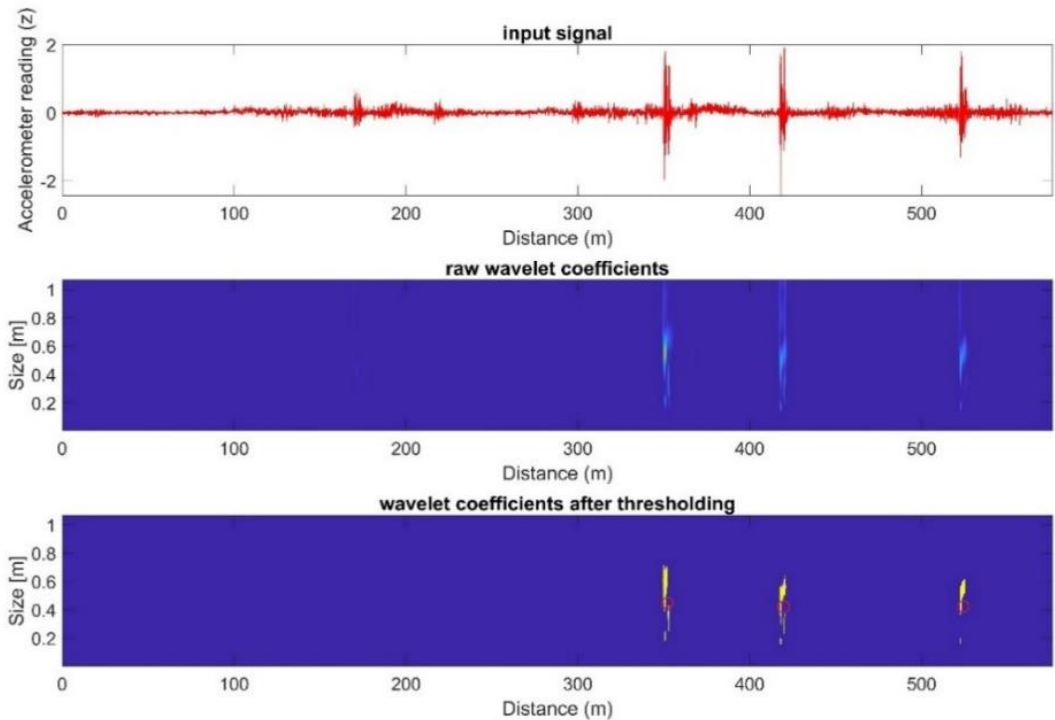
Figure 4.5 Wavelet analysis results.

4.2.2.2. Pothole Size Estimation

CWT generates a high value response when the wavelet shifts to a pothole location (Figure 4.5).

90

The raw wavelet coefficient images, however, do not come with a meaningful scale that corresponds to pothole size and usually capture irrelevant information such as random road noise and the vibration of the engine. Therefore, we further process the wavelet coefficient images with these following steps:

1) Convert the unitless wavelet scales to physical scales in meters using the algorithm provided by MATLAB Wavelet Toolbox (Misiti et al. 2015).

2) Multiply the scale axis by a scaling factor, which relates the converted wavelet scales to the sizes of target. This scaling factor is determined by field experiments at a test site and is kept as a constant unless the data acquisition platform is changed (in this study, we get a value of 0.3 for generic vehicles including sedan and SUV).

3) Clean the wavelet coefficient images by thresholding (only keep values that are greater than N times of overall average, and in this case, we use $N = 18$).

4) Apply 2-D Gaussian filter to remove noise and combine detections that correspond to the same pothole. Then the center of each highlighted zone is considered as the center of a detected pothole.

5) Get the size estimation for each detected pothole (highlighted zones on the wavelet coefficient image).

The final result contains two pieces of information: pothole location (step 4) and pothole size (step 5). It is necessary to state that the choice of scaling factor and threshold value may subject to change in other data acquisition settings, because the signals can be influenced by the coupling between road and vehicle. For example, the

data acquired by a pickup truck with a large tire and harder suspension may require a different set of processing parameters. Also note that since mobile device mainly measures vehicle vibrations along driving path, we only estimate the maximum driving-dimensional length of road anomalies in this study. Here, the driving-dimension of anomalies is parallel to the road driving direction, as illustrated in Figure 4.6.

Figure 4.6 Illustration of the measuring dimension for road anomalies.

4.2.3. Result Optimization by Clustering Crowd Sensed Data

Using smartphone sensors to detect vehicle jerks is a high-efficient solution to identify road anomalies; however, it also has some significant drawbacks. For example, the detection result purely depends on if the vehicle kicks up road anomalies. But vehicle

wheels only run over a smart portion of pavement surface, which significantly limits the detection coverage. Meanwhile, a single user's detection result can be influenced by various factors, such as vehicle models, phone models, driving skills, etc. Therefore, in this study, we implement a crowdsensing solution to optimize the detection results by mining public contributed data. We hypothesize that the significant similarities among crowd sensed data could be used to obtain more reliable detection results than single user's results.

In this study, we innovatively implement spatial clustering methods to group crowd sensed results into clusters based on their similarities. Then, each cluster's member points are further synthesized to form a unique point using weighting schemes, which represents a confirmed road anomaly.

4.2.3.1. Density-Based Clustering

Density-Based Spatial Clustering of Applications with Noise (DBSCAN) has been extensively utilized to analyze spatial patterns, which can effectively identify concentrated points (clusters) and discrete points (noises) (Esri 2019; Ester et al. 1996). Implementing DBSCAN requires two parameters, including 1) minimum points to form a cluster (C_{min}) and 2) search distance (d) to define neighbors. The clustering procedure can classify data points into three classes, including (Ester et al. 1996):

- **Core point**—a point which has at least C_{min} neighbors—points within the d distance to the tested point are counted as its neighbors.

- **Border point**—a point which is counted as a neighbor to core points but doesn't have sufficient its own neighbors (less than C_{min}).

- **Noise point**—a point which is neither a core point nor a border point.

The clustering procedure of DBSCAN contains the following main steps:

1) Choose a random sample point from the dataset as a starting point (p).

2) Identify the neighbors of p using a customized search distance.

3) If p was a core point, it would be marked as visited, a cluster would be formed with the core point and all its connected points. Connected points include p's neighbors and all reachable points (within a d radius) of its neighbors.

4) If p was not a core point, DBSCAN would retrieve an unvisited point from the dataset as a new starting point and repeat the process.

5) The process will end until all points are marked as visited or all points are assigned to a cluster.

Hierarchical DBSCAN (HDBSCAN) is an enhanced density-based clustering method proposed by Campello et al in 2013 (Campello, Moulavi, and Sander 2013). This method integrates DBSCAN with hierarchical clustering algorithm, which significantly extends the ability of DBSCAN to identify clusters of varying densities. As one of the most data-driven clustering methods, HDBSCAN only has one required parameter C_{min}. One prominent advantage of HDBSCAN is that it can generate probability scores for the sample points. The probability score indicates the likelihood of a point to be involved in a cluster. Refer to ("How HDBSCAN Works" n.d.) for a detailed explanation of HDBSCAN.

In this study, we implement HDBSCAN to group the crowd sensed road anomalies. Each identified cluster is recognized as a unique road anomaly. Meanwhile,

this process can also aid in filtering out low-quality public detected results though a simple procedure—points labeled as noises or with low probability scores are eliminated from the clustering result.

4.2.3.2. Weighting Schemes

After removing the low-quality crowd sensed data, we utilize two weighting schemes to synthesize each cluster's members into one data point. First, we calculate the weighted median center for each cluster to represent the locations of final determined anomalies. Median center is the location which minimizes the distance to all features in a group. Median center is less influenced by outliers than the mean center, which is a more reliable measure of central tendency (J. Lee and Wong 2001). Mathematically, median center needs to satisfy the following objective function (J. Lee and Wong 2001):

$$\text{Min} \sum_{i=1}^{n} w_i \sqrt{(x_i - u)^2 + (y_i - v)^2}, \tag{4.9}$$

where x_i and y_i are coordinates of the ith point, u and v are coordinates of weighted median center, w_i is the weight of the ith point, which refers to the probability score in this study, and n is number of points.

Meanwhile, a weighted average scheme is used to optimize the size estimation result for each cluster.

$$S_{opt} = \frac{\sum_{i=1}^{n} s_i w_i}{\sum_{i=1}^{n} w_i}, \tag{4.10}$$

where n is number of points in a cluster, s_i the estimated size of the ith point, w_i is the weight of the ith point, which refers to the probability score in this study, and S_{opt} is the recalculated size for each cluster.

Through these two weighting schemes, we can effectively leverage crowd sensed data to obtain an optimized detection result.

4.3. Experiments and Results

This section details our experiments, data analyses, and result validation.

4.3.1. Experiment Settings

To verify the effectiveness of our method, we manually collected 24 road anomalies from two parking lots at Texas A&M University. These anomalies were positioned through a high-accuracy hand-held GPS. Meanwhile, we carefully measured each pothole's driving-dimensional length using a ruler to form a ground-truth dataset. Figure 4.7 illustrates the spatial distribution of the obtained ground truth data.
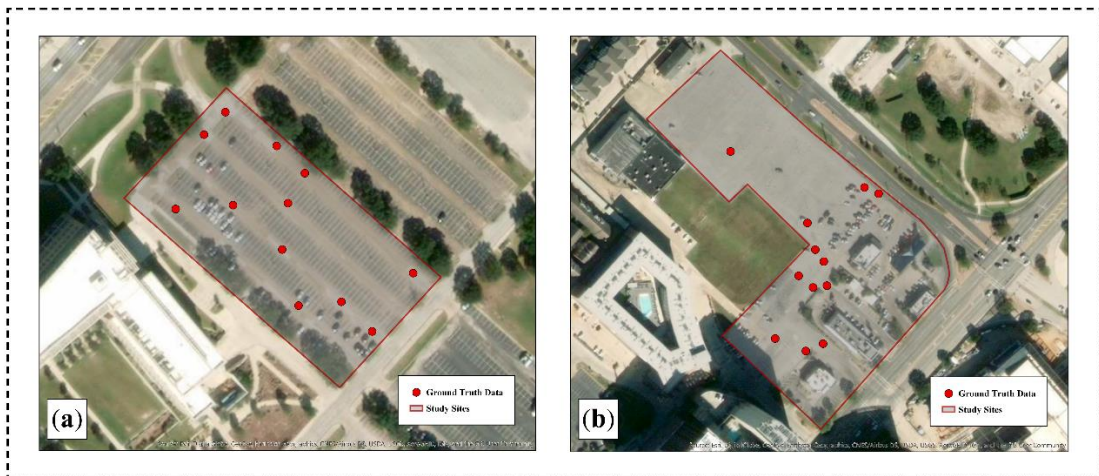
Figure 4.7 Study sites: (a) parking lot 1; (b) parking lot 2.

Table 4.1 Experiment Settings.

	Lot 1	Lot2
Data acquisition time	02/24/2019 2:10 pm	06/01/2019 11:10 am
Road anomalies	12 potholes	8 potholes and 4 bumps
Vehicles models	2009 Toyota Corolla & 2009 Toyota RVA4	2009 Toyota Corolla & 2009 Toyota RVA4
Phone models and apps	Moto X Pure: *PotholeAnalyzor* iPhone 8: *CrowdSense*	Moto X Pure: *PotholeAnalyzor* iPhone 8: *CrowdSense*
Sensors sampling rates	Accelerometer: 100Hz GPS: 1Hz	Accelerometer: 100Hz GPS: 1Hz
Driving tests	2 drivers. Driver 1: test 3 times using Moto X Pure. Driver2: test 2 times using iPhone 8.	2 drivers. Driver 1: test 3 times using Moto X Pure. Driver2: test 2 times using iPhone 8.
Ground Truth Acquisition	Manually collected with GARMIN GPSMAP 78 and ruler.	Manually collected with GARMIN GPSMAP 78 and ruler.

Table 4.1 shows our experiment settings. In this study, we tested each parking lot five times by two different drivers, with approximately 30 km/h driving speed. One driver drove a 2009 Toyota Corolla with a Moto X Pure phone running our *PotholeAnalyzor* to detect each parking lot three times. Another driver drove a 2009 Toyota RVA4 with an iPhone 8 running a similar iOS app *CrowdSensor* to detect each parking lot twice. Drivers' explicit permission was required before collecting sensors' data. The sampling rates of accelerometers for both phones were set to 100 Hz. GPS was set to 1 Hz. Through increasing the variability of the experiment (such as drivers,

phones, vehicles, etc.), we were able to effectively assess the performance of our method for processing crowd sensed data.

4.3.2. Wavelet Analysis Results

After data collection, we first eliminated the noise of Z-axis acceleration data and geotagged each data point using GPS readings. Then, we analyzed the processed Z-axis acceleration series to identify road anomalies and measure their sizes.

As illustrated in Figure 4.5, the upper subplot shows the input signals—preprocessed Z-axis acceleration. Then, we performed CWT on the signals to calculate its similarity with mother wavelet at continuous scales, as shown in the middle subplot. The lower subplot shows the filtered high wavelet coefficients, which indicates the high possibility that an anomaly exists with a specific size. The red circles indicate the location and size of ground truth points. Results demonstrated that wavelet analysis can efficiently identify, locate, and measure abnormal signals caused by hitting road anomalies.

4.3.3. Optimized Detection Results by Mining Crowd Sensed Data

After obtaining detection results from each driving test, we implemented HDBSCAN to group the ten times detection results (five times for each study sites) based on their similarities, which can aid in eliminating low-quality public contributed data and enhancing detection accuracy.
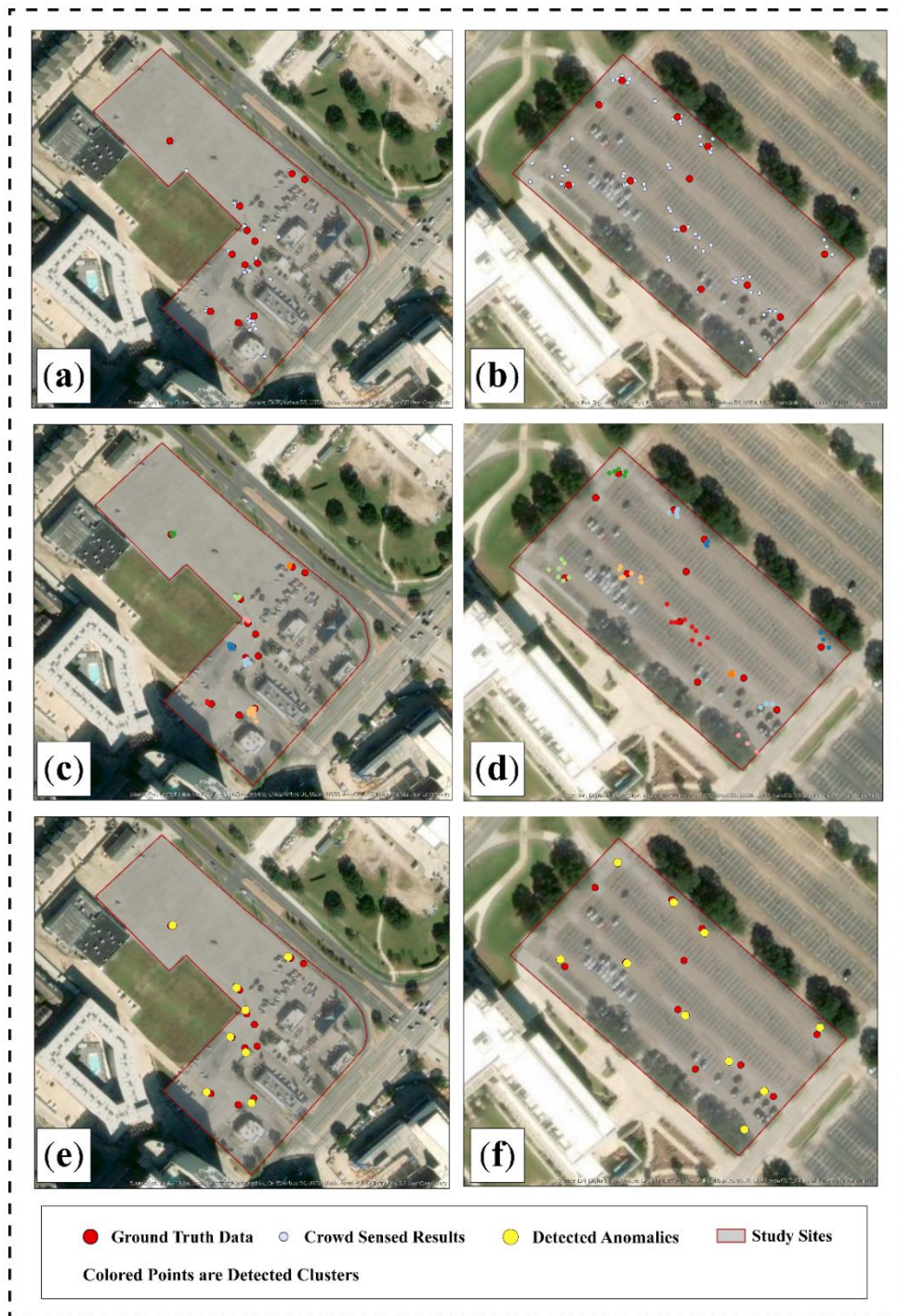
Figure 4.8 Crowd sensed data integration results: (a) and (b) are detection results of five driving tests for two study sites; (c) and (d) show the clustering results after eliminating low-quality contributed points; (e) and (f) are the optimized detection results by synthesizing each clusters' member points.

Figure 4.8a and Figure 4.8b illustrate detection results obtained from five driving tests for both study sites. These two subplots show that some detected anomalies are concentrated around ground truth points; however, there are some detected points with a relatively far distance to ground truth points. It implies that the detection results obtained from one single driving test is not reliable.

To optimize our results, we first implemented HDBSCAN on the five times detection results to form clusters. HDBSCAN can automatically group sample points into clusters or noises based on their spatial density patterns. Meanwhile, it also generates a probability score for each point, indicating its likelihood of being involved in a cluster. In this study, clustering noises and cluster member points with low probability scores (less than 0.5) were regarded as low-quality contributed points and eliminated from the detection results. Figure 4.8c and Figure 4.8d show the clustering results for both study sites after eliminating low-quality contributed points. Through this procedure, some points with a far distance to the cluster centers can be successfully removed. Finally, we calculated the weighted median center for each cluster to synthesize multiple contributed points into one point, which represents the optimized location of a detected road anomaly. Figure 4.8e and Figure 4.8f show that the optimized detection results (yellow dots) can perfectly match with ground truth points (red dots). Meanwhile, we also used a weighted average scheme based on cluster probability scores to recalculate the driving-dimensional size for each final confirmed road anomaly.

4.3.4. Result Evaluation

To better evaluate the performance of this enhanced crowdsensing solution in road anomaly detection, we compared our method with a widely utilized threshold-based method—Z-THRESH (Method 1) (Mednis et al. 2011) and a preliminary crowdsensing approach proposed by Li et al. (Method 2).

- Method 1: Z-axis accelerometer measurements exceeding $0.4g$ m/s^2 are counted as road anomalies.

- Method 2: An improved threshold-based detection method integrated with a simple crowdsensing strategy—anomalies need to be reported by more than three users before finally confirmed. The location for the confirmed anomaly is calculated by averaging all the contributed points.

Since Method 1 does not mention how the crowd sensed data was synthesized, we integrated the same crowdsensing strategy used in Method 2 to Method 1 for fusing five driving tests' results. In this study, we compared these two methods with our enhanced solution in terms of detection efficiency and position accuracy.

The detection efficiency is evaluated from three perspectives:

1) Precision: Correctly detected anomalies (N_{CDA}) / Total detected anomalies.

2) Recall: Detected ground truth points (N_{DGT})/ Total ground truth points.

3) Detection Redundancy: (N_{CDA} - N_{DGT}) / (N_{CDA})

In this study, the detected anomalies within a 10-meter radius to any ground truth points are counted as correctly detected anomalies. For each ground truth point, if it can match with any detected anomalies within a 10-meter radius, it would be counted as

detected ground truth points. Please note each ground truth point may be matched with more than one detected anomaly; therefore, we also checked detection redundancy for each method.

Meanwhile, we calculated the distance between detected anomalies to their corresponding ground truth points to compare the positioning accuracy while performing different methods.

Table 4.2 represents the comparison results among these three methods. The results demonstrate that the proposed enhanced crowdsensing solution achieved the highest precision value (94.44%), which is far superior to the other two methods (43.90% and 64.71%). Our approach also achieved the same recall value compared to Method 2. Moreover, by applying spatial clustering methods, we can dramatically synthesize crowd sensed points into high-reliable detection results with no redundant detected anomalies and higher positioning accuracy.

Table 4.2 Performance Comparison Among Three Methods.

		Method 1	**Method 2**	**Our Method**
Detection Efficiency	Precision	43.90%	64.71%	94.44%
	Recall	66.67%	70.83%	70.83%
	Detection Redundancy	11.11%	22.22%	00.00%
Positioning Accuracy (meter)	Min	0.60	0.73	0.58
	Mean	3.47	4.07	3.29
	Max	9.88	7.27	6.21
	STEDV	2.58	2.41	1.56
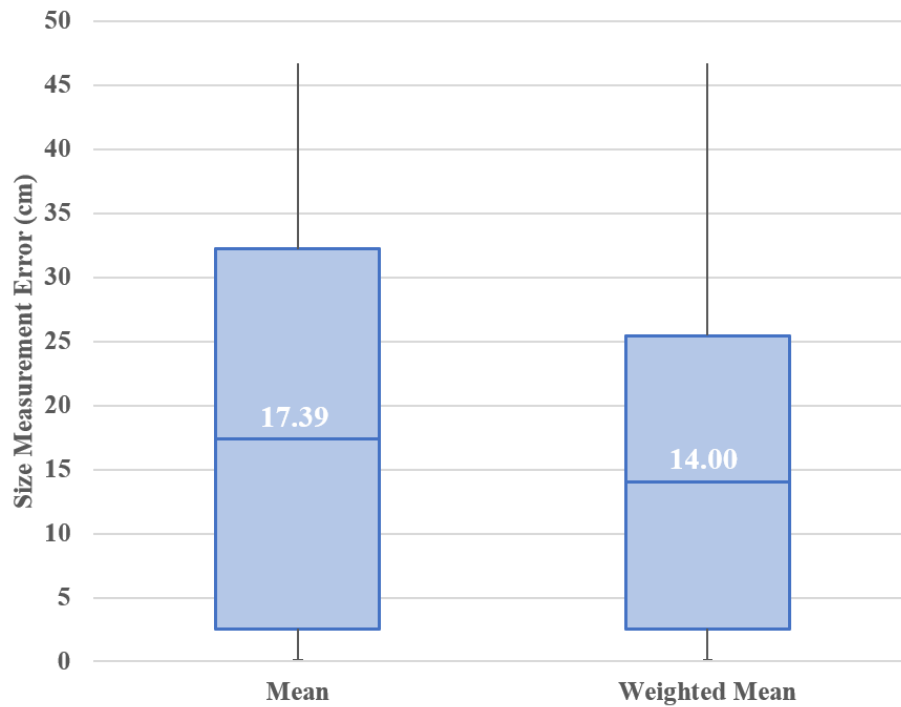
Figure 4.9 Result evaluation for anomaly size estimation.

More importantly, this study added a new dimension to road anomaly detections to estimate the driving-dimensional size for each road anomalies. In this study, we used two methods to synthesize the size estimation results of cluster member points into one final result. One is to average all member points' estimation values. Another is to calculate the weighted mean based on the cluster probability scores of each member point. Figure 4.9 shows the size estimation results by implementing these two methods. The centerline of the box represents the mean value of estimation errors. The box upper and lower bounds represent the mean plus and minus standard deviation, respectively. This figure indicates that our method can effectively estimate the driving-dimensional size for road anomalies with an acceptable detection error. Meanwhile, the weighted

mean shows a lower mean error and a smaller standard deviation in Figure 4.9. It indicates that using the weighted average scheme can better synthesize crowd sensed than calculating the average.

4.4. Discussion and Conclusion

Road anomaly detection is of great importance in road maintenance and management. Continuously monitoring road anomalies with a low-cost and high-efficiency solution is a fundamental social need; however, it remains to be a complicated and unsolved research task.

In this study, we proposed an enhanced crowdsensing approach to detect road anomalies and measure their sizes using smartphone sensors. Different from existing studies, we made the first attempt to utilize continuous wavelet transform to analyze mobile sensors' measurements. Results demonstrated that wavelet analysis outperforms conventional threshold-based methods, which can more effectively identify abnormal vehicle vibrations when hitting road anomalies through analyzing mobile sensed data. Meanwhile, it can also estimate the driving-dimensional size of bumps and potholes based on the calculated wavelet coefficients. Moreover, we innovatively utilized a spatial clustering method to synthesize crowd sensed results based on their spatial density patterns. Experiments demonstrated that this enhanced crowdsensing solution could accurately detect road anomalies (94.44%) with a high positioning accuracy (within 3.29 meters in average) and an acceptable size estimation error (with a mean error of 14 cm).

The proposed solution is efficient to detect road anomalies; however, there are still some limitations to be addressed in future work, including:

1) **Propose a new anomaly size estimation solution.** In this study, we only estimate the driving-dimensional size of road anomalies. In fact, the depth of potholes is also a critical factor for assessing pothole damages. In future work, we will propose a better solution to measure road anomaly size.

2) **Improve the performance of crowdsensing solution.** Using spatial clustering methods can efficiently eliminate low-quality contributed data points and optimize detection results. However, the density-based clustering method may mis-cluster two neighboring potholes into the same group, which could influence the detection accuracy. In future work, we will further investigate how to synthesize crowd sensed data with further improved accuracy.

3) **Put forward a real-time road anomaly detection system.** Drivers can sense road surface using smartphones at real-time. With a certain number of reliable data contributors, we can potentially update road detection results on a daily, or even hourly basis. In future work, we will put forward a real-time road anomaly monitoring system by leveraging mobile crowd sensed data.

Leveraging crowd sensed data to detect road anomalies could substantially improve the effectiveness of traditional road monitoring systems. It can continuously monitor road surface condition with little additional economic cost. It is worth noting that some technical barriers exist, which limits the implementation of crowdsensing solutions at the current stage. For example, mobile crowdsensing is significantly

constrained by smartphone hardware. Low-quality mobile sensors' data may lead to

unreliable detection results. Collecting mobile sensors' data at a high sampling rate can

drain phone battery in several hours, or even faster. However, fueled by the rapid

development of mobile sensing technique, this proposed solution remains to be

promising and more efficient in the foreseeable future.

5. ENHANCING DRIVING SAFETY: DISCOVERING INDIVIDUALIZED HAZARDOUS DRIVING SCENES USING GIS AND MOBILE SENSING[*]

5.1. Introduction

Can driving safety be improved? This has been a frequently asked question for over decades in the automobile industry and academia. Road traffic collisions have been socially acknowledged as an extremely severe threat to public health. According to the World Health Organization's statistics, vehicle crashes represent the leading cause of death among young adults (15-59 years) and the eighth cause of death globally (World Health Organization 2018). The U.S. National Highway Traffic Safety Administration estimates that ninety-four percent of U.S. traffic collisions are caused by human error such as speeding, sharp turns, and hard brake (The U.S. National Highway Safety Administration 2015). Accordingly, detecting and geo-analyzing driving mistakes can be an extremely promising solution to enhance traffic safety and require immediate attention.

Aggressive driving behaviors have been shown to have a significant positive correlation with traffic collisions, which exposes both the driver and other road users to potential collision risks (Nataanen and Summala 1976; World Health Organization 2018; J. D. Lee 2008; Xi et al. 2016). To better assess one's driving behavior, in-vehicle

---

sensing techniques have been widely adopted to collect and analyze various driving-related data (Boyce and Geller 2002; Jensen, Wagner, and Alexander 2011; Toledo, Musicant, and Lotan 2008). However, these in-vehicle sensing platforms are typically very costly and only commercially available, which directly limits their applicability to the public. Driving behavior recognition and assessment has begun to take hold in the research community thanks to the rapid development of mobile sensing in the past several years. The sensor-rich smartphones have become promising data collection and geo-computing platforms allowing us to achieve driving behavior profiling with limited user cost (Macias, Suarez, and Lloret 2013; R. Chen, Chu, Liu, Chen, et al. 2014; Li and Goldberg 2018). Since 2000, researchers have investigated the detection of dangerous driving behaviors using mobile-sensed data (Fazeen et al. 2012; Bergasa et al. 2014; Johnson and Trivedi 2011).

It is worth noting that the assessment of driving safety is a spatially complex and temporally dynamic process, which is also impacted by numerous behavioral factors. As early as 1996, Kim and Levine (1996) identified that the integration of driver behaviors and spatial characteristics as the key to understanding traffic collisions better. However, to date, the study of individual-based driving safety analysis has been limited, and the correlation between driving error occurrence and geospatial features are still underexplored. In this study, we innovatively integrate driving errors with driving-related geospatial features to discover hazardous driving scenes that characterize *when* and *where* drivers are prone to producing more driving errors.

5.1.1. Related Work

Numerous studies have been conducted to address traffic collisions related concerns such as: identifying collision concentrations, looking for significant contributing factors, predicting collision likelihood at a specific location. Among these studies, Geographic Information Science (GIS) plays an essential role not only in managing and manipulating traffic collision data but also in providing abundant spatiotemporal methods and theories for better understanding and facilitating traffic safety (Goodchild 1992). Since the 1990s, GIS-aided methods have begun to be utilized for analyzing traffic collisions because of the rapid spread and advancement of GIS techniques. Since then, GIS enabled traffic safety analysis has transitioned from storing and visualizing traffic collision points to modeling traffic risk scenarios (Levine, Kim, and Nitz 1995; Zhang and Virrantaus 2010; Plug, Xia, and Caulfield 2011; Harirforoush and Bellalite 2016; Anderson 2009; Yao, Loo, and Yang 2016). However, these existing geographic studies mainly focus on regional traffic safety analysis. The most influential component in traffic safety, driving behavior, is excluded from most of these geographic studies.

Driving behavior, as a crucial contributing factor, closely relates to road safety. Irregular driving behaviors such as speeding, drunken driving, and irregular overtaking not only threaten driving safety but also put pedestrians at significant risk (T. Chen, Zhang, and Xu 2016; J. D. Lee 2008; Manepalli and Bham 2013; Nataanen and Summala 1976). However, most prior studies did not take driving behavioral factors into account due to data acquisition difficulties. With the emergence of various sensor-rich

mobile devices, a growing number of studies have begun to focus on the detection of erratic driving behaviors extracted from mobile-sensed data (Johnson and Trivedi 2011; Castignani et al. 2015; Júnior et al. 2017).

Threshold techniques have been extensively used in driving errors detection. Chakravarty et al. (2013) created a mobile application (app) called *MobiDriveScore* to assess driving risk based on mobile-sensed data. 3-axis accelerometer and GPS data were utilized to capture and calculate the "jerk" energy caused by erratic driving behaviors such as hard cornering, stop, or acceleration. By comparing jerk energy with a preset threshold, these driving errors could be successfully detected. A similar study conducted by Zeeman and Booysen (2013) identified reckless driving patterns also through GPS and accelerometer. Different from (Chakravarty et al. 2013), driving events in this study were first pre-classified into urban driving and highway driving. Then operating speed and acceleration were considered to model jerk energy for each class. Threshold techniques were utilized to assess the acceleration peaks to determine if the peak value exceeded a "safe-driving" range.

Several studies have investigated the capability of Dynamic Time Warping (DTW) for driving behavior detection. Eren et al. (2012) proposed a cost-efficient and user-friendly system to estimate the driving behavior using smartphones. In this study, the built-in smartphone accelerometer and gyroscope were used to collect driving information. A smoothing algorithm was applied to remove noise in the data. An end-point detection algorithm was performed on the smoothed data to identify dangerous driving events. The DTW was then adopted to compare the detected event with the

110

training event. After the above process, a driving behavior was labeled as "safe" or "unsafe" using a Bayesian Classifier. Johnson and Trivedi (2011) created a similar mobile system called *MIROAR* to recognize aggressive driving events. This study integrated Endpoint Detection and DTW and applied them on sensor-fused data. Their results demonstrated that performing DTW on the integration of y-axis acceleration, x-axis gyroscope, and pitch could accurately detect aggressive driving events.

Machine Learning Analysis has also been tested for assessing driving behaviors (Hong, Margines, and Dey 2014; Meiring and Myburgh 2015; Júnior et al. 2017). Júnior et al. (2017) attempted to identify the best combinations of mobile sensors and machine learning algorithms (MLAs) to recognize aggressive driving behaviors. In this study, the researchers tested four different MLAs including Artificial Neural Networks, Random Forrest, Bayesian Network, and Support Vector Machine. 3-axis accelerometer, gyroscope, and magnetometer were used for data collection. Mobile-sensed data was transformed and used to generate attribute vector data sets for characterizing the driving behaviors over a sliding window. The attribute vectors were then used to train, test, and evaluate the performance of these four MLAs. The results demonstrated that accelerometer and gyroscope were the best combinations, and Random Forrest outperformed the other three MALs for driving behavior detection.

5.1.2. Knowledge Gaps

Through a careful study of the relevant literature, the following knowledge gaps were identified:

1) The conventional geographical studies have been built based upon the aggregated

111

data (e.g., average daily traffic volume, annual number of crashes, road network length, etc.) to examine a relatively macro-level geographic unit (e.g., counties, census tract, etc.). The individual-based traffic safety analysis remained lacking.

2) Most driving behavior detection has been conducted by employing threshold techniques or machine learning methods. However, the widespread use of threshold-based methods has been limited due to replication difficulties. Machine learning methods, on the other hand, usually require an extensive training process based on a massive volume of labeled data, which has been found laborious to collect and less efficient.

3) Studies have been carried out for understanding driving risk from different perspectives including road, driver, and environment. However, to date, there are still no solutions that can estimate driving risk by comprehensively synthesizing these different types of data.

5.1.3. Key Contributions

To address these gaps, we propose a new approach to discover individualized hazardous driving scenes by integrating driving errors with other spatiotemporal features (i.e., *when, where,* and *what*). In this study, an enhanced driving error detection method is created by using built-in smartphone sensors. The spatiotemporal distribution of dangerous driving behaviors is first characterized. Then, mobile-sensed driving errors are integrated with road networks and trajectory features (e.g., start point, end point, trip purpose, etc.), which can help track dangerous driving habits and depict individualized hazardous driving scenes.

Compared with previous studies, our contributions to enhancing driving safety are threefold:

1) **Integrating different types of driving-related data to address traffic risks:** Studies have demonstrated that driving behaviors significantly influence traffic safety; however, most of the prior studies did not consider them due to driving errors acquisition difficulties. This study innovatively integrates the driving errors detected from mobile sensed data with the road network and driving trajectories to achieve a more comprehensive road safety analysis.

2) **Proposing a new driving error detection method:** Different from conventional in-vehicle sensing platforms, this study explores the flexibility of using smartphone sensors to detect aggressive driving behaviors. A new multi-feature-fusion framework for driving errors detection is proposed, which can successfully capture the abnormal signals from the mobile sensed data and classify them into different types when performing aggressive driving behaviors.

3) **Conducting individual-based traffic safety analysis:** To the best of our knowledge, this study is among the first that focuses on individualized traffic safety analysis—depicting individualized hazardous driving scenes. Hazardous driving scenes refer to some combinations of factors which negatively influence an individual's driving performance and may vary across different drivers. Extracting individualized hazardous driving scenes can aid drivers better in understanding their driving errors and avoiding potential driving risks.

5.2. Methods

In this study, we develop an innovative approach to discover individualized hazardous driving scenes using GIS and mobile sensing techniques. The research progresses through three main stages including 1) driving error detection, 2) driving error scenic tuple construction, and 3) individualized hazardous driving scenes extraction. Through this workflow, we aim to effectively map driving errors and extract error-prone driving scenes to individual drivers, as illustrated in Figure 5.1. Three types of data sources are utilized in this study including smartphone sensors' data (3-axis accelerometer and gyroscope), driving trajectories generated from the smartphone GPS, and road network. In this section, we discuss the methods and data used in these three main stages sequentially. First, a new multi-feature-fusion framework for driving errors detection using smartphone accelerometer and gyroscope measurements is introduced. Then we illustrate a new approach - scenic tuple construction for representing the occurrence of driving mistakes. The detected driving errors are integrated with the road network and driving trajectory, which can aid in representing and characterizing the occurrence of each driving error. Lastly, a detailed explanation of hazardous driving scenes extraction is described. Two clustering methods, i.e., K-modes clustering and Hierarchical Clustering on Principal Components (HCPC) are utilized to investigate the significant similarities among an individual's driving errors through an in-depth analysis of a long-term collection of error scenic tuples.
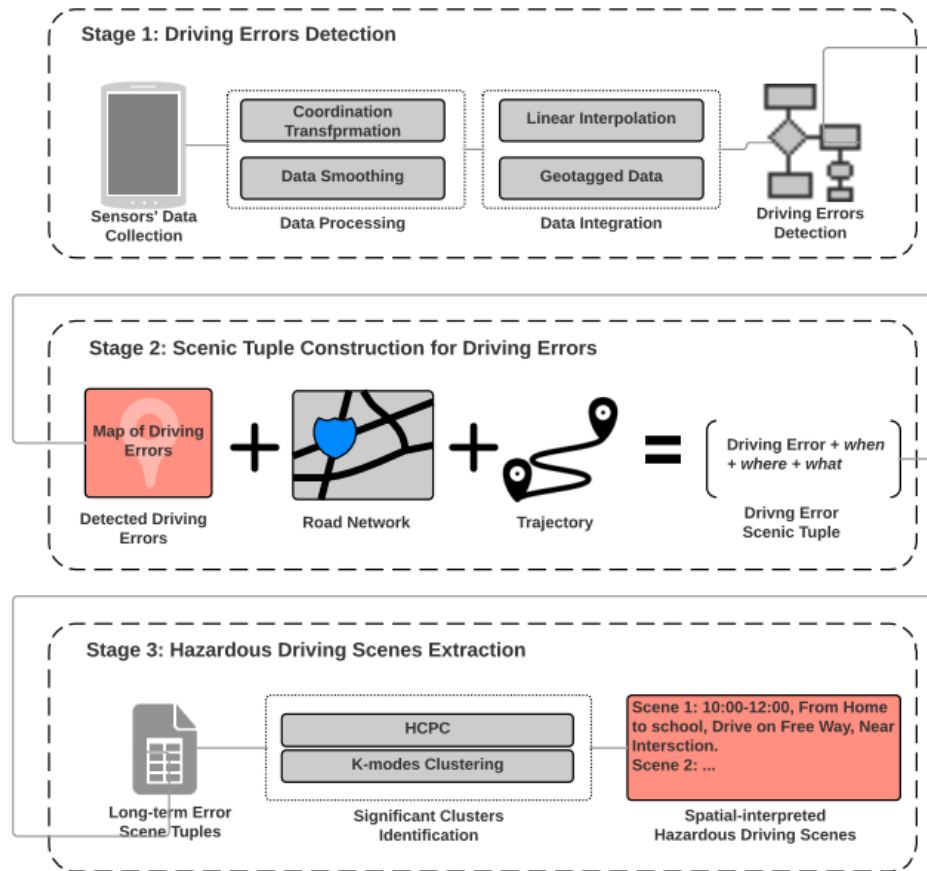
Figure 5.1 Research workflow.

5.2.1. Driving Error Detection

First, we put forward a multi-feature-fusion framework to extract driving errors from mobile-sensed data. Figure 5.2 illustrates the detection process which contains three steps: mobile sensors' data sampling and smoothing, data process (performing multi-feature-fusion framework on smoothed data), and data combination.
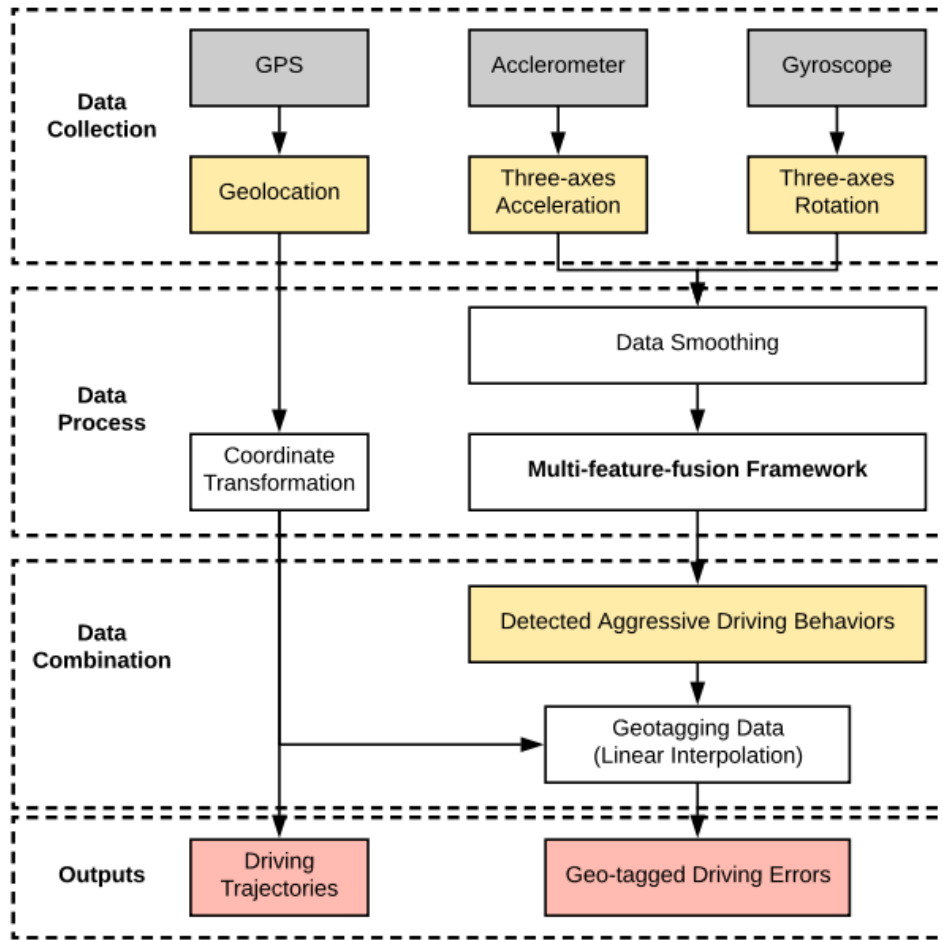
Figure 5.2 The flow chart of driving error detection.

5.2.1.1. Mobile Sensors' Data Sampling and Smoothing

In this study, we identify six types of aggressive driving behaviors including hard brake, fast acceleration, sharp left-turn, sharp right-turn, aggressive left-lane-change, and aggressive right-lane-change using smartphone GPS and sensors. Studies have demonstrated that aggressive driving behaviors (e.g., hard brake, sharp turn, fast acceleration, etc.) generate "jerk energy", which can be sensed and measured by mobile sensors, especially by the 3-axis accelerometer and gyroscope sensors with a high

116

sampling rate (50Hz-100Hz). In this study, these two smartphone sensors are utilized to capture vehicle jerks caused by driving errors. A smartphone is horizontally placed in a vehicle with its axes aligned with the vehicle's axes in the current version, which will be improved to achieve a constraint-free smartphone placement in future work. The accelerometer measures the vehicle's acceleration (m/s^2) in a 3-axis frame, which can effectively capture the "jerk energy". The gyroscope detects the vehicle's rotation (°/s) and aids in inferring turning events and lane changes (Hong, Margines, and Dey 2014; Meiring and Myburgh 2015; Júnior et al. 2017). The smartphone built-in GPS data is adopted to record driving trajectories and geotag detected driving mistakes, which is detailed in Sec 5.2.1.3. To better analyze the mobile-sensed data, a high-pass filter (Equations 5.1-5.2) is applied on each sensor's raw data to eliminate noise and highlight abnormal signals, as shown in Figure 5.3.
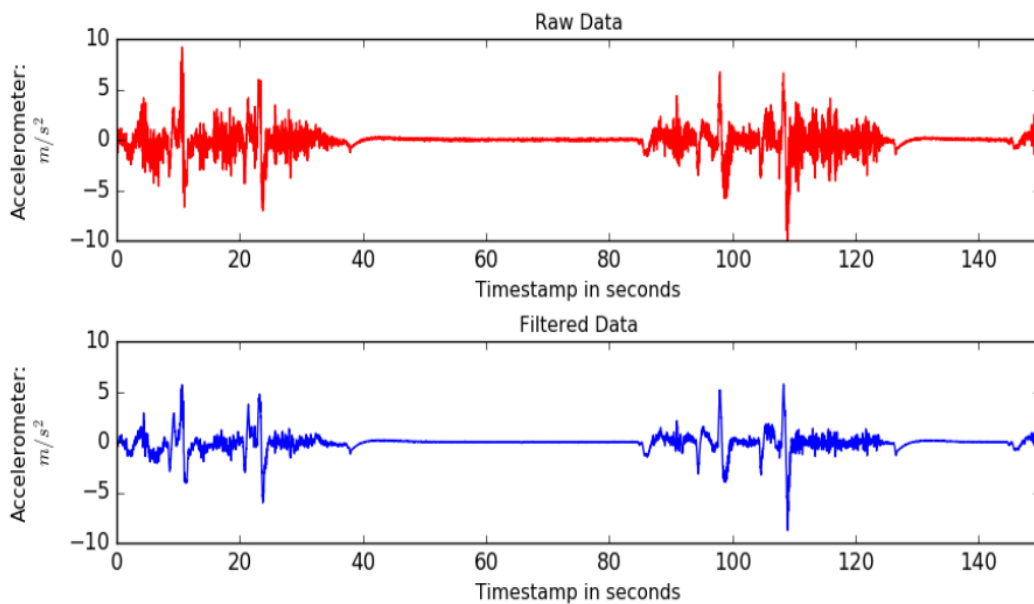
Figure 5.3 The comparison between raw data and filtered data.

$$y[i] = \alpha * y[i-1] + \alpha * (x[i] - x[i-1]), \quad i \in [1, n-1] \qquad (5.1)$$

where

$$\alpha = \frac{t}{t+dT} \qquad (5.2)$$

x[i] represents the *ith* sample data, *y[i]* represents the *ith* filtered data, *t* represents the

current time tag, and *dT* is the event delivery rate.

5.2.1.2. The Multi-Feature-Fusion Framework for Driving Error Detection

Figure 5.4 shows the sensor output from built-in smartphone accelerometer and

gyroscope when performing the pre-selected driving errors described above. This figure

illustrates that the "jerk energy" caused by aggressive driving behaviors can be

represented as sequential peak values on the sensor's data curve making it distinct from

other regular driving events. Further, different driving errors generate unique data

patterns, which can be captured by the accelerometer and gyroscope. In this study, we

quantitatively examine the mobile sensed data collected from the 3-axis accelerometer

and gyroscope from four perspectives to characterize the unique abnormal signals

generated by different aggressive driving behaviors:

1) Abnormal session: An abnormal session is defined as a session of accelerometer

   readings, which contains more than five sequential peaks (greater than 0.38g

   m/s^2) per second. Through empirical tests and the results of the prior work

   described above, 0.38g m/s^2 is used as the threshold peak value to separate

   driving errors from normal driving behaviors (Zeeman and Booysen 2013;

   Chakravarty et al. 2013; Júnior et al. 2017).

2) The mean value of Z-axis gyroscope (mean Z-gyro) readings: The Z-axis

118

readings of gyroscope directly reflects a vehicle's rotation caused by performing turn or lane change. Empirical tests show that sharp left-turns and aggressive left-lane-changes generate positive values for mean Z-gyro. Sharp right-turns and aggressive right-lane-changes generate negative values.

3) The duration of driving errors: The duration of lane-change is significantly shorter than other driving events (< 1.5 s).

4) The variation tendency of X-axis acceleration: The X-axis of the accelerometer aligns with a vehicle's X-axis and directly senses the acceleration of driving. The varying tendency can aid in differentiating accelerating and braking.
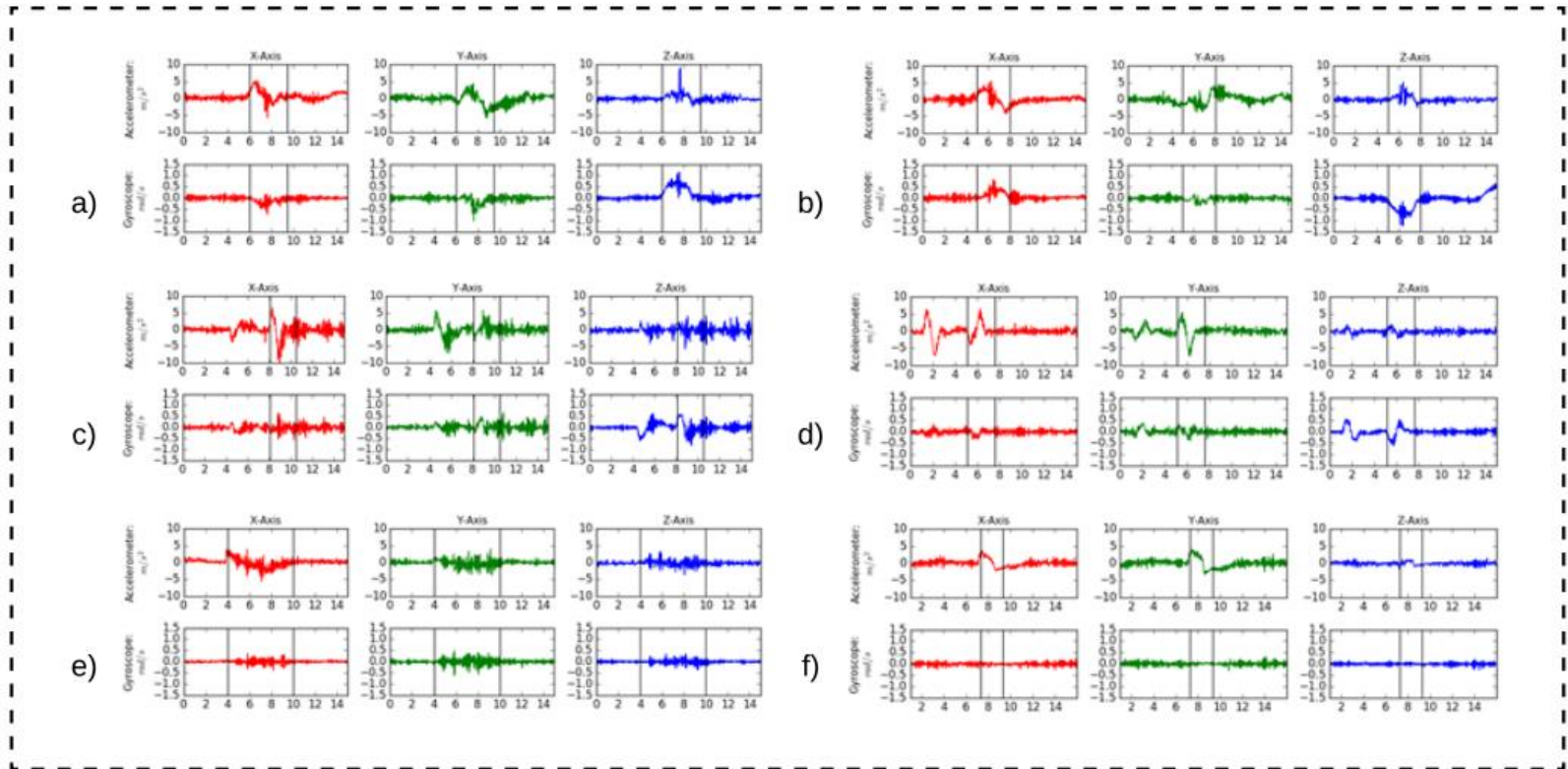
Figure 5.4 Samples of abnormal signals caused by driving errors gathered from 3-axis accelerometer and gyroscope (a: sharp left-turn, b: sharp right-turn, c: aggressive left-lane-change, d: aggressive right-lane-change, e: fast acceleration, and f: hard brake).

Table 5.1 summarizes the features of aggressive driving behaviors extracted from the mobile-sensed data. By analyzing and combining these features, a multi-feature-fusion framework is created for labeling the types of aggressive driving behavior.

Table 5.1 Features in Mobile-Sensed Data Pattern for Six Types of Aggressive Driving Behaviors.

Driving Errors	Descriptions of features for sensors' data pattern
Sharp left-turn	Abnormal sessions can exist in all three axes of accelerometer; The mean value of Z-axis reading of gyroscope are much greater than other event (positive value).
Sharp right-turn	Abnormal sessions can exist in all three axes of accelerometer; The mean value of Z-axis reading of gyroscope are much smaller than other event (negative value).
Aggressive left-lane-change	Abnormal sessions can exist in all three axes of accelerometer; The mean value of Z-axis reading of gyroscope are positive, but much smaller than sharp-left turn. The behavior duration is usually less than 1.5 s.
Aggressive right-lane-change	Abnormal sessions can exist in all three axes of accelerometer; The mean value of Z-axis reading of gyroscope are positive, but much smaller than sharp-left turn. The behavior duration is usually less than 1.5 s.
Fast acceleration	Abnormal sessions with an increasing tendency can be detected from X-axis of accelerometer; The mean value of Z-axis reading of gyroscope is close to zero.
Hard brake	Abnormal sessions with decreasing tendency can be detected from X-axis of accelerometer; The mean value of Z-axis reading of gyroscope is close to zero.

Figure 5.5 illustrates our approach for detecting aggressive driving behaviors, which proceeds through the following steps:

1) Detect potential driving errors: Analyze accelerometer data to identify the abnormal sessions;

2) Check mean Z-gyro: For each abnormal session, check its corresponding mean Z-gyro. If the value is in [-0.1, 0.1], it means that no apparent rotational motion is detected. The abnormal session is pre-labeled as speed-event (brake and accelerate). Otherwise, it is pre-labeled as a left-rotation-event (left turn and left-lane-change) or a right-rotation event (right turn and right-lane-change) by checking if the mean Z-gyro is positive or negative;

3) Calculate error duration: For the left- and right-rotation-event, we furtherly calculate its time duration. If the duration is less than 1.5 s and its mean Z-gyro is smaller than 0.3, this error is labeled as lane-change. Otherwise, it is treated as turn event.

4) Examine changing tendency: For the speed-event, we furtherly examine the changing trend of its X-axis acceleration. An increasing tendency represents fast acceleration. Decreasing implies hard brake.
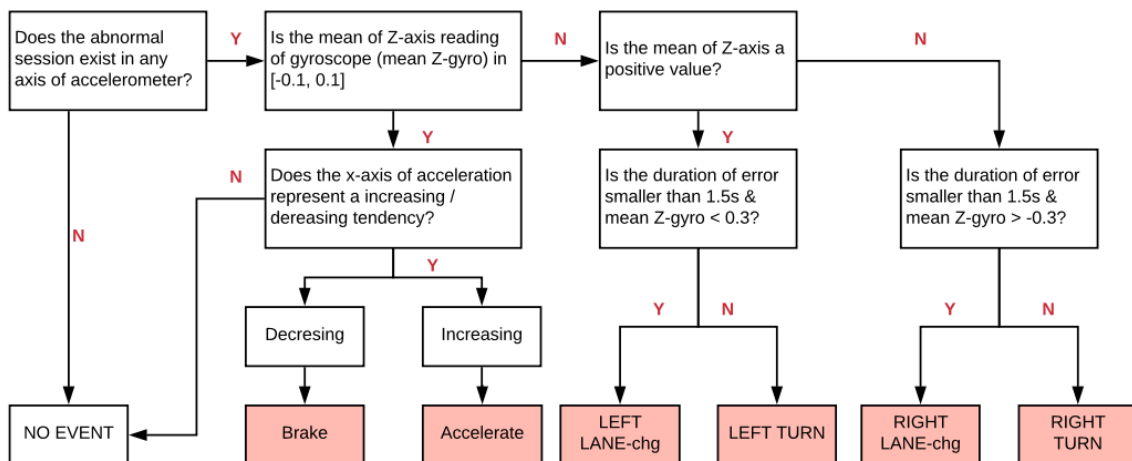
Figure 5.5 The multi-feature-fusion framework for aggressive driving behaviors detection.

5.2.1.3. Geotagging Data

Last, we calculate the geolocation for each detected driving error using GPS readings. The output rate of the GPS receiver is typically 1Hz, which is far lower than the motion sensors (which can often by up to 100 Hz). By matching timestamps, we can find two consecutive GPS sample points with the nearest timestamps for each detected driving error. To calculate the driving error's geolocation, first, the original geodetic coordinates (latitude, longitude, ellipsoidal height) are converted into Earth-Centered, Earth-Fixed coordinates (x, y, z) through the method provided in (Li and Goldberg 2018). Then, the coordinates of the driving error are calculated by applying a linear interpolation scheme as in Equations (5.3) - (5.5):

$$x = x_0 + \frac{(t-t_0)(x_1-x_0)}{(t_1-t_0)} \tag{5.3}$$

$$y = y_0 + \frac{(t-t_0)(y_1-y_0)}{(t_1-t_0)} \tag{5.4}$$

$$z = z_0 + \frac{(t-t_0)(z_1-z_0)}{(t_1-t_0)} \tag{5.5}$$

where *(x, y, z)* are the calculated coordinates for the detected driving error, t is the error's timestamp, *(x_0, y_0, z_0)* and *(x_1, y_1, z_1)* are two consecutive GPS points collected at time t_0 and t_1.

5.2.2. Scenic Tuples Construction for Driving Errors

In the second stage of this study, we investigate the spatiotemporal distribution of dangerous driving behaviors. The detected driving trajectories generated from the

smartphone GPS readings and the detected driving errors are mapped and geo-statistically analyzed to extract several individualized driving patterns including 1) driving error hotspots, 2) hazardous time periods, and 3) most visited road segments.

Studies have demonstrated that traffic collisions are not randomly distributed, and factors exist that cause them to occur more frequently in some places than others (Effati et al. 2012; Vorko-Jović, Kern, and Biloglav 2006). Burdett, Starkey, and Charlton (2017) stated that driving close to home poses a significantly higher risk to road crashes which might be influenced by drivers' complacency when driving on familiar road segments. Road category, distance to road intersections, and driving in rush hours also constitute significantly contributing factors to traffic collisions (Beshah and Hill 2010; Steenberghen et al. 2004). In this study, we also attempt to investigate if factors exist to trigger more driving errors to drivers. Through a careful study of prior literature, we carefully select seven factors, which have been proven contributing to driving risks, to characterize the occurrence of each driving error as listed in Table 5.2. A "Scenic Tuple" is built by integrating these factors to characterize and depict when, where, and what a driving error occurs.

Figure 5.6 illustrates the procedure of scenic tuple construction. In this study, each scenic tuple contains seven components including timestamp (C1), near home (C2), near intersections (C3), road category (C4), start point of trip (C5), end point of trip (C6), trip purpose (C7). These are generated from three data sources: 1) detected driving errors, 2) road network, and 3) driving trajectory. Driving errors are detected with timestamps from the mobile sensor data by utilizing the proposed multi-feature-fusion

framework. Driving trajectories are generated from GPS readings. We project the

detected driving errors to their nearest road segments and mapped them with the road

network and driving trajectories using ArcGIS Pro. Through spatial joining these data

layers, we can append the attributes of driving errors with more road- and driving-related

information. A detailed description of scenic tuple components is listed in Table 5.2.

Table 5.2 Description of Scenic Tuple Components.

Components	Description	Values	Data Source
C1: Timestamp	Time periods in which the driving errors occur.	Each two-hour session is considered as one period. Twelve time periods in total (e.g. 8:00-10:00; 10:00-12:00 etc.)	Driving errors
C2: Near Home	Whether or not a driving error occurred within 100 meters to home?	Y or N	Detected errors + apartments shapefile
C3: Near Intersection	Whether or not a driving error occurred within 3 meters to a road intersection?	Y or N	Driving errors + road network shapefile
C4: Road Type	Classification of road network.	Twelve types of road including: Major Arterial, Major Collector, Minor Arterial, Minor Collector, Private Street, Local Street, Freeway, Alley, Campus Road, Access Easement, and Public Access.	Road network shapefile
C5: Start Point	Start point of a driving trajectory which contains driving errors.	Home, School/Workplace, Restaurant, Shop, Residential Area, Hospital, Church, and Others.	Driving errors + trajectories
C6: End Point	End point of a driving trajectory which contains driving errors.	Home, School/Workplace, Restaurant, Shop, Residential Area, and Others.	Driving errors + trajectories
C7: Trip Purpose	The purpose of a driving in which driving errors exist	Go home, Go to school/work, Go shopping, Go eating, Visiting (e.g., friends' home, church, hospital etc.), and Others.	Manually record
Note: Driving errors and trajectories are detected using smartphone sensors; apartment shapefiles and road network shapefiles are downloaded from City of College Station – GIS Open Data Files.			

No.	C1	C2	C3	C4	C5	C6	C7
1	8-10	N	N	MAJORA	Home	School	School
2	12-14	N	Y	MAJORA	School	Restaurant	Eating
3	18-20	Y	Y	MAJORC	School	Mall	Shopping
				......			
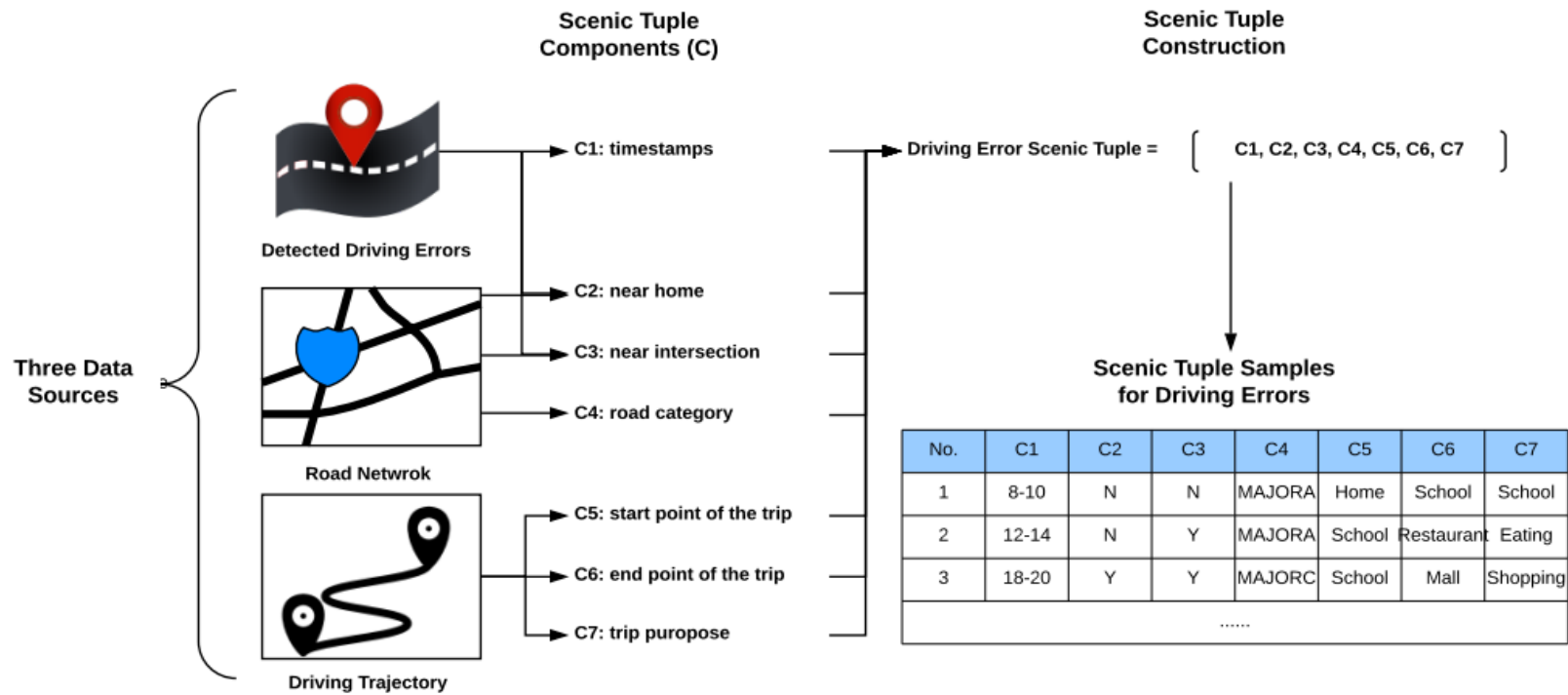
Figure 5.6 Illustration of scenic tuple construction for driving errors.

126

5.2.3. Hazardous Driving Scenes Extraction

In our last step, we attempt to characterize hazardous driving scenes for individual drivers based on the seven factors used in scenic tuples. Hazardous driving scenes refer to some combinations of factors which negatively influence an individual's driving performance and may vary across different drivers. Studies have demonstrated that crashes do not occur randomly. Instead, in some specific driving scenes, drivers are prone to making more driving errors, therefore leading to potential traffic collisions. In this study, we investigate the significant similarities among individual's driving errors through an in-depth analysis of a long-term collection of error scenic tuples. Different from the spatiotemporal clusters of driving errors (e.g., driving error hotspots, hazardous time periods), clustering driving errors based on the selected scenic tuple factors can aid drivers in better understanding what specific driving scenes are more likely for them to make mistakes and how to avoid the potentially hazardous driving conditions.

Cluster analysis has been extensively utilized to divide samples into different homogeneous subgroups to facilitate discovering significant similarities and patterns from each subset (Kumar and Toshniwal 2016; Shikhar et al. 2016; Chaturvedi et al. 2001). All scenic tuple components are categorical data, therefore two clustering methods that are proven to be useful for dealing with categorical data are adopted to identify the significant clusters of error scenic tuples including: 1) K-modes clustering, and 2) Hierarchical Clustering on Principal Components (HCPC).

5.2.3.1. K-modes Clustering

K-modes clustering, as an enhanced version of K-means clustering, can more

effectively group similar samples into "K" number of clusters, especially for processing categorical data (Huang 1997; Chaturvedi et al. 2001; Jain 2010). The procedure of K-modes clustering contains the following main steps (Huang 1997; Kumar and Toshniwal 2015):

1) Initialize "K" number of cluster centers (aka modes).

2) Calculate the dissimilarity between sample points to each cluster centers. The dissimilarity can be calculated through Equations (5.6) – (5.8).

3) Assign sample points to the cluster whose dissimilarity is minimum.

4) Reset the center for the cluster and repeat from step 2 until the center remains the same as the previous center.

The dissimilarity between two categorical objectives X and Y can be calculated as follows:

$$X = [X_1, X_2, \dots X_n] , Y = [Y_1, Y_2, \dots Y_n] \tag{5.6}$$

$$D(X, Y) = \sum_{i=1}^{n} \delta(X_i, Y_i) \tag{5.7}$$

Where,

$$\delta(X_i, Y_i) = \begin{cases} 0, & X_i = Y_i \\ 1, & X_i \neq Y_i \end{cases} \tag{5.8}$$

In Equations (5.6) – (5.8), X and Y represent two objectives containing n categorical attributes. X_i and Y_i are the *ith* categorical attributes in X and Y. The dissimilarity D (X,

Y) is calculated by counting the number of different categorical attribute between *X* and *Y*.

5.2.3.2. Hierchical Clustering on Principal Components (HCPC)

The HCPC is a hybrid method which combines Hierarchical Clustering (HC) with Multiple Correspondence Analysis (MCA) (Husson et al. 2010). HC has been broadly used to form clusters sequentially in a tree structure. The objects with the highest similarity are grouped firstly. Then the groups are further merged based on the maximum similarity among them. With the decrease of the similarity, all clusters are finally forced into a single group (Odong et al. 2013; Murtagh and Legendre 2014). MCA is an extension of principal component analysis, which is designed for processing categorical dataset. In HCPC's procedure, first, MCA is applied to transform categorical objects into numerical variables (aka principal components) and reduce data dimensions. Then, the HC is performed on the selected principal components using Ward's criterion. Lastly, clusters are generated by cutting the hierarchical tree. Studies have demonstrated that HCPC can yield a more robust clustering result by excluding the last principal components. Refer to (Murtagh and Legendre 2014) for a detailed explanation of HCPC.

In this study, we implement both methods (K-Modes and HCPC) to group similar scenic tuples into clusters. By spatially interpreting the significant clusters, we can discover individualized hazardous driving scenes.

5.3. Experiments and Results

This section details the experiments, data analysis, and results. First, we tested our proposed driving error detection method on a high-quality open dataset to evaluate

its performance for detecting aggressive driving errors. Then, we conducted a one-month long driving test in College Station, TX to record a tester's daily driving dynamics. Through an in-depth spatiotemporal analysis of the detected driving errors, we identified the spatial and temporal concentrations of driving errors for the test driver. More importantly, by constructing and clustering the error scenic tuples, we successfully extracted three hazardous driving scenes for the test driver.

5.3.1. The Validation of Proposed Driving Errors Detection

To verify the feasibility and effectiveness of the proposed driving error detection framework, we tested it on a high-quality open dataset of driving errors created by Ferreira Júnior and utilized in many similar studies (Júnior et al. 2017; Carvalho et al. 2017). This dataset contains smartphone sensor measurements captured while performing seven different types of driving events. An Android-based Motorola XT1058 phone was fixed on a 2011 Honda Civic for sensing driving errors. The smartphone was not moved during the data collection. The sampling rate of the mobile sensors varied between 50Hz to 100 Hz. Sixty-nine driving events including fifty-five aggressive driving events and fourteen regular driving events, as listed in Table 5.3, were collected from four driving trips. Each driving test took about thirteen minutes in average and was performed on dry, paved, asphalt road. These driving events were executed by two drivers – each has more than fifteen years of driving experience. The start and end timestamps of the driving events were manually recorded for result validation.

Table 5.3 The Number of Samples for Seven Types of Driving Events.

Driving Event Type	Number of driving events
Hard brake	12
Fast acceleration	12
Sharp left-turn	11
Sharp right-turn	11
Aggressive left-lane-change	4
Aggressive right-lane-change	5
Regular driving event	14
Total	69

We executed the proposed behavior detection framework on the open dataset. The result demonstrated that the proposed framework could effectively separate aggressive driving events and regulars driving events with an accuracy of 92.75% (64/69), as shown in Table 5.4. It implies that "jerk energy" is a tightly associated with aggressive driving behaviors. The same dataset was also tested by other studies. (Júnior et al. 2017; Carvalho et al. 2017) built and evaluated different machine learning models to find the best performing model for detecting each type of driving events; however, their study couldn't provide a single model to classify different driving events. Compared with those studies, our approach achieved a relatively high detection accuracy and outperformed these studies in terms of the ease of implement and high-efficiency (no need for extensive model training).

Table 5.4 Confusion Matrix for the Classification of Aggressive Driving and Regular Driving.

Number of Irregular Driving Events: 55		Classified Events	
Number of Regular Driving Events: 14		Irregular Driving	Regular Driving
Actual Events	Irregular Driving	50	5
	Regular Driving	0	14

Table 5.5 Confusion Matrix for Driving Event Detection.

Number of Events: 69		Classified Events						
		1	2	3	4	5	6	7
Actual Events	1	10	1	0	0	0	0	1
	2	1	9	0	0	0	0	2
	3	0	0	9	0	2	0	0
	4	0	0	0	10	0	0	1
	5	0	0	1	0	3	0	0
	6	0	0	0	1	0	3	1
	7	0	0	0	0	0	0	14
1-hard brake, 2-fast acceleration, 3-sharp left-turn, 4-sharp right-turn, 5-aggressive left-lane-change, 6-aggressive right-lane-change, 7-regular driving event								

Table 5.5 lists the detailed evaluation results, in which the diagonal cells contain the number of correctly classified driving events, while the remainder of cells shows the number of misclassified results. The results indicated that our approach achieved a high success rate (≥75%) for identifying the type of each aggressive event except for the case of "aggressive right-lane-change," which may be caused by 1) the limited samples of

aggressive right-lane-change, and 2) the high similarity between a lane-change event and a turn event.

5.3.2. Spatiotemporal Analysis of Hazardous Driving Patterns

After verifying the accuracy of the proposed driving error detection method with the open dataset, we carried out a one-month long driving test in College Station, TX to record a tester's daily driving dynamics for investigating and discovering the hazardous driving patterns for the test driver. To achieve a comparable data collection, we carefully followed the experiment settings of the open dataset. The data of the one-month long driving test were collected through an Android app *AndroSensor* using an Android-based Moto X Pure. The phone was securely taped in the cabin of a 2009 Toyota Corolla. Two motion sensors (3-axis accelerometer and gyroscope) and the GPS receiver were utilized to sense driving behaviors and track driving trajectories. The output rate of the motion sensors was set to 80Hz, while the GPS generated sample points at 1Hz.

Figure 5.7 Detected driving errors and trajectories (a: spatial distribution of driving errors, b: temporal distribution of driving errors, c: most-visited roads and driving mistake hotspots).

By analyzing the mobile-sensed data, fifty-one driving errors were detected including thirty hard bake, six fast acceleration, two sharp left-turn, ten sharp right-turn, and three aggressive left-lane-change as shown in Figure 5.7a. It is worth noting that 86% of the driving errors occurred close to road intersections. These results suggest that the test driver needed to improve driving ability when crossing road intersections. Figure 5.7b shows the temporal distribution of the detected aggressive driving behaviors. Three hazarded driving periods (i.e., 8AM-10AM, 10AM-12PM, 6PM-8PM) were identified, which contain a predominance of driving errors. By combing the driving errors with driving trajectories, the driving error hotspots and most visited road segments could be detected. As Figure 5.7c shows, three significant driving error hotspots were detected, and the most visited road segments were highlighted, which can help the drivers to avoid error-prone driving zones.

5.3.3. Extracting Hazardous Driving Scenes from Scenic Tuples

To understand the occurrence of aggressive driving events more fully, we first built a driving error scenic tuple for each detected driving event, as shown in Table 5.6. Fifty-one driving error scenic tuples were constructed by integrating detected errors, driving trajectories, and road network data for the one-month long driving test.

Next, we applied two clustering methods (i.e., K-modes clustering and HCPC) on the scenic tuples to extract the significant similarities among the detected driving errors. HCPC can consecutively group the most similar objects in a tree structure. One main advantage of HCPC is it can automatically determine the optimal number of clusters based on the loss of inertia (a higher relative loss indicates a better clustering result). By

performing HCPC, the scenic tuples were grouped into six clusters (three significant

clusters and three weak ones) as illustrated in Figure 5.8, the top-right histogram shows

the loss of inertia with an increasing number of clusters.

Table 5.6 Samples of Constructed Scenic Tuples for Driving Errors.

OBJECTID	Timestamp	Near Intersection	Near Home	RoadType	Startpoint	Endpoint	TripPurpose
1	8_10	N	N	MAJORA	Home	Church	School
2	8_10	Y	N	MAJORA	Home	Church	School
3	18_20	Y	N	MAJORA	School	Res_Area	Visiting
4	18_20	Y	N	MAJORA	School	Res_Area	Visiting
5	18_20	Y	N	MAJORA	School	Res_Area	Visiting
…							
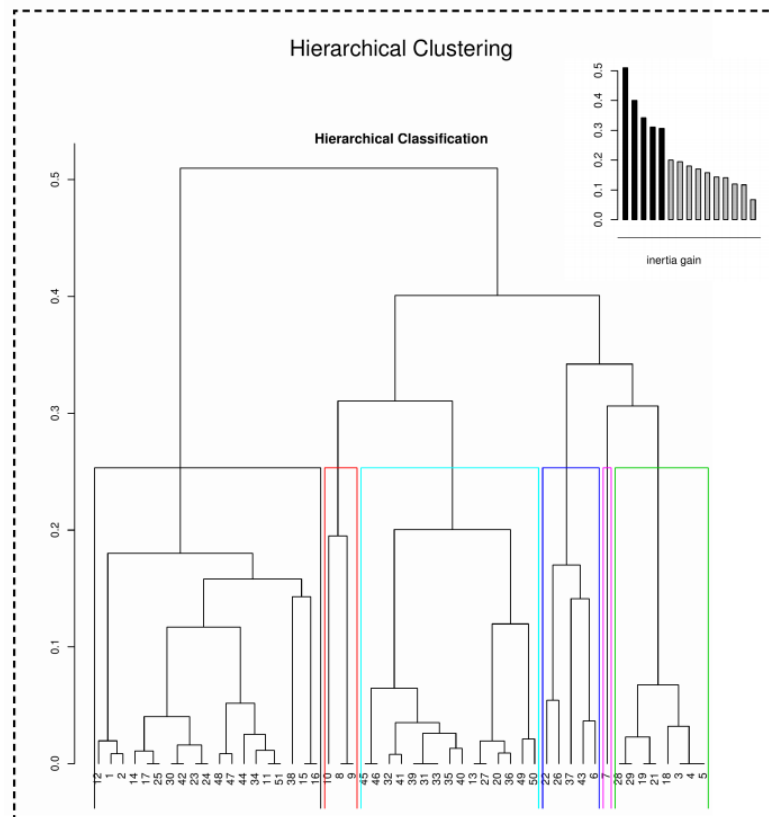
Figure 5.8 Hierarchical clustering tree generated by HCPC.

In addition, K-modes clustering was conducted to assign scenic tuples into different clusters. Applying K-modes clustering requires the specification of K (the number of clusters), which significantly impacts the clustering results. The "cost" of K-modes clustering is widely used to examine the model's performance— "cost" is defined as the sum of dissimilarities between each sample point to its closest centroid. A good clustering model typically yields a low-cost value with a small K. In this study, we calculated the cost of 10 different models (K = 1, 2, 3, ……, 10). Figure 5.9 illustrates the decreasing tendency of cost value with an increasing number of K. Based on this figure, we selected the model with three clusters since no noticeable improvement was observed following this value.
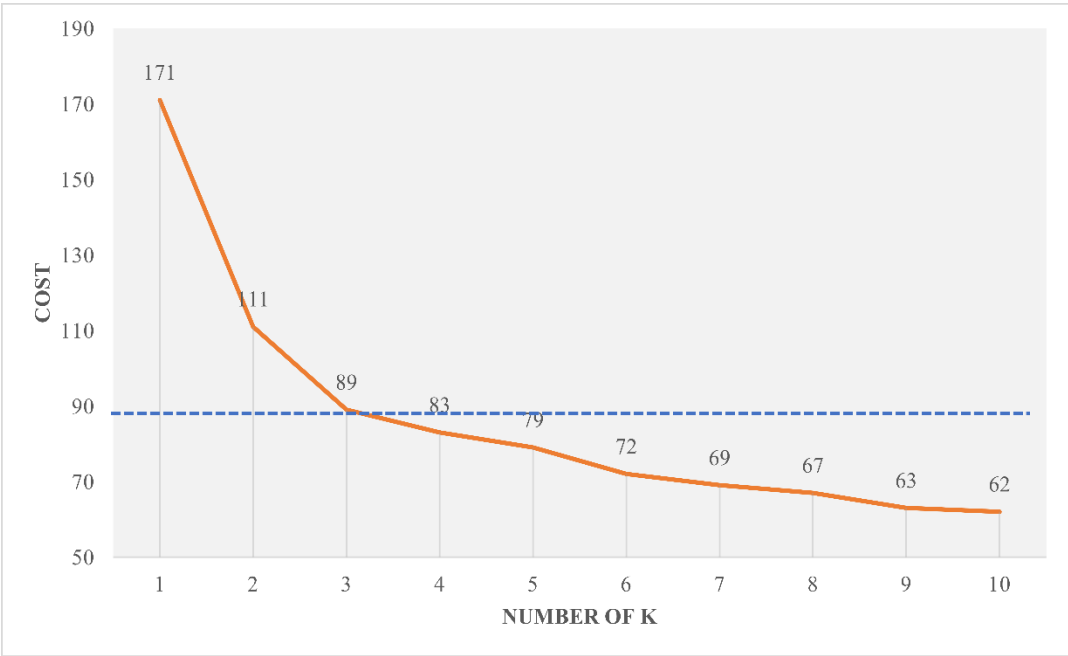
Figure 5.9 The cost values for ten different K-modes models (K = 1, 2, 3, ..., 10).

The results of K-modes clustering and HCPC are detailed in Table 5.7 indicating that K-modes' result has a very high similarity with the significant clusters generated by HCPC. Through the consolidation of the results obtained from these two methods, three clusters (hazardous driving scenes) were selected.

Table 5.7 The Result Comparison Between K-modes Clustering and HCPC.

	Scenic Tuples' ID	
	K-modes	HCPC
Cluster 1	6, 8, 9, 13, 20, 22, 26, 27, 31, 32, 33, 35, 36, 37, 39, 40, 41, 45, 46, 49, 50	13, 20, 26, 27, 31, 32, 33, 35, 36, 39, 40, 41, 45, 46, 49, 50
Cluster 2	3, 4, 5, 7, 18, 19, 21, 28, 29	3, 4, 5, 18, 19, 21, 28, 29
Cluster 3	1, 2, 10, 11, 12, 14, 15, 16, 17, 23, 24, 25, 30, 34, 38, 42, 43, 44, 47, 48, 51	1, 2, 11, 12, 14, 15, 16, 17, 23, 24, 25, 30, 34, 38, 42, 44, 47, 48, 51
The following IDs are in weak clusters (4, 5&6) detected by HCPC: 6, 7, 8, 9, 10, 22, 37, 43		

Table 5.8 The Clusters' Centroids Generated by K-modes.

Cluster	Timestamp	Near Intersection	Near Home	Road Type	Start point	End point	Trip Purpose
1	22_24	Y	N	MAJORA	School	Home	Home
2	18_20	Y	N	MAJORA	School	Res_Area	Visiting
3	10_12	Y	N	Campus	Home	School	School

Table 5.8 lists the centroid for each identified cluster. By interpreting and characterizing these centroids, three hazardous driving scenes were depicted as:

- Scene 1: During midnight (22:00-24:00), when driving back home from school, the driver was observed to be prone to making driving errors at the intersections of major arterial roads.

- Scene 2: During evening rush hours (18:00-20:00), when driving from school to visit a friend, the driver was again observed to be prone to making driving errors at intersections of major arterial roads.

- Scene 3: During 10:00-12:00, when driving from home to school, the driver was observed to be prone to making driving errors at the intersections of campus roads.

5.4. Discussion and Conclusion

Aggressive driving behaviors are significant contributors to driving risks; however, few studies have detected and integrated them into road safety analysis, especially into individual-based driving safety analysis. In this study, we put forward a novel approach to discover the significant spatiotemporal similarities among individual's driving errors to answer a fundamental but underexplored road safety research question: *when* and *where* drivers are more prone to making driving errors? To the best of our knowledge, this is the first study to integrate different types of driving-related data to assess driving risks—depicting individualized hazardous driving scenes.

We utilized mobile sensed data collected by smartphone built-in accelerometer and gyroscope to capture the "jerk energy" when performing aggressive driving behaviors. Our experiment demonstrated that different driving errors generate unique sensors' data pattern, which can be, in turn, utilized to classify the detected driving

errors. Meanwhile, by integrating the mobile sensed driving errors with road networks and driving trajectories, we depicted and characterized each driving error with seven carefully selected spatiotemporal factors. Through an in-depth analysis of long-term collected driving errors, we not only can help drivers to identify their hazardous driving patterns (e.g., hazardous driving time periods, most visited roads, and driving error hotspots), but more, assist drivers with recognizing their dangerous driving habits and hazardous driving scenes.

The proposed approach was validated on a high-quality open dataset for driving errors. The result demonstrated our proposed behavior detection framework could effectively identify six types of driving errors (e.g., hard brake, fast acceleration, sharp left-turn, sharp right-turn, aggressive left-lane-change, and aggressive right-lane-change) using mobile sensed data with an accuracy rate of 84.05%. It outperforms prior studies tested on the same dataset in terms of accuracy and efficacy. In addition, a one-month long driving test was carried out in College Station, TX. Fifty-one driving errors were accurately identified through the driving test. By integrating the mobile sensed driving errors, road networks, and driving trajectories, we successfully identified hazardous driving time periods; mapped the most visited roads and driving error hotspots; and extracted three typical hazardous driving scenes from the test driver's one-month driving dynamics. The integration of driver behaviors with associated spatiotemporal characteristics paves the way for us to better understand and characterize potential traffic risks. This study can be of great benefit to drivers, allowing them to assess their driving performance, correct their driving errors and, avoid potential traffic risks.

140

With the rapid development of GIS and mobile sensing technologies, the proposed solution is promising for providing personalized driving-risk analysis and offering customized safe-driving assistance for drivers. However, to achieve a deeper understanding of driving risks, the proposed approach could be further improved in the following ways:

1) **The adoption of a better driving error detection method.** This study mainly focuses on the detection of six types of driving errors using a multi-feature-fusion framework. These features are generated through empirical tests for obvious driving errors, which can maximize the accuracy of detection. However, other driving errors which do not manifest these features may not be detected. An advanced detection framework covering more driving error types needs to be proposed and evaluated. It should be noted that until the present, there have not been universal standards to characterize or quantity driving mistakes. In prior studies, driving errors are identified by comparing empirical thresholds, matching of template driving events, or human judgment. A unified standard for assessing driving behaviors needs to be generated.

2) **More scenic tuple components can be included.** In this study, each driving error scenic tuple contains seven components. These components are primarily generated from driving trajectories and road network. However, driving error occurrence can be influenced by various factors. Studies have proved that driving risks are strongly correlated with weather conditions, traffic volume, road surface condition, etc. Theofilatos and Yannis (2014) reported that taking use of real-

141

time data sources (e.g., weather conditions, traffic volume) could capture more short-term effects, yielding a better understanding of traffic risk. Nowadays, massive amounts of traffic-related data sources are becoming available (e.g., real-time traffic volume, real-time weather conditions), offering a great opportunity for road safety researchers to discover insights into driving risk detection. In future studies, we will integrate additional traffic-related data sources to more comprehensively present and analyze driving error occurrences;

3) **A longer period of data collection is suggested.** In this study, the driving test only captures the one-month of driving data. Although this is enough for extracting some driving patterns, we believe a more reliable hazardous driving scenes extraction can be achieved by mining longer-term datasets.

6. CONCLUSION[*]

6.1. Summary

Mobile sensing technology has advanced rapidly over the past few years (Li et al. 2019; W. Xu et al. 2015; R. Chen, Chu, Liu, Chen, et al. 2014). Equipped with miniaturized sensors (e.g., accelerometer, gyroscope, GPS, camera), smartphones have become promising data acquisition and computing platforms, which could achieve a high-sampling rate with little or zero economic cost. Smartphones are ubiquitous today, which empower the citizens to sense their surroundings, generate data, and contribute their observations to achieve a continuous monitoring system in an unprecedented manner (Guo et al. 2016, 2014; Panichpapiboon and Leakkaw 2017). By leveraging the power of citizens and the rich sensing resources, mobile crowd sensing has become a popular researching paradigm for large-scale sensing and monitoring.

This study innovatively explored the possible implementations of MCS-based approaches for solving traffic-safety-related issues. Four distinctive research works were conducted to enhance road safety from three perspectives: 1) capture unreported traffic risks; 2) identify bumpy road segments and detect road anomalies; and 3) discover individualized hazardous driving scenes, in which drivers are prone to making driving mistakes.

---

[*]Part of this section is reprinted with permission from "Embracing Crowdsensing: An Enhanced Mobile Sensing Solution for Road Anomaly Detection" by Xiao Li, Da Huo, Daniel W. Goldberg, Tianxing Chu, Zhengcong Yin, and Tracy Hammond, 2018. ISPRS International Journal of Geo-Information, Copyright 2019 by Xiao Li. https://doi.org/10.3390/ijgi8090412

In Section 2, we created a new research scheme to utilize mobile crowdsourced Waze incident reports (WIR) to capture unreported traffic risks (near-crashes and traffic incidents). The researchers analyzed four weeks WIRs and PCRs obtained from the I-35 corridor in North Texas. The researchers collected a whole week data from four different months: August, October, November, December of 2016. First, the authors developed a new method to reduce data redundancy and obtain unique Waze incidents (unique WIRs). The researchers then matched the unique WIRs with the observed crashes and compared their spatial and temporal distributions. Besides, the researchers estimated predicted crashes through safety performance functions (SPFs) and crash modification factors (CMFs), to assess whether the WIR data can be used as a reliable surrogate of these safety measures (i.e., observed crash frequency and predicted crashes) for identifying high-risk locations. This study shows that Waze is an invaluable source of data for safety researchers, which is tremendously useful for capturing unreported traffic incidents. Meanwhile, WIRs and PCRs are spatially correlated, which implies that WIRs could be potentially used as a surrogate safety measure in the absence of crash data. Moreover, by combining WIRs with PCRs, more high-risk road segments can be identified compared to the results generated from PCRs.

In Section 3 and Section 4, we proposed crowdsensing solutions to assess road surface conditions and detect road anomalies. Section 3 presents a novel crowdsensing-based system for road surface assessment using smartphones. The built-in GPS and accelerometer in smartphones are utilized to compute two assessment indexes that aid in determining the road quality. Filed tests demonstrated that the smartphone accelerometer

144

could successfully capture irregular vehicle vibrations while driving on the bumpy road segments. The overall road surface condition can be accurately judged and labeled by mining mobile sensed data. By implementing a crowdsensing solution, the road surface conditions can be continuously monitored. In Section 4, we proposed an enhanced mobile crowdsensing solution by implementing wavelet analysis and spatial clustering methods. This study further addressed two unanswered research questions: 1) it effectively estimated the size of road anomalies using a wavelet-based approach; 2) it successfully optimized road anomaly detection results by spatial clustering mobile crowd sensed detection results.

In Section 5, we proposed a novel approach to discovering the significant spatiotemporal similarities among individual's driving errors to answer a fundamental but underexplored road safety research question: *when* and *where* drivers are more prone to making driving errors? This study utilized mobile sensed data collected by smartphone built-in accelerometer and gyroscope to capture the "jerk energy" when performing aggressive driving behaviors. Our experiment demonstrated that different driving errors generate unique sensors' data patterns, which can be, in turn, utilized to classify the detected driving errors. Meanwhile, by integrating the mobile sensed driving errors with road networks and driving trajectories, we depicted and characterized each driving error with seven carefully selected spatiotemporal factors. Through an in-depth analysis of long-term collected driving errors, we not only can help drivers to identify their hazardous driving patterns, but more, assist drivers with recognizing their dangerous driving habits and hazardous driving scenes.

This dissertation demonstrated that the mobile crowd sensed data is an invaluable source for safety researchers to rethink road safety studies. Leveraging crowdsourced data can substantially advance traditional road safety analysis. It can effectively capture unreported traffic risks, continuously monitor road surface conditions with few economic costs, and assist drivers in recognizing their dangerous driving habits and hazardous driving scenes.

6.2. Limitations and Future Work

Although mobile crowdsensing solution shows great potential for solving various large-scale monitoring tasks and can substantially improve the current road safety studies, there are still some barriers exist, which limits the implementation of crowdsensing solutions at the current stage.

1) Crowdsourced data may have severe inaccuracy and redundancy issues. Since the public voluntarily contributes their data, many people may report the same event, which could generate a massive volume of redundant data. Meanwhile, inaccurate information may also be reported because of the crowdsourcers' mistakes.

2) Mobile crowdsensing is significantly constrained by smartphone hardware. Low-quality mobile sensors' data may lead to unreliable detection results. Collecting mobile sensors' data at a high sampling rate can drain phone battery in several hours, or even faster.

3) The success of crowdsensing solution heavily relies on the constant contribution of high-quality crowd sensed data. However, how to recruit a group of reliable

crowdsourcers to ensure the effectiveness of crowd sensed result is still an

unanswered question.

To overcome these limitations, a comprehensive crowdsensing-quality-control

strategy should be proposed and formalized in future work, which could further

eliminate the low-quality crowd sensed data (e.g., data collected using low-quality

sensors or devices, data collected while driving at high speed). Meanwhile, we could

further optimize the mobile-based analyzing algorithm, reduce computing load, and

choose a more appropriate sensor sampling rate instead of using 100 Hz, which may

potentially extend the smartphone battery life. Meanwhile, future work should focus

more attention on how to take full advantage of mobile sensed data. For example, we can

test different spatial clustering methods, compare their performances, and further form a

formalized crowdsensing strategy to synthesize crowd sensed data with further improved

accuracy. More importantly, the future works need to be built based on the reliable

crowd data sources, for example, we could recruit vehicles from local governments (e.g.,

garbage truck, police vehicles) to put forward a real-time road anomaly monitoring

system, which could continuously monitor road surface conditions with high accuracy.

6.3. Next-Generation Approach—Crowd Vehicular Sensing

It is worth noting that, to make autonomous vehicles a reality, vehicular sensing

techniques are undergoing an unprecedented revolution, which also shows great

potential for facilitating the implementation of crowdsensing solutions for assessing road

qualities. Nowadays, each commercial vehicle is equipped with approximately 4,000

sensors (Massaro et al. 2017; Fugiglando et al. 2019). These sensors empower vehicles

to collect thousands of signals through the controller area network (CAN) bus technology, which could monitor the vehicle and its surrounding environment in real-time. These vehicular sensors have a higher sampling rate and a better data quality than that of a smartphone, which facilitates achieving a more precise detection result than smartphone sensors.

Meanwhile, light detection and ranging (LiDAR) provides a compelling sensing ability to autonomous vehicles (Schwarz 2010; H. Wang et al. 2017). The vehicular LiDAR can simultaneously scan and generate high-resolution 3-D representations of the immediate vicinity, which could help us identify road anomalies and bumpy road segments more effectively.

Therefore, we believe, the vehicular crowdsensing system could be the next-generation approach for large-scale sensing and monitoring with higher data quality, faster data transmission, and better precision. This proposed solution remains to be promising and efficient in the foreseeable future.

REFERENCES

AAA. 2016. "Pothole Damage Costs U.S. Drivers $3 Billion Annually." AAA. 2016.

> https://www.oregon.aaa.com/2016/02/pothole-damage-costs-u-s-drivers-3-billion-

> annually/.

Abdesslem, Fehmi Ben, Andrew Phillips, and Tristan Henderson. 2009. "Less Is More:

> Energy-Efficient Mobile Sensing with SenseLess." In *SIGCOMM 2009 -*

> *Proceedings of the 2009 SIGCOMM Conference and Co-Located Workshops,*

> *MobiHeld 2009*. https://doi.org/10.1145/1592606.1592621.

Aleadelat, Waleed, and Khaled Ksaibati. 2017. "Estimation of Pavement Serviceability

> Index through Android-Based Smartphone Application for Local Roads."

> *Transportation Research Record*. https://doi.org/10.3141/2639-16.

Aleadelat, Waleed, Ksaibati, and Khaled. 2017. "TRR 2639." *Transportation Research*

> *Record: Journal of the Transportation Research Board*, no. 2639: 129–35.

> https://doi.org/10.3141/2639-16.

Allouch, Azza, Anis Koubaa, Tarek Abbes, and Adel Ammar. 2017. "RoadSense:

> Smartphone Application to Estimate Road Conditions Using Accelerometer and

> Gyroscope." *IEEE Sensors Journal*. https://doi.org/10.1109/JSEN.2017.2702739.

Amador-Jiménez, Luis, and Nagham Matout. 2014. "A Low Cost Solution to Assess

> Road ' s Roughness Surface Condition for Pavement Management." *TRB 2014*

> *Annual Meeting*.

American Association of State Highway and Transportation Officials. 2010. *Highway*

Safety Manual, 1st Edition. 1st ed. https://www.amazon.com/Highway-Safety-Manual-1st-AASHTO/dp/B0048EZQPS.

Amin-Naseri, Mostafa, Pranamesh Chakraborty, Anuj Sharma, Stephen B. Gilbert, and Mingyi Hong. 2018. "Evaluating the Reliability, Coverage, and Added Value of Crowdsourced Traffic Incident Reports from Waze." *Transportation Research Record*. https://doi.org/10.1177/0361198118790619.

Anderson, Tessa K. 2009. "Kernel Density Estimation and K-Means Clustering to Profile Road Accident Hotspots." *Accident Analysis and Prevention*. https://doi.org/10.1016/j.aap.2008.12.014.

Astarita, Vittorio, Maria Vittoria Caruso, Guido Danieli, Demetrio Carmine Festa, Vincenzo Pasquale Giofrè, Teresa Iuele, and Rosolino Vaiana. 2012. "A Mobile Application for Road Surface Quality Control: UNIquALroad." *Procedia - Social and Behavioral Sciences*. https://doi.org/10.1016/j.sbspro.2012.09.828.

Bellis, Rayla, Beth Osborne, and Stephen Lee Davis. 2019. "Repair Priorities 2019." Washington, DC. http://t4america.org/wp-content/uploads/2019/05/Repair-Priorities-2019.pdf.

Bello-Salau, H., A.M. Aibinu, A.J. Onumanyi, E.N. Onwuka, J.J. Dukiya, and H. Ohize. 2018. "New Road Anomaly Detection and Characterization Algorithm for Autonomous Vehicles." *Applied Computing and Informatics*. https://doi.org/10.1016/j.aci.2018.05.002.

Bergasa, Luis M., Daniel Almeria, Javier Almazan, J. Javier Yebes, and Roberto Arroyo. 2014. "DriveSafe: An App for Alerting Inattentive Drivers and Scoring Driving

Behaviors." In *IEEE Intelligent Vehicles Symposium, Proceedings*.
https://doi.org/10.1109/IVS.2014.6856461.

Beshah, Tibebe, and Shawndra Hill. 2010. "Mining Road Traffic Accident Data to
Improve Safety: Role of Road-Related Factors on Accident Severity in Ethiopia."

Beuving, E, T De Jonghe, D Goos, T Lindahl, and A Stawiarski. 2004. "Fuel Efficiency
of Road Pavements." *Proceedings of the 3Rd Eurasphalt and Eurobitume Congress
Held Vienna, May*.

Bham, G H, Arthur Charpentier, Ewen Gallic, Haiyang Hao Yu, Pan Liu, Jun Chen, Hao
Wang, et al. 2017. "Spatial and Temporal Visualisation Techniques for Crash
Analysis." *Accident Analysis and Prevention* 20 (1): 1–18.
https://doi.org/10.1016/j.aap.2007.05.004.

Bhoraskar, Ravi, Nagamanoj Vankadhara, Bhaskaran Raman, and Purushottam
Kulkarni. 2012. "Wolverine: Traffic and Road Condition Estimation Using
Smartphone Sensors." In *2012 4th International Conference on Communication
Systems and Networks, COMSNETS 2012*.
https://doi.org/10.1109/COMSNETS.2012.6151382.

Bonneson, James A., and Michael P. Pratt. 2009. "Roadway Safety Design Workbook."
FHWA/TX-09/0-4703-P2.

Boyce, Thomas E., and E. Scott Geller. 2002. "An Instrumented Vehicle Assessment of
Problem Behavior and Driving Style: Do Younger Males Really Take More
Risks?" *Accident Analysis and Prevention*. https://doi.org/10.1016/S0001-
4575(00)00102-0.

Bruce, Voorst. 2001. "Why America Has So Many Potholes." 2001.

    http://content.time.com/time/magazine/article/0,9171,159579,00.html.

Burdett, Bridget R.D., Nicola J. Starkey, and Samuel G. Charlton. 2017. "The Close to

    Home Effect in Road Crashes." *Safety Science*.

    https://doi.org/10.1016/j.ssci.2017.04.009.

Campello, Ricardo J.G.B., Davoud Moulavi, and Joerg Sander. 2013. "Density-Based

    Clustering Based on Hierarchical Density Estimates." In *Lecture Notes in Computer*

    Science (Including Subseries Lecture Notes in Artificial Intelligence and Lecture

    Notes in Bioinformatics), 7819 LNAI:160–72. https://doi.org/10.1007/978-3-642-

    37456-2_14.

Cao, Yuejian, Joseph Labuz, and Bojan Guzina. 2011. "Evaluation of Pavement System

    Based on Ground-Penetrating Radar Full-Waveform Simulation." *Transportation*

    Research Record. https://doi.org/10.3141/2227-08.

Carvalho, Eduardo, Bruno V. Ferreira, Jair Ferreira, Cleidson de Souza, Hanna V.

    Carvalho, Yoshihiko Suhara, Alex Sandy Pentland, and Gustavo Pessin. 2017.

    "Exploiting the Use of Recurrent Neural Networks for Driver Behavior Profiling."

    In *2017 International Joint Conference on Neural Networks (IJCNN)*, 3016–21.

    IEEE. https://doi.org/10.1109/IJCNN.2017.7966230.

Castignani, German, Thierry Derrmann, Raphael Frank, and Thomas Engel. 2015.

    "Driver Behavior Profiling Using Smartphones: A Low-Cost Platform for Driver

    Monitoring." *IEEE Intelligent Transportation Systems Magazine*.

    https://doi.org/10.1109/MITS.2014.2328673.

Celaya-Padilla, Jose M., Carlos E. Galván-Tejada, F. E. López-Monteagudo, O. Alonso-González, Arturo Moreno-Báez, Antonio Martínez-Torteya, Jorge I. Galván-Tejada, Jose G. Arceo-Olague, Huizilopoztli Luna-García, and Hamurabi Gamboa-Rosales. 2018. "Speed Bump Detection Using Accelerometric Features: A Genetic Algorithm Approach." *Sensors (Switzerland)*. https://doi.org/10.3390/s18020443.

Chakravarty, Tapas, Avik Ghose, Chirabrata Bhaumik, and Arijit Chowdhury. 2013. "MobiDriveScore — A System for Mobile Sensor Based Driving Analysis: A Risk Assessment Model for Improving One's Driving." In *2013 Seventh International Conference on Sensing Technology (ICST)*, 338–44. IEEE. https://doi.org/10.1109/ICSensT.2013.6727671.

Chaturvedi, Anil, Kraft Foods, Paul E. Green, and J. Douglas Carroll. 2001. "K-Modes Clustering." *Journal of Classification*. https://doi.org/10.1007/s00357-001-0004-3.

Chen, Kongyang, Mingming Lu, Guang Tan, and Jie Wu. 2014. "CRSM: Crowdsourcing Based Road Surface Monitoring." In *Proceedings - 2013 IEEE International Conference on High Performance Computing and Communications, HPCC 2013 and 2013 IEEE International Conference on Embedded and Ubiquitous Computing, EUC 2013*. https://doi.org/10.1109/HPCC.and.EUC.2013.308.

Chen, Ruizhi, Tianxing Chu, Jingbin Liu, Yuwei Chen, Liang Chen, Wenchao Xu, Xiao Li, Juha Hyyppa, and Jian Tang. 2014. "Development of a Contextual Thinking Engine in Mobile Devices." In *2014 Ubiquitous Positioning Indoor Navigation and Location Based Service (UPINLBS)*, 90–96. IEEE.

https://doi.org/10.1109/UPINLBS.2014.7033714.

Chen, Ruizhi, Tianxing Chu, Jingbin Liu, Xiao Li, Yuwei Chen, Liang Chen, and
Wenchao Xu. 2014. "DGNSS-C: A Differential Solution for Enhancing
Smartphone GNSS Performance." In *27th International Technical Meeting of the
Satellite Division of the Institute of Navigation, ION GNSS 2014*.

Chen, Ruizhi, and Robert Guinness. 2014. *Geospatial Computing in Mobile Devices*.
Artech House.

Chen, Tao, Chu Zhang, and Lifeng Xu. 2016. "Factor Analysis of Fatal Road Traffic
Crashes with Massive Casualties in China." *Special Issue Article Advances in
Mechanical Engineering* 8 (4): 1–11. https://doi.org/10.1177/1687814016642712.

Clynch, James R. 2006. "Geodetic Coordinate Conversions." *East*.

Constandache, Ionut, Shravan Gaonkar, Matt Sayler, Romit Roy Choudhury, and
Landon Cox. 2009. "EnLoc: Energy-Efficient Localization for Mobile Phones." In
Proceedings - IEEE INFOCOM. https://doi.org/10.1109/INFCOM.2009.5062218.

Das, Tathagata, Prashanth Mohan, Venkata N. Padmanabhan, Ramachandran Ramjee,
and Asankhaya Sharma. 2010. "PRISM: Platform for Remote Sensing Using
Smartphones." In *MobiSys'10 - Proceedings of the 8th International Conference on
Mobile Systems, Applications, and Services*.
https://doi.org/10.1145/1814433.1814442.

Daubechies, Ingrid. 1992. "Ten Lectures of Wavelets." *Springer-Verlag*.

Douangphachanh, Viengnam, and Hiroyuki Oneyama. 2013. "Estimation of Road
Roughness Condition from Smartphones under Realistic Settings." In *2013 13th*

International Conference on ITS Telecommunications, ITST 2013.
https://doi.org/10.1109/ITST.2013.6685585.

Effati, Meysam, Mohammad Ali Rajabi, Farhad Samadzadegan, and J. A. Rod Blais.
2012. "Developing a Novel Method for Road Hazardous Segment Identification
Based on Fuzzy Reasoning and GIS." *Journal of Transportation Technologies*, 32–
40.

Eren, H., S. Makinist, E. Akin, and A. Yilmaz. 2012. "Estimating Driving Behavior by a
Smartphone." In *IEEE Intelligent Vehicles Symposium, Proceedings*.
https://doi.org/10.1109/IVS.2012.6232298.

Eriksson, Jakob, Lewis Girod, Bret Hull, Ryan Newton, Samuel Madden, and Hari
Balakrishnan. 2008. "The Pothole Patrol: Using a Mobile Sensor Network for Road
Surface Monitoring." In *MobiSys'08 - Proceedings of the 6th International
Conference on Mobile Systems, Applications, and Services*.
https://doi.org/10.1145/1378600.1378605.

Esri. 2016. "How Hot Spot Analysis (Getis-Ord Gi*) Works." *How Hot Spot Analysis
(Getis-Ord Gi*) Works*.

———. 2019. "How Density-Based Clustering Works." 2019.
https://pro.arcgis.com/en/pro-app/tool-reference/spatial-statistics/how-density-
based-clustering-works.htm.

Ester, Martin, Hans-Peter Kriegel, Jörg Sander, and Xiaowei Xu. 1996. "A Density-
Based Algorithm for Discovering Clusters in Large Spatial Databases with Noise."
In *Proceedings of the 2nd International Conference on Knowledge Discovery and*

Data Mining.

Fazeen, Mohamed, Brandon Gozick, Ram Dantu, Moiz Bhukhiya, and Marta C
González. 2012. "Safe Driving Using Mobile Phones." *IEEE Transactions on
Intelligent Transportation Systens* 13 (3).
https://doi.org/10.1109/TITS.2012.2187640.

Fire, Michael, Dima Kagan, Rami Puzis, Lior Rokach, and Yuval Elovici. 2012. "Data
Mining Opportunities in Geosocial Networks for Improving Road Safety." In *2012
IEEE 27th Convention of Electrical and Electronics Engineers in Israel, IEEE
2012*. https://doi.org/10.1109/EEEI.2012.6377049.

Flynn, DB, MM Gilmore, and EA Sudderth. 2018. "Estimating Traffic Crash Counts
Using Crowdsourced Data: Pilot Analysis of 2017 Waze Data and Police Accident
Reports in Maryland." https://rosap.ntl.bts.gov/view/dot/37256.

Fugiglando, Umberto, Emanuele Massaro, Paolo Santi, Sebastiano Milardo, Kacem
Abida, Rainer Stahlmann, Florian Netter, and Carlo Ratti. 2019. "Driving Behavior
Analysis through CAN Bus Data in an Uncontrolled Environment." *IEEE
Transactions on Intelligent Transportation Systems*.
https://doi.org/10.1109/TITS.2018.2836308.

Goodall, Noah, and Eun Lee. 2019. "Comparison of Waze Crash and Disabled Vehicle
Records with Video Ground Truth." *Transportation Research Interdisciplinary
Perspectives* 1 (June): 100019. https://doi.org/10.1016/j.trip.2019.100019.

Goodchild, Michael F. 1992. "Geographical Information Science3." *International
Journal of Geographical Information Systems*.

https://doi.org/10.1080/02693799208901893.

———. 2015. "Space, Place and Health." *Annals of GIS*.

https://doi.org/10.1080/19475683.2015.1007895.

Guo, Bin, Chao Chen, Zhiwen Yu, Daqing Zhang, and Xingshe Zhou. 2015. "Building

Human-Machine Intelligence in Mobile Crowd Sensing." *IT Professional*.

https://doi.org/10.1109/MITP.2015.50.

Guo, Bin, Chao Chen, Daqing Zhang, Zhiwen Yu, and Alvin Chin. 2016. "Mobile

Crowd Sensing and Computing: When Participatory Sensing Meets Participatory

Social Media." *IEEE Communications Magazine*.

https://doi.org/10.1109/MCOM.2016.7402272.

Guo, Bin, Zhiwen Yu, Xingshe Zhou, and Daqing Zhang. 2014. "From Participatory

Sensing to Mobile Crowd Sensing." In *2014 IEEE International Conference on

Pervasive Computing and Communication Workshops, PERCOM WORKSHOPS

2014*. https://doi.org/10.1109/PerComW.2014.6815273.

Harikrishnan, P. M., and Varun P. Gopi. 2017. "Vehicle Vibration Signal Processing for

Road Surface Monitoring." *IEEE Sensors Journal*.

https://doi.org/10.1109/JSEN.2017.2719865.

Harirforoush, Homayoun, and Lynda Bellalite. 2016. "A New Integrated GIS-Based

Analysis to Detect Hotspots: A Case Study of the City of Sherbrooke." *Accid. Anal.

Prev. Accident Analysis and Prevention* xxx.

https://doi.org/10.1016/j.aap.2016.08.015.

Hayhoe, GF. 2009. "Spectral Characteristics of Longitudinal Highway Profiles as

Related to Ride Quality." In *Vehicle, Tire, Pavement Interface*.

https://doi.org/10.1520/stp15908s.

Hong, Jin-Hyuk, Ben Margines, and Anind K. Dey. 2014. "A Smartphone-Based

Sensing Platform to Model Aggressive Driving Behaviors." In *Proceedings of the

32nd Annual ACM Conference on Human Factors in Computing Systems - CHI '14*.

https://doi.org/10.1145/2556288.2557321.

"How HDBSCAN Works." n.d. Accessed August 5, 2019.

https://hdbscan.readthedocs.io/en/latest/how_hdbscan_works.html.

Huang, Zhexue. 1997. "A Fast Clustering Algorithm to Cluster Very Large Categorical

Data Sets in Data Mining." *Data Mining and Knowledge Discovery* 3 (8): 34–39.

http://citeseerx.ist.psu.edu/viewdoc/download?doi=10.1.1.134.83&rep=rep1&type=

pdf.

Husson, François, Agrocampus Julie Josse, Agrocampus Jérôme, and Pagès

Agrocampus. 2010. "Principal Component Methods-Hierarchical Clustering-

Partitional Clustering: Why Would We Need to Choose for Visualizing Data?"

http://www.agrocampus-ouest.fr/math/.

Jain, Anil K. 2010. "Data Clustering: 50 Years beyond K-Means." *Pattern Recognition

Letters*. https://doi.org/10.1016/j.patrec.2009.09.011.

Jensen, M., J. Wagner, and K. Alexander. 2011. "Analysis of In-Vehicle Driver

Behaviour Data for Improved Safety." *International Journal of Vehicle Safety*.

https://doi.org/10.1504/IJVS.2011.042850.

Jinfeng Zhao. 2011. "Road Traffic Safety Evaluation Index System Based on Complex

System-Entropy Theory." In *2011 International Conference on Electric Technology and Civil Engineering (ICETCE)*, 1521–24. IEEE. https://doi.org/10.1109/ICETCE.2011.5776393.

Johnson, Derick A., and Mohan M. Trivedi. 2011. "Driving Style Recognition Using a Smartphone as a Sensor Platform." In *IEEE Conference on Intelligent Transportation Systems, Proceedings, ITSC*. https://doi.org/10.1109/ITSC.2011.6083078.

Júnior, Jair Ferreira, Eduardo Carvalho, Bruno V. Ferreira, Cleidson De Souza, Yoshihiko Suhara, Alex Pentland, and Gustavo Pessin. 2017. "Driver Behavior Profiling: An Investigation with Different Smartphone Sensors and Machine Learning." *PLoS One*. https://doi.org/10.1371/journal.pone.0174959.

Kalim, Faria, Jaehoon Jeong, and Muhammad U. Ilyas. 2016. "CRATER: A Crowd Sensing Application to Estimate Road Conditions." *IEEE Access* 4: 8317–26. https://doi.org/10.1109/ACCESS.2016.2607719.

Kim, Y. R. 2001. "Assessing Pavement Layer Condition Using Deflection Data." In *NCHRP Research Results Digest No.254*, Transportation Research Board, National Research Council, Washington D.C.

Kumar, Sachin, and Durga Toshniwal. 2015. "A Data Mining Framework to Analyze Road Accident Data." *Journal of Big Data*. https://doi.org/10.1186/s40537-015-0035-y.

———. 2016. "A Data Mining Approach to Characterize Road Accident Locations." *Journal of Modern Transportation*. https://doi.org/10.1007/s40534-016-0095-5.

Lee, Jay, and David W.S. Wong. 2001. "Point Descriptors." In *Statistical Analysis with ArcView GIS*, 33–58. John Wiley & Sons, Inc.

Lee, John D. 2008. "Fifty Years of Driving Safety Research." *Human Factors: The Journal of the Human Factors and Ergonomics Society*. https://doi.org/10.1518/001872008X288376.

Levine, Ned, Karl E. Kim, and Lawrence H. Nitz. 1995. "Spatial Analysis of Honolulu Motor Vehicle Crashes: II. Zonal Generators." *Accident Analysis and Prevention*. https://doi.org/10.1016/0001-4575(95)00018-U.

Li, Xiao, Ruizhi Chen, and Tianxing Chu. 2014. "A Crowdsourcing Solution for Road Surface Roughness Detection Using Smartphones." In *27th International Technical Meeting of the Satellite Division of the Institute of Navigation, ION GNSS 2014*.

Li, Xiao, and Daniel W. Goldberg. 2018. "Toward a Mobile Crowdsensing System for Road Surface Assessment." *Computers, Environment and Urban Systems*. https://doi.org/10.1016/j.compenvurbsys.2017.12.005.

Li, Xiao, Daniel W. Goldberg, Tianxing Chu, and Andong Ma. 2019. "Enhancing Driving Safety: Discovering Individualized Hazardous Driving Scenes Using GIS and Mobile Sensing." *Transactions in GIS*. https://doi.org/10.1111/tgis.12540.

Lima, Lucas Cedro, Vicente Jose Peixoto Amorim, Igor Muzetti Pereira, Filipe Nunes Ribeiro, and Ricardo Augusto Rabelo Oliveira. 2017. "Using Crowdsourcing Techniques and Mobile Devices for Asphaltic Pavement Quality Recognition." In *Brazilian Symposium on Computing System Engineering, SBESC*. https://doi.org/10.1109/SBESC.2016.029.

Macias, Elsa, Alvaro Suarez, and Jaime Lloret. 2013. "Mobile Sensing Systems."
Sensors (Switzerland). https://doi.org/10.3390/s131217292.

Manepalli, U.R.R., and Ghulam Bham. 2013. "Identification of Crash-Contributing
Factors." *Transportation Research Record Journal of the Transportation Research
Board Transportation Research Board of the National Academies*, no. 2386: 179–
88. https://doi.org/10.3141/2386-20.

Massaro, Emanuele, Chaewon Ahn, Carlo Ratti, Paolo Santi, Rainer Stahlmann, Andreas
Lamprecht, Martin Roehder, and Markus Huber. 2017. "The Car as an Ambient
Sensing Platform." In *Proceedings of the IEEE*.
https://doi.org/10.1109/JPROC.2016.2634938.

Mednis, Artis, Girts Strazdins, Reinholds Zviedris, Georgijs Kanonirs, and Leo Selavo.
2011. "Real Time Pothole Detection Using Android Smartphones with
Accelerometers." In *2011 International Conference on Distributed Computing in
Sensor Systems and Workshops, DCOSS'11*.
https://doi.org/10.1109/DCOSS.2011.5982206.

Meiring, Gys Albertus Marthinus, and Hermanus Carel Myburgh. 2015. "A Review of
Intelligent Driving Style Analysis Systems and Related Artificial Intelligence
Algorithms." *Sensors (Switzerland)*. https://doi.org/10.3390/s151229822.

Misiti, Michel, Yves Misiti, Georges Oppenheim, Jean-Michel Poggi, and MathWorks.
2015. "Wavelet Toolbox User's Guide." *The MathWorks, Inc*.

Monge-Fallas, Jorge, Franklin Hernandez-Castro, Sofia Gonzalez-Villalobos, Evelyn
Barquero-Rodriguez, and Johnnie Esquivel-Piedra. 2016. "Traffic Data

Visualization in Costa Rica: A Visualization of Top 100 Routes with the Highest Traffic Density in Costa Rica." *PONTE International Scientific Researchs Journal* 72 (11). https://doi.org/10.21506/j.ponte.2016.11.19.

Moore, Samuel. 2018. "Superaccurate GPS Chips Coming to Smartphones in 2018." IEEE Spectrum. 2018. https://spectrum.ieee.org/tech-talk/semiconductors/design/superaccurate-gps-chips-coming-to-smartphones-in-2018.

"Motion Sensors." n.d. Android Developers. Accessed August 5, 2019. https://developer.android.com/guide/topics/sensors/sensors_motion.

Murtagh, Fionn, and Pierre Legendre. 2014. "Ward's Hierarchical Agglomerative Clustering Method: Which Algorithms Implement Ward's Criterion?" *Journal of Classification* 31 (3): 274–95. https://doi.org/10.1007/s00357-014-9161-z.

Nataanen, R, and H Summala. 1976. "Road-User Behavior and Traffic Accidents." *Publication of: North-Holland Publishing Company*.

Odong, T. L., J. van Heerwaarden, T. J.L. van Hintum, F. A. van Eeuwijk, and J. Jansen. 2013. "Improving Hierarchical Clustering of Genotypic Data via Principal Component Analysis." *Crop Science*. https://doi.org/10.2135/cropsci2012.04.0215.

Panichpapiboon, Sooksan, and Puttipong Leakkaw. 2017. "Traffic Density Estimation: A Mobile Sensing Approach." *IEEE Communications Magazine*. https://doi.org/10.1109/MCOM.2017.1700693.

Parnami, Archit, Prajval Bavi, Dimitris Papanikolaou, Srinivas Akella, Minwoo Lee, and Siddharth Krishnan. 2018. "Deep Learning Based Urban Analytics Platform:

Applications to Traffic Flow Modeling and Prediction." In *ACM SIGKDD Workshop on Mining Urban Data (MUD3)*. London : ACM.

Paterson, William D. O., and Busby Attoh-Okine. 1992. "Summary Models of Paved Road Deterioration Based on HDM-III." *Transportation Research Record*.

Peng, Jia, Yanmin Zhu, Qingwen Zhao, Hongzi Zhu, Jian Cao, Guangtao Xue, and Bo Li. 2017. "Fair Energy-Efficient Sensing Task Allocation in Participatory Sensing with Smartphones." *Computer Journal*. https://doi.org/10.1093/comjnl/bxx015.

Perez Espinosa, Adriana, Ruben F Estrada-S, Alejandro Molina, Adriana Perez-Espinosa, Araceli L Reyes-C, Jose L Quiroz-F, and Emilio Bravo-G. 2016. "Zonification of Heavy Traffic in Mexico City." https://www.researchgate.net/publication/322644686.

Perez, Gabriela V. Angeles, Jose Castillejos Lopez, Araceli L. Reyes Cabello, Emilio Bravo Grajales, Adriana Perez Espinosa, and Jose L. Quiroz Fabian. 2018. "Road Traffic Accidents Analysis in Mexico City through Crowdsourcing Data and Data Mining Techniques" *International Journal of Computer and Information Engineering*. https://doi.org/10.5281/ZENODO.1340532.

Perttunen, Mikko, Oleksiy Mazhelis, Fengyu Cong, Mikko Kauppila, Teemu Leppänen, Jouni Kantola, Jussi Collin, et al. 2011. "Distributed Road Surface Condition Monitoring Using Mobile Phones." In *Lecture Notes in Computer Science (Including Subseries Lecture Notes in Artificial Intelligence and Lecture Notes in Bioinformatics)*. https://doi.org/10.1007/978-3-642-23641-9_8.

Pesyna, Kenneth M., Robert W. Heath, and Todd E. Humphreys. 2014. "Centimeter

Positioning with a Smartphone-Quality GNSS Antenna." In *27th International Technical Meeting of the Satellite Division of the Institute of Navigation, ION GNSS 2014*.

Plug, Charlotte, Jianhong Xia, and Craig Caulfield. 2011. "Spatial and Temporal Visualisation Techniques for Crash Analysis." *Accident Analysis and Prevention*. https://doi.org/10.1016/j.aap.2011.05.007.

Rishiwal, Vinay, and Hamshan Khan. 2016. "Automatic Pothole and Speed Breaker Detection Using Android System." In *2016 39th International Convention on Information and Communication Technology, Electronics and Microelectronics, MIPRO 2016 - Proceedings*. https://doi.org/10.1109/MIPRO.2016.7522334.

Sabir, Naveed, Anzal Ali Memon, and Faisal Karim Shaikh. 2019. "Threshold Based Efficient Road Monitoring System Using Crowdsourcing Approach." *Wireless Personal Communications* 106 (4): 2407–25. https://doi.org/10.1007/s11277-019-06324-y.

Santos, Salatiel Ribeiro Dos, Clodoveu A. Davis, and Rodrigo Smarzaro. 2016. "Integration of Data Sources on Traffic Accidents." In *Proceedings of the Brazilian Symposium on GeoInformatics*, 2016-November:192–203. National Institute for Space Research, INPE.

Sattar, Shahram, Songnian Li, and Michael Chapman. 2018. "Road Surface Monitoring Using Smartphone Sensors: A Review." *Sensors (Switzerland)*. MDPI AG. https://doi.org/10.3390/s18113845.

Sayers, Michael W., Thomas D. Gillespie, and Cesar a V. Queiroz. 1986. *The

International Road Roughness Experiment - Establishing Correlation and a

Calibration Standard for Measurements. The World Bank Technical Paper.

Sayers, Michael W, and Steven M Karamihas. 1998. "The Little Book of Profiling Basic

Information about Measuring and Interpreting Road Profiles."

https://deepblue.lib.umich.edu/bitstream/handle/2027.42/21605/90151.pdf?sequenc

e=1&isAllowed=y.

Schwarz, Brent. 2010. "Lidar: Mapping the World in 3D." *Nature Photonics*.

https://doi.org/10.1038/nphoton.2010.148.

Shen, Warren. 2012. "Introducing New Fusion Tables API." 2012.

https://research.googleblog.com/search/label/Fusion Tables.

Shikhar, Abhinav, J. S. Naveen, B. J. Sowmya, and K. G. Srinivas. 2016. "Data

Analytics on Accident Data for Smarter Cities and Safer Lives." In *2016*

International Conference on Computation System and Information Technology for

Sustainable Solutions, CSITSS 2016.

https://doi.org/10.1109/CSITSS.2016.7779365.

Silva, Nuno, Vaibhav Shah, João Soares, and Helena Rodrigues. 2018. "Road Anomalies

Detection System Evaluation." *Sensors (Switzerland)*.

https://doi.org/10.3390/s18071984.

Silva, Thiago H., Pedro O.S. Vaz De Melo, Aline Carneiro Viana, Jussara M. Almeida,

Juliana Salles, and Antonio A.F. Loureiro. 2013. "Traffic Condition Is More than

Colored Lines on a Map: Characterization of Waze Alerts." In *Lecture Notes in*

Computer Science (Including Subseries Lecture Notes in Artificial Intelligence and

Lecture Notes in Bioinformatics), 8238 LNCS:309–18. https://doi.org/10.1007/978-3-319-03260-3_27.

Silveira Rodrigues, Ricardo, Marcia Pasin, Alice Kozakevicius, and Vinicius Monego. 2019. "Pothole Detection in Asphalt: An Automated Approach to Threshold Computation Based on the Haar Wavelet Transform." In *2019 IEEE 43rd Annual Computer Software and Applications Conference (COMPSAC)*, 306–15. IEEE. https://doi.org/10.1109/COMPSAC.2019.00053.

Singh, Gurdit, Divya Bansal, and Sanjeev Sofat. 2017. "A Smartphone Based Technique to Monitor Driving Behavior Using DTW and Crowdsensing." *Pervasive and Mobile Computing*. https://doi.org/10.1016/j.pmcj.2017.06.003.

Songchitruksa, Praprut, and Xiaosi Zeng. 2010. "Getis-Ord Spatial Statistics to Identify Hot Spots by Using Incident Management Data." *Transportation Research Record: Journal of the Transportation Research Board*. https://doi.org/10.3141/2165-05.

Steenberghen, T., T. Dufays, I. Thomas, and B. Flahaut. 2004. "Intra-Urban Location and Clustering of Road Accidents Using Gis: A Belgian Example." *International Journal of Geographical Information Science*. https://doi.org/10.1080/13658810310001629619.

Tan, Guang, Mingming Lu, Fangsheng Jiang, Kongyang Chen, Xiaoxia Huang, and Jie Wu. 2014. "Bumping: A Bump-Aided Inertial Navigation Method for Indoor Vehicles Using Smartphones." *IEEE Transactions on Parallel and Distributed Systems*. https://doi.org/10.1109/TPDS.2013.194.

Texas DOT. 2019a. "Crash Records Information System." 2019.

https://cris.dot.state.tx.us/public/Purchase/app/home/welcome.

———. 2019b. "Roadway Inventory." 2019. https://www.txdot.gov/inside-txdot/division/transportation-planning/roadway-inventory.html.

"The Pothole Facts." 2019. 2019. https://www.pothole.info/the-facts/.

The U.S. National Highway Safety Administration. 2015. "Critical Reasons for Crashes Investigated in the National Motor Vehicle Crash Causation Survey." https://crashstats.nhtsa.dot.gov/Api/Public/ViewPublication/812115.

———. 2019. "Crash Rate Calculations." 2019. https://safety.fhwa.dot.gov/local_rural/training/fhwasa1109/app_c.cfm.

Theofilatos, Athanasios, and George Yannis. 2014. "A Review of the Effect of Traffic and Weather Characteristics on Road Safety." *Accident Analysis and Prevention*. https://doi.org/10.1016/j.aap.2014.06.017.

Toledo, Tomer, Oren Musicant, and Tsippy Lotan. 2008. "In-Vehicle Data Recorders for Monitoring and Feedback on Drivers' Behavior." *Transportation Research Part C: Emerging Technologies*. https://doi.org/10.1016/j.trc.2008.01.001.

U.S. National Highway Traffic Safety Administration. 2016. "Traffic Safety Facts 2016 Data." 2016. https://crashstats.nhtsa.dot.gov/Api/Public/ViewPublication/812580.

Vittorio, Astarita, Vaiana Rosolino, Iuele Teresa, Caruso Maria Vittoria, P. Giofrè Vincenzo, and De Masi Francesco. 2014. "Automated Sensing System for Monitoring of Road Surface Quality by Mobile Devices." *Procedia - Social and Behavioral Sciences*. https://doi.org/10.1016/j.sbspro.2014.01.057.

Vorko-Jović, Ariana, Josipa Kern, and Zrinka Biloglav. 2006. "Risk Factors in Urban

Road Traffic Accidents." *Journal of Safety Research*.

https://doi.org/10.1016/j.jsr.2005.08.009.

Wang, Heng, Bin Wang, Bingbing Liu, Xiaoli Meng, and Guanghong Yang. 2017.

"Pedestrian Recognition and Tracking Using 3D LiDAR for Autonomous Vehicle."

Robotics and Autonomous Systems. https://doi.org/10.1016/j.robot.2016.11.014.

Wang, Jing, Jian Tang, Guoliang Xue, and Dejun Yang. 2017. "Towards Energy-

Efficient Task Scheduling on Smartphones in Mobile Crowd Sensing Systems."

Computer Networks. https://doi.org/10.1016/j.comnet.2016.11.020.

Watanatada, Thawat, Clell Harral, William Paterson, Ashok Dhareshwar, Anil Bhandari,

and Koji Tsunokawa. 1987. "The Highway Design and Maintenance Model:

Description of the HDM-III Model." *The Highway Design and Maintenance

Standards Series*.

Waze. 2019. "Waze Company Factsheet." 2019. https://assets.brandfolder.com/p31v19-

dpmnts-ci9it3/original/Waze Company Factsheet.pdf.

Wei, Liu, T. F. Fwa, and Zhao Zhe. 2005. "Wavelet Analysis and Interpretation of Road

Roughness." *Journal of Transportation Engineering*.

https://doi.org/10.1061/(asce)0733-947x(2005)131:2(120).

World Health Organization. 2015. "Global Status Report on Road Safety." *Injury

Prevention*.

https://doi.org/http://www.who.int/violence_injury_prevention/road_safety_status/2

015/en/.

———. 2018. "Global Status Report On Road Safety 2018." WHO. World Health

Organization. 2018.

https://www.who.int/violence_injury_prevention/road_safety_status/2018/en/.

Xi, Jianfeng, Zhonghao Zhao, Wei Li, and Quan Wang. 2016. "A Traffic Accident

Causation Analysis Method Based on AHP-Apriori." In *Procedia Engineering*.

https://doi.org/10.1016/j.proeng.2016.01.305.

Xu, Bing, S. Ranji Ranjithan, and Y. Richard Kim. 2002. "New Relationships between

Falling Weight Deflectometer Deflections and Asphalt Pavement Layer Condition

Indicators." In *Transportation Research Record*. https://doi.org/10.3141/1806-06.

Xu, Wenchao, Ruizhi Chen, Tianxing Chu, Lei Kuang, Yanqin Yang, Xiao Li, Jingbin

Liu, and Yuwei Chen. 2015. "A Context Detection Approach Using GPS Module

and Emerging Sensors in Smartphone Platform." In *2014 Ubiquitous Positioning*

Indoor Navigation and Location Based Service, UPINLBS 2014 - Conference

Proceedings. https://doi.org/10.1109/UPINLBS.2014.7033723.

Yao, Shenjun, Becky P.Y. Loo, and Bruce Zi Yang. 2016. "Traffic Collisions in Space:

Four Decades of Advancement in Applied GIS." *Annals of GIS*.

https://doi.org/10.1080/19475683.2015.1085440.

Zandbergen, Paul A. 2009. "Accuracy of IPhone Locations: A Comparison of Assisted

GPS, WiFi and Cellular Positioning." In *Transactions in GIS*.

https://doi.org/10.1111/j.1467-9671.2009.01152.x.

Zandbergen, Paul A., and Sean J. Barbeau. 2011. "Positional Accuracy of Assisted GPS

Data from High-Sensitivity GPS-Enabled Mobile Phones." *Journal of Navigation*.

https://doi.org/10.1017/S0373463311000051.

Zang, Kaiyue, Jie Shen, Haosheng Huang, Mi Wan, and Jiafeng Shi. 2018. "Assessing
and Mapping of Road Surface Roughness Based on GPS and Accelerometer
Sensors on Bicycle-Mounted Smartphones." *Sensors (Switzerland).*
https://doi.org/10.3390/s18030914.

Zappatore, Marco, Antonella Longo, and Mario A. Bochicchio. 2016. "Using Mobile
Crowd Sensing for Noise Monitoring in Smart Cities." In *2016 International
Multidisciplinary Conference on Computer and Energy Science, SpliTech 2016*.
https://doi.org/10.1109/SpliTech.2016.7555950.

Zeeman, A. S., and M. J. Booysen. 2013. "Combining Speed and Acceleration to Detect
Reckless Driving in the Informal Public Transport Industry." In *IEEE Conference
on Intelligent Transportation Systems, Proceedings, ITSC*.
https://doi.org/10.1109/ITSC.2013.6728322.

Zhang, Zhe, and Kirsi Virrantaus. 2010. "Analysis of Vulnerability of Road Networks
on the Basis of Graph Topology and Related Attribute Information." *Smart
Innovation, Systems and Technologies*. https://doi.org/10.1007/978-3-642-14616-
9_34.

Zhuang, Zhenyun, Kyu Han Kim, and Jatinder Pal Singh. 2010. "Improving Energy
Efficiency of Location Sensing on Smartphones." In *MobiSys'10 - Proceedings of
the 8th International Conference on Mobile Systems, Applications, and Services*.
https://doi.org/10.1145/1814433.1814464.